DYNAMIC NUMERICAL ANALYSIS OF TYPICAL MONOPILE FOUNDATIONS FOR OFFSHORE WIND TURBINE APPLICATIONS

MASTER'S DEGREE THESIS

ABDUH KIWANUKA

MERSIN UNIVERSITY
INSTITUTE OF SCIENCES

CIVIL ENGINEERING
DEPARTMENT

SUPERVISOR
Prof. Dr. ÖZGÜR LÜTFİ ERTUĞRUL

JUNE-2023

MERSİN

DYNAMIC NUMERICAL ANALYSIS OF TYPICAL MONOPILE FOUNDATIONS FOR OFFSHORE WIND TURBINE APPLICATIONS

MASTER'S DEGREE THESIS

ABDUH KIWANUKA
ORCID : 0000-0002-7975-7609

MERSIN UNIVERSITY
INSTITUTE OF SCIENCES

CIVIL ENGINEERING
DEPARTMENT

SUPERVISOR
Prof. Dr. ÖZGÜR LÜTFİ ERTUĞRUL
ORCID : 0000-0002-1270-3649

JUNE-2023

MERSİN

ABSTRACT

DYNAMIC NUMERICAL ANALYSIS OF TYPICAL MONOPILE FOUNDATIONS FOR OFFSHORE WIND TURBINE APPLICATIONS.

Offshore wind energy has become an important source of renewable energy in recent years, with large-diameter monopile foundations serving as the primary support structures for offshore wind turbines. The design of these monopiles requires an understanding of their structural behavior and interaction with the surrounding soil. Within this study, a 7.5m diameter monopile embedded in a dense sand soil was analysed using finite element method and the simplified design procedures available in the literature. The effect of structural and soil parameters on the monopile behavior was examined, and results indicated that the stiffness of the soil and internal friction angle have a nonlinear and negative relationship with the monopile's lateral displacement and rotation. The simplified design procedure and elastic solution in combination with the Winkler model underestimated the pile displacement and rotation, while the finite element analysis accurately predicted the behavior of the monopile. Based on the results obtained from the finite element simulations, regression equations that can be used for the initial design of monopiles embedded in dense sand soil conditions were presented.

In conclusion, this study provides insight into the behavior of large-diameter monopiles embedded in granular soils which is quite common in offshore wind energy applications and offers recommendations for their design. The regression equations generated within this study can be used as a preliminary design tool for large-diameter monopiles in dense sand soil conditions.

Keywords: Monopile, Monotonic lateral load, Offshore Wind Turbine, Finite Element Analysis, Simplified Design Procedure.

Advisor: Prof. Dr. Özgür Lütfi ERTUĞRUL, Department of Civil Engineering, Mersin University.

GENİŞLETİLMİŞ ÖZET

DENİZ RÜZGAR TÜRBİNİ UYGULAMALARI İÇİN TİPİK TEK KAZIKLI TEMELLERİN DİNAMİK SAYISAL ANALİZİ

Küresel ısınmanın temel kaynağı olan karbondioksit emisyonlarının olumsuz etkilerini azaltmak için günümüzde alternatif enerjiye yönelim giderek artmaktadır. Rüzgar enerjisi, güneş enerjisinden sonra ikinci önemli alternatif olarak karşımıza çıkmaktadır. Rüzgar potansiyelinin en yüksek olduğu lokasyonlar ise genellikle denizlerdir. Başta Hollanda ve Norveç olmak üzere, Avrupa ülkeleri ve Amerika Birleşik Devletleri rüzgar enerjisini kullanılabilir hale getirmek için yoğun bir çaba içerisindedir. Türkiye, Akdeniz, Karadeniz ve Ege Denizi tarafından çevrelenmekte olup önemli bir rüzgar enerjisi potansiyeline sahiptir. Ancak mevcut rüzgar enerjisi stokunu kullanılabilir hale getirebilmek için ülkemizde yeteri düzeyde çalışma yapılmamaktadır. Açık deniz rüzgar çiftliklerine yatırım yapmak ve yenilenebilir enerji farkındalığını teşvik etmek, açık deniz rüzgar türbinlerinin temeli olarak tek kazıklı yapıların kullanılması yoluyla maliyetleri düşürürken sürdürülebilir bir geleceğe ve daha temiz bir çevreye katkıda bulunabilir. Açık deniz rüzgar çiftlikleri, fosil yakıtlara bağımlılığı azaltarak ve enerji karışımını çeşitlendirerek daha güçlü ve daha tutarlı rüzgar kaynaklarından yararlanabilir. Geniş çaplı tek kazıklı temeller kullanılarak deniz ortamında kurulacak rüzgar çiftlikleri zorlu deniz koşullarına dayanabilmektedir. Bu şekilde tasarlanmış rüzgar türbinleri, Amerika ve Kuzey Avrupa kıyılarında çok büyük bir hızla yer almaya başlamıştır. Yenilenebilir enerji farkındalığının her fırsatta vurgulanması, halkın desteğini ve katılımını sağlamak için çok önemlidir. Türkiye gibi ülkeler rüzgar enerjisini benimseyerek ve üç tarafı denizlerle çevrili Türkiye'nin bu devasa imkanından yararlanarak karbondioksit emisyonlarını azaltabilir, iklim değişikliğiyle mücadele edebilir ve daha sürdürülebilir bir geleceğin yolunu açabilir.

Açık deniz rüzgar enerjisi son on yılda, yenilenebilir bir enerji kaynağı olarak giderek daha önemli hale gelerek tek kazıklı (monopile) temeller, açık deniz rüzgar türbinleri için birincil destek yapıları olarak yaygın şekilde kullanılmaya başlanmıştır. Büyük çaplı çelik tüp profillerden imal edilen tekil kazıklı temelleri etkili bir şekilde tasarlamak için, yapısal davranışlarını ve çevresindeki zeminle nasıl etkileşime girdiklerini anlamak çok önemlidir. Bu çalışma kapsamında kum zemin profiline gömülmüş 7,5 m çapındaki tüp tekil kazığın kazığın davranışına odaklanılmaktadır. Bu amaçla, tez çalışması kapsamında, sonlu elemanlar analizi (SEA), basitleştirilmiş tasarım prosedürleri ve çoklu regresyon analizi teknikleri kullanılmaktadır. SEA, stres dağılımı ve yük taşıma kapasitesi gibi faktörlerin değerlendirilmesini sağlayarak karmaşık yükler altındaki yapıların simülasyonuna izin vermektedir. Basitleştirilmiş tasarım prosedürleri ise, basitleştirilmiş varsayımlar ve hesaplamalar vasıtasıyla tasarımcılara yol gösterebilecek düzeyde verimli çözümler sunar. Literatürde yer alan mevcut çalışmalardan farklı olarak bu tez çalışması kapsamında, tek kazıklı temelin davranışını çeşitli girdi parametreleriyle ilişkilendiren ampirik denklemler veya modeller geliştirmek için çoklu regresyon analizleri yapılmıştır. Bu yaklaşımlar neticesinde elde edilen veriler birleştirilerek, tekil kazıklı temelin davranışı ve çevredeki toprakla etkileşimi hakkında kapsamlı bir anlayış sağlanması amaçlanmıştır. Elde edilen bulgular açık deniz rüzgar türbin temelleri için tasarım kılavuzlarının geliştirilmesine yardımcı olabilecek niteliktedir.

Basitleştirilmiş tasarım prosedürü, tek kazık davranışını değerlendirmek için kullanışlı ve hızlı bir değerlendirme imkanı sunmaktadır. Tez çalışması kapsamında, bu prosedürlerden bir tanesi, Excel yazılımına entegre edilerek, monopile kazıklar için zemin-kazık etkileşimi Winkler yaklaşımıyla irdelenmiştir. Elde edilen bulgular, Abaqus yazılımı sonuçları ile karşılaştırılarak monopile kazığın çeşitli yük koşulları altındaki karmaşık davranışı ele alınmıştır. Elde edilen bulgular istatistiksel olarak değerlendirilmek üzere Statistica yazılımı kullanılarak yapılan çoklu regresyon analizleri ile büyük çaplı tek kazıklı temellerin ön tasarımı için kapalı form formüllerinin türetilmesi sağlanmıştır.

Sayısal modelleme amacıyla Abaqus yazılımı kullanılarak 7.5 m çapındaki tüp tekil kazığın kazığın davranışını ve çevredeki toprakla etkileşimini üç boyutlu olarak simüle etmek için sonlu elemanlar modelleme yaklaşımı kullanılmıştır. Sayısal analizler için tekil kazık ve çevreleyen zeminin üç boyutlu bir modeli oluşturulmuştur. Doğru bir simülasyon sağlamak için modelleme işlemi sırasında sınır koşulları ve temas bölgesindeki davranışın gerçekçi şekilde dikkate alınmaya çalışılmıştır. Modelleme sürecinde, tekil kazığın geometrisinin doğru bir şekilde temsil edilmesi, uygun sınır koşullarının seçimi, kazık-zemin etkileşimi ve temas bölgesi davranışının dikkate alınması ve ilgili malzemelerin davranışını temsil edecek uygun eleman tipleri ile malzeme modellerinin seçimi önem arz etmiştir. Simülasyonlar iki adımda gerçekleştirilmiştir. İlk olarak, başlangıç koşullarını oluşturabilmek için kazık modeline ve zemine yer çekimi etkisi uygulanmıştır. Daha sonra, rüzgar ve dalga kuvvetlerinin tek kazık üzerindeki etkisini simüle etmek için yanal yük ve devrilme momenti uygulanmıştır. Kapsamlı bir veri seti oluşturmak üzere toplam 324 tane simülasyon gerçekleştirilmiştir. Elde edilen sonuçlar daha önce bahsedilen çoklu regresyon analizinde kullanılmıştır. Ayrıca, zemin ve yapısal parametre değerlerinin uygun aralıklarını belirlemek için parametrik bir çalışma yapılmıştır. Bu çalışmayla, açık deniz rüzgar çiftliği sahalarının değişken özellikleri dikkate alınarak elde edilen denklemlerin gerçekçi saha koşullarını yansıtabilmesi amaçlanmıştır. Parametrik analizlerde araştırılan değişkenler arasında kazık et kalınlığı, gömülü uzunluk, zeminin içsel sürtünme açısı ve elasitisite modülü yer almaktadır. Bu araştırma, sonlu elemanlar modelleme yaklaşımını kullanarak ve kapsamlı bir parametrik çalışma yürüterek, tek kazıklı temelin yapısal davranışı ve çevredeki toprakla etkileşimi hakkında değerli bilgiler ortaya koymayı amaçlamıştır. Elde edilen bulgular, daha gerçekçi tasarım kılavuzlarının geliştirilmesine katkıda bulunabilir ve açık deniz rüzgar türbini temel tasarımının geliştirilmesine yardımcı olabilir.

İçi boş silindirik kazıklar günümüzde yüksek dayanımlı çelik kullanılarak imal edilmektedir. Modelleme çalışmasında da bu malzemenin özellikleri dikkate alınmıştır. Kazığın içinde yer alan zemin ortamının ise kohezyonsuz sıkı kum olduğu düşünülmüştür. Sıkı kumun birim hacim ağırlığı, oedometrik rijitlik parametreleri, Poisson oranı, içsel sürtünme açısı gibi geoteknik özellikleri dikkate alınmıştır. Benzer şekilde, tekil kazık gövdesini oluşturan malzeme için de kütle yoğunluğu, elastisite modülü, Poisson oranı ve kalınlık gibi çelik malzeme özellikleri analizlerde dikkate alınmıştır. Bu tez çalışması, monopile kazık ve çevreleyen zeminin etkileşimini doğru bir şekilde yakalamayı amaçlamaktadır.

Sayısal modelleme kısmında, farklı yapısal ve zemin parametrelerinin monopile tekil kazıkların davranışı üzerindeki etkisi, Abaqus yazılımı kullanılarak üç boyutlu sonlu elemanlar analizi vasıtasıyla incelenmiştir. Analizler, çeşitli koşullar altında tek kazığın tepkisine ilişkin öngörü sağlamayı amaçlamıştır. Çalışmanın bulguları, zemin rijitliği, içsel sürtünme açısı ve tekil kazığın yanal yer değiştirmesi ve rotasyonu arasında doğrusal olmayan ve negatif bir ilişki olduğunu göstermiştir. Bu durum, zemin rijitliği ve içsel sürtünme açısı arttıkça, monopile tekil kazığın yanal yer değiştirmesinin ve dönmesinin azaldığını göstermektedir. Bu ilişkiler, tek kazıklı temellerin stabilitesini ve performansını anlamada çok önemlidir. Ayrıca çalışma neticesinde, basitleştirilmiş tasarım prosedürünün Winkler modeli ve elastik çözümle birleştiğinde kazık yer değiştirmesini ve dönüşünü olması gerekenden daha düşük tahmin etmekte olduğunu ortaya çıkmıştır. Buna karşılık, sonlu eleman analizi, tek kazığın davranışını doğru bir şekilde tahmin edebilmektedir. Bu durum, tekil kazığın dinamik yükler altındaki karmaşık davranışını doğru bir şekilde yakalamak için sonlu elemanlar analizi gibi daha karmaşık analiz teknikleri kullanmanın önemini vurgulamaktadır. Çalışmamızda, sonlu elemanlar analizi simülasyonlarından elde edilen sonuçlar üzerinde regresyon analizi yaparak, sıkı kum zemin koşullarında geniş çaplı tek kazıklar için bir ön tasarım aracı olarak hizmet edebilecek regresyon denklemleri türetilmiştir. Bu denklemler, mühendislere ve tasarımcılara tekil kazığın davranışını ve performansını tahmin etmek için pratik bir araç sağlayarak tasarım sürecine yardımcı olacak ve açık deniz rüzgar türbini temellerinin stabilitesini ve güvenilirliğini için oluşturulabilecek standartlara katkıda bulunacaktır. Genel olarak değerlendirildiğinde, elde ettiğimiz bulgular, monopile kazığın davranışını doğru bir şekilde değerlendirmek için gelişmiş sayısal analiz tekniklerini kullanmanın önemini göstermektedir. Elde edilen regresyon denklemleri, sıkı kum zemin koşullarında tek kazıklı temellerin ön tasarımı için değerli bilgiler sunarak etkili ve verimli açık deniz rüzgar enerjisi projelerinin geliştirilmesine katkıda bulunmaktadır.

Bu çalışmada yürütülen analizin doğruluğunu ve uygulanabilirliğini artırmak için, gelecekteki araştırmalar, gerçek saha koşullarındaki boşluk suyu basıncı, çevrimsek yükler altında zeminde direnç kaybı ve yanı sıra rüzgar ve dalga özellikleri hakkında ayrıntılı bilgileri analizlere dahil etmeyi düşünmelidir. Bu ek faktörler, açık deniz ortamlarında tek kazığın davranışını ve performansını doğru bir şekilde değerlendirmede çok önemli bir rol oynar. Ayrıca, açık deniz rüzgar türbinleri dinamik yükleme koşullarına tabi olduğundan, tekil kazığın çevrimsel yükleme davranışının araştırılması önerilir. Döngüsel yükleme altındaki monopile kazığın tepkisinin irdelenmesi de tasarımları ve uzun vadeli performansları için değerli bilgiler sağlayabilir. Ek olarak, analizi 4m, 5m, 6m ve 8m gibi farklı çaplara sahip tek kazıklı temelleri içerecek şekilde genişletmek, değişen boyutlardaki tek kazığın davranışının daha kapsamlı bir şekilde anlaşılmasına katkıda bulunacaktır. Benzer şekilde, kil ve kum gibi farklı zemin koşullarının dikkate alınması, zemin özelliklerinin silindirik tüp profil tekil kazık performansı üzerindeki etkisine ilişkin fikir verebilecektir. Son olarak, çok değişkenli doğrusal olmayan regresyon analizlerinin uygulanması, tek kazıklı temellerin ön tasarımı için kapalı formüller önererek tasarım sürecini daha da geliştirebilir. Bu formüller, tasarım sürecini basitleştirerek mühendislerin tek kazıklı temellerin davranışını daha verimli bir şekilde tahmin etmelerini sağlar. Bu araştırma alanlarını ele alan gelecekteki çalışmalar, monopile kazık davranışı anlayışını ilerletebilir ve açık deniz rüzgar türbini temelleri için daha doğru ve güvenilir tasarım kılavuzlarının geliştirilmesine katkıda bulunabilir.

Bu tez çalışması, açık deniz rüzgar enerjisi uygulamalarında büyük çaplı tekil kazıklı (monopile) temelin davranışına ilişkin değerli bilgiler sağlamakta ve tasarım önerileri sunmaktadır. Elde edilen regresyon denklemleri, yoğun kum zemin koşullarına gömülü 7.5 m çapındaki tekil kazığın davranışını anlamak için bir ön tasarım aracı olarak hizmet edebilecektir. Çalışmamızda elde edilen bulgular, monopile kazık rotasyonu ve deplasmanları üzerinde önemli bir etkiye sahip olan zemin elastisite modülü ve içsel sürtünme açısı gibi zemin parametrelerinin öneminin altını çizmektedir. Daha yüksek toprak rijitliği, daha düşük yanal yer değiştirme ve dönme ile sonuçlanırken, artan içsel sürtünme açısı, çamur çizgisi seviyesinde (mudline) kazık yer değiştirmesini ve dönüşünü azaltır. Yanal tasarım ağırlıklı olarak deformasyon davranışı tarafından yönetildiğinden, bu araştırmanın odak noktası nihai dirençten ziyade öncelikle deformasyon davranışı olmuştur. Zemin direncini ve akma davranışını doğru bir şekilde tahmin etmede, basitleştirilmiş tasarım prosedürünün sınırlamaları göz önünde bulundurularak sonlu elemanlar analizi ile tamamlanması önerilir. Gelecekteki analizlerde gerçekçi çelik davranışı ve geliştirilmiş zemin modellerinin yanı sıra boşluk basıncının hesaba katılması, silindirik tüp profilden imal edilen tekil kazıklı offshore temellerin tasarımının doğruluğunu ve güvenilirliğini daha da artıracaktır.

Anahtar Kelimeler: Tek kazıklı temel, Monoton yanal yük, Açık deniz Rüzgar Türbini, Sonlu Elemanlar Analizi, Basitleştirilmiş Tasarım Prosedürü.

Danışman: Prof. Dr. Özgür Lütfi ERTUĞRUL, İnşaat Mühendisliği Bölümü, Mersin Üniversitesi.

ACKNOWLEDGEMENTS

I would like to thank my advisor, Prof. Dr. Özgür Lütfi ERTUĞRUL for all his help and patience. I could not have achieved it without his continuous support and guidance. A special thanks also go to Civil Engineering Department Staff, all Civil Engineering Graduate Students, and all the international students studying at Mersin University. My experience at Mersin University was wonderful because of all the great people. Thank you to my family especially my father for all the financial and emotional support. I will forever be grateful to Turkish Scholarship Programme. Without Turkey's government support, I could not complete this thesis.

CONTENTS

LIST OF FIGURES

LIST OF TABLES

ABBREVIATIONS AND SYMBOLS

SDP	Simplified Design Procedure
E_s	soil Young’s modulus
L_p	Monopile embedded length
t_p	Monopile wall thickness in millimeters
U	Horizontal displacement at mudline in meters
UR	The magnitude of the node rotation at mudline
OWT	Offshore Wind Turbine
FEA	Finite Element Analysis
BEM	Beam Element Model
CFD	Computational Fluid Dynamics
ϕ	Internal angle of friction in degrees
E_p	pile material Young’s modulus
NREL	National Renewable Energy Laboratory

1. INTRODUCTION

1.1. Monopile definition

A monopile is a large diameter open-ended tubular pipe loaded by vertical loads from the weight of the tower and the turbine, and large lateral forces and bending moments due to wind and ocean waves and currents. It transfers the load to the seabed by mobilizing horizontal earth pressures in competent upper soil layers (Arshad and O'Kelly, 2016). A typical 7.5 m diameter monopile is shown in Figure 1-1 below. Also Figure 1-2 shows an already installed monopile foundation.

A 7.5 m diameter monopile for Gode Wind Offshore Wind Farm. DONG Energy. (Online version in colour.)

Figure 1-1: 7.5 m diameter monopile at the production plant (Kallehave et al., 2015).

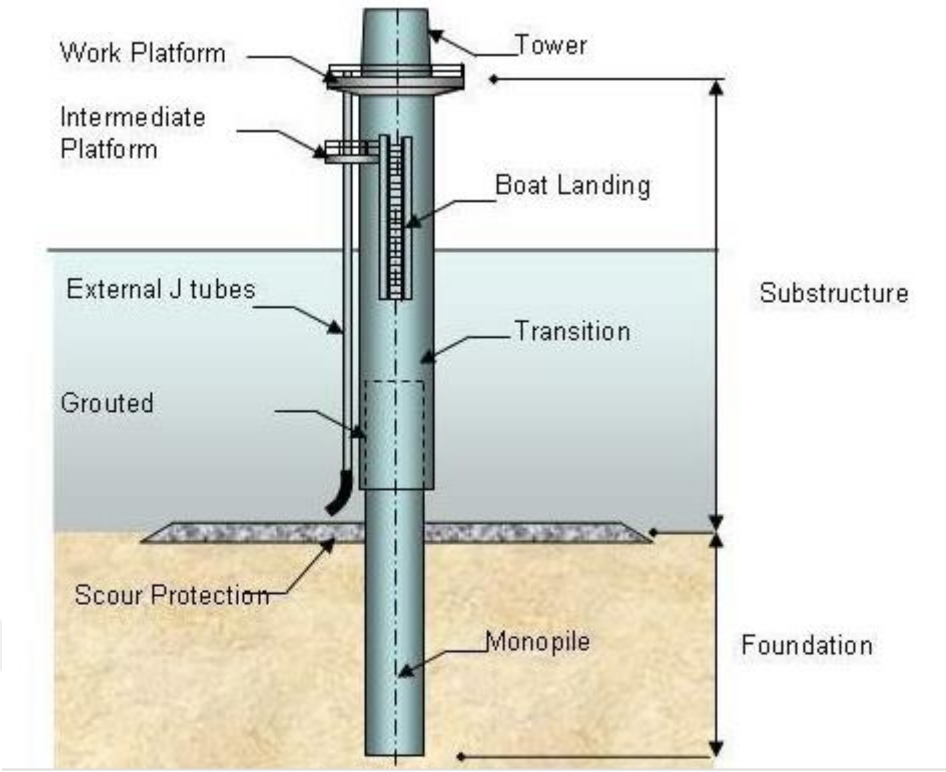

Figure 1-2: A sample cross section of a monopile foundation (Piante et al., 2019).

1.1.2. Components of an offshore wind turbine

An offshore wind turbine typically consists of several key components, including a foundation, tower, nacelle, and blades. The foundation of an offshore wind turbine is typically a monopile, a large diameter steel pipe that is driven into the seabed to provide support for the turbine. The monopile is connected to the tower by a transition piece, which extends above the water level and provides a platform for the nacelle and blades. The tower, which is typically made of steel, supports the nacelle, which houses the generator, gearbox, and other mechanical and electrical components of the turbine. The blades, which are typically made of composite materials, are attached to the nacelle and are responsible for capturing the wind's energy and converting it into electricity. Together, these components work to generate clean, renewable energy from the wind. A sample Offshore Wind Turbine is shown in Figure 1-3.

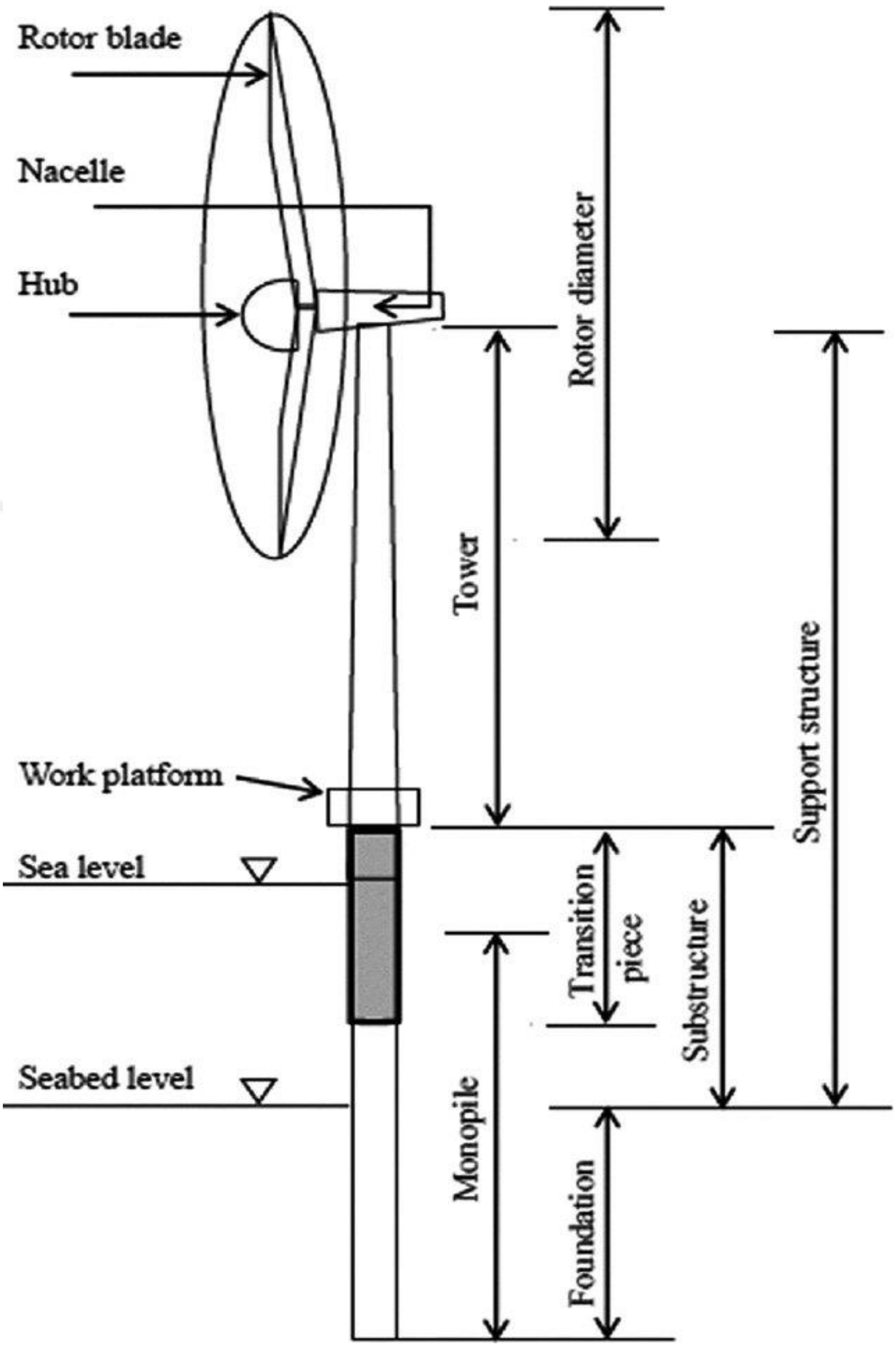

Figure 1-3: Main components of an offshore wind turbine system (Arshad and O'Kelly, 2016).

1.2. Aim of the study

This study aims to explore the potential for the adoption of wind energy as a means of mitigating the negative impacts of carbon dioxide emissions, particularly concerning the escalation of climatic temperatures. As a rich country with abundant water bodies, including the Mediterranean Sea, Black Sea, and Aegean Sea, Turkey has the potential to develop offshore wind farms as a clean and renewable energy source. To support the growth and success of the wind industry, it is essential to reduce costs for future projects, which can be achieved through the use of monopile structures as foundations for offshore wind turbines. The government of Turkey should consider investing in offshore wind farm technology and increasing awareness about the benefits of renewable energy to reduce usage of fossil-fuel-based energy sources. The essence of this thesis project is focused on numerical analysis of an offshore wind turbine monopile foundation using;

1. The simplified design procedure was implemented in Excel software.
2. The finite element analysis using Abaqus software.
3. Multiple regression analysis using Statistica software.

Well documented characteristics of a National Renewable Energy Laboratories (NREL) 5MW baseline wind turbine was considered in the study.

1.3. Advantages of the monopile foundations in offshore wind energy applications

There are several advantages of using monopile foundations for offshore wind turbines:

- Flexibility in design: To meet the unique environmental and soil conditions at a specific site, the pile penetration depth can be adjusted. This gives the design and installation procedure more flexibility, allowing the monopile to sustain the wind turbine effectively in a variety of situations.
- Ease of installation: Installing monopile foundations is not too difficult because they don't need elaborate anchoring or foundations. They are therefore a sensible choice for offshore wind farms.
- Durability: Monopile foundations are renowned for their toughness and capacity to survive harsh offshore environments. High-strength steel is often used to make them, and they are built to withstand the forces of wind, waves, and currents.
- Suitability for areas with moveable seabeds: As they can efficiently transfer the load of the wind turbine to the seabed without too much local scour in the vicinity of foundation, monopile foundations are ideally suited for use in regions with movable seabeds, such as sand or silt. They are thus a good option for application in various offshore locales.

1.4. Limitations of the monopile foundation for the offshore applications

There are several limitations of using monopile foundations for offshore wind turbines:

- Limited water depth range: Monopile foundations are best suited for use in water depths up to 30 meters. Monopiles might be too flexible in deeper waters to support the wind turbine adequately. There may be buckling and flexibility issues for long monopiles thus reducing their cost efficiency.
- Deflection and vibration: Since excessive movement might reduce the stability and dependability of the wind turbine, the monopile's total deflection and vibration may be a limiting factor in its utilization.
- Cost: Although monopile foundations are typically thought of as a cost-effective choice for offshore wind farms, they could cost more to install in some places due to the specific equipment and labor needed.
- Environmental impact: The pushing of the piles into the seabed may disturb the sea floor and perhaps harm marine organisms, hence the installation of monopile foundations may affect the local marine environment. To reduce any negative effects, careful design and understanding of the local environment is crucial.
- Limited soil types: Sand or clay soils with moderate to high carrying capability are ideal for using monopile foundations. They might not work well in soil types with poor bearing capability, including soft or loose sediments.

1.5. Working mechanism of a wind turbine

A clean and renewable energy source, wind turbines use the wind's energy to produce electricity. Typically, these enormous turbines are installed in wind farms, which are frequently situated offshore where the wind is stronger and more reliable.

The selection of an appropriate site is the first step in the installation of a wind turbine. Once a location has been chosen, piles are installed by hammering into the seafloor to serve as the turbine's foundation. The turbine assembly is then supported by a tower that is built on top of the piles, which also gives access to maintenance workers.

A typical three-bladed rotor that is attached to a drive system that actuates an electrical generator makes up the turbine itself. The nacelle, which houses the gearbox, generator, and other vital parts of the wind turbine, is where the rotor is installed. Service staff have access to the nacelle, which is placed on top of the tower, for maintenance and repairs.

The rotor blades rotate around a horizontal hub that is attached to a shaft inside the nacelle when the wind blows. The gearbox transfers the rotor's rotational energy to the shaft, increasing rotational speed and driving the generator to produce power. Each blade of a modern wind turbine is around 27 meters (80 feet) long and is built like an airplane wing to capture as much wind as possible to maximize energy production. Wind turbines, despite their size and power, have very little adverse effects on the environment and are an important part of the future of sustainable energy.

2. LITERATURE REVIEW

As a clean and renewable source of electricity, offshore wind energy has recently attracted a lot of attention. Moving wind turbines offshore, where there are stronger winds, more reliable airflow, and more free space, has become the trend in the wind energy sector. Offshore wind energy projects cost 50–100% more per installed rotor area than onshore facilities, which is currently a significant barrier to their widespread development. The extra difficulty of laying foundations and power cables in a sea bed is one of the key factors contributing to the greater cost of offshore wind generation. Up to 35% of the installed cost of an offshore wind project goes into the foundation itself, which is another key cost factor. Therefore, it is essential for the development of offshore wind farms to optimize the foundation design of offshore wind turbines.

This chapter includes a review of the literature on pile lateral loading, pile-soil interaction, offshore wind turbine dynamic behavior and frequency, load simulation, and modeling methodology.

2.1. Laterally loaded piles

The size and shape of the pile are critical considerations when building a pile foundation to withstand lateral loads. Larger-diameter piles or piles with a cross-sectional design that resists bending, like a square or rectangular shape, are typically better at withstanding lateral loads than smaller or more slender piles.

The pile's ability to withstand lateral stresses is also influenced by how stiff it is, or how resistant it is to deformation. In general, piles built of high-stiffness materials, like concrete or steel, are better able to resist lateral loads than piles composed of low-stiffness materials, like wood or plastic.

Another crucial aspect to think about is the soil's stiffness, which will determine where the pile will be placed. The pile will often receive more support from soils with high stiffness, such as clay or dense sand, and be better able to withstand lateral stresses than soils with low stiffness, like loose sand or peat.

Another key factor to take into account is the fixity of the pile's ends, or how securely the pile's ends are fixed to the ground. In comparison to piles with free ends, which are ends that are not secured into the ground, piles with fixed ends, where the ends are anchored firmly into the earth, are better equipped to resist lateral stresses.

In addition to these factors, the pile's placement depth can also have an impact on how well it can withstand lateral loads. Because the soil is often more stable and supportive at greater depths, deeper piles may be more successful at resisting lateral loads than shallower ones.

In general, the capacity of a pile foundation to withstand lateral loads depends on the interaction of all of these variables, as well as the unique design of the pile and the projected loading circumstances. To ensure that a pile foundation is capable of efficiently resisting lateral loads, engineers will carefully take into account each of these aspects while designing it. The variation of deflection, moment, and shear force for a short pile is indicated in the Figure 2-1 below.

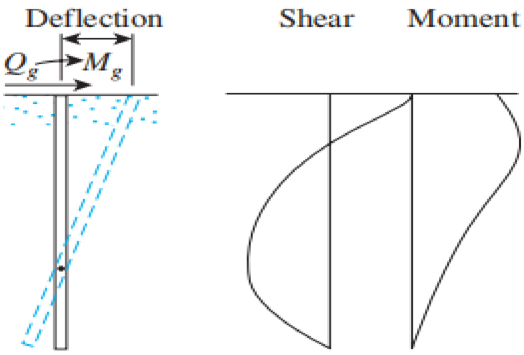

Figure 2-1: Typical shear and moment distribution along the pile length for a short pile.

When subjected to lateral loads, a short pile will rotate as a single unit. When the maximum load is reached, it is believed that the soil in contact with the pile will fail in shear (Haiderali et al., 2013).

2.1.1. Brom's solution

The idea of subgrade reaction is used to determine Brom's solution, sometimes referred to as Brom's method, which determines the lateral deflection of piles at ground level under operating loads. The lateral force the soil applies to the base of the pile in response to a lateral load imposed on the pile's top is known as subgrade reaction. The basic idea of Brom's approach is the presumption that when the applied load is less than one-half to one-third of the pile's ultimate lateral resistance, the pile's deflection grows linearly with the applied load.

For piles embedded in cohesive soils (like clay) and cohesionless soils (like sand), as well as for short or stiff piles and long or elastic piles, Brom's approach offers solutions. The approach accounts for the soil's stiffness as well as the pile's stiffness, as well as the pile's shape, size, and fixity at its ends.

The geotechnical engineer in charge of design must first calculate the projected lateral load on the pile and its ultimate lateral resistance before applying Brom's solution, which can be done using the Broms method or other techniques. The engineer can then compute the anticipated deflection of the pile at ground level at working loads using Brom's approach. The pile foundation can be designed using this information to make sure it is capable of properly resisting lateral loads. The solutions are illustrated using the following graphs presented in Figure 2-2 to Figure 2-7.

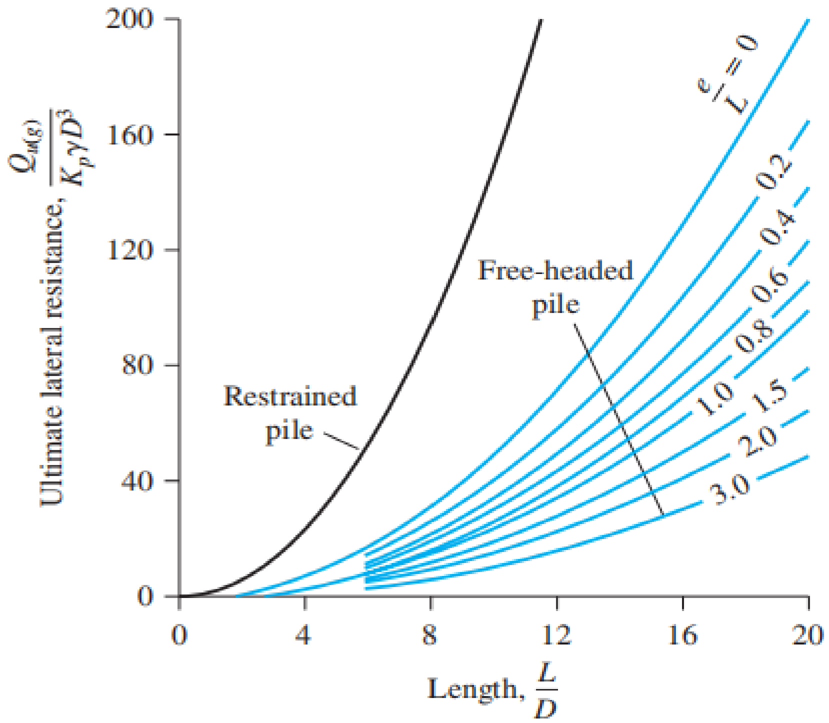

Figure 2-2: Brom’s solution for ultimate lateral resistance of short piles in sand**.**

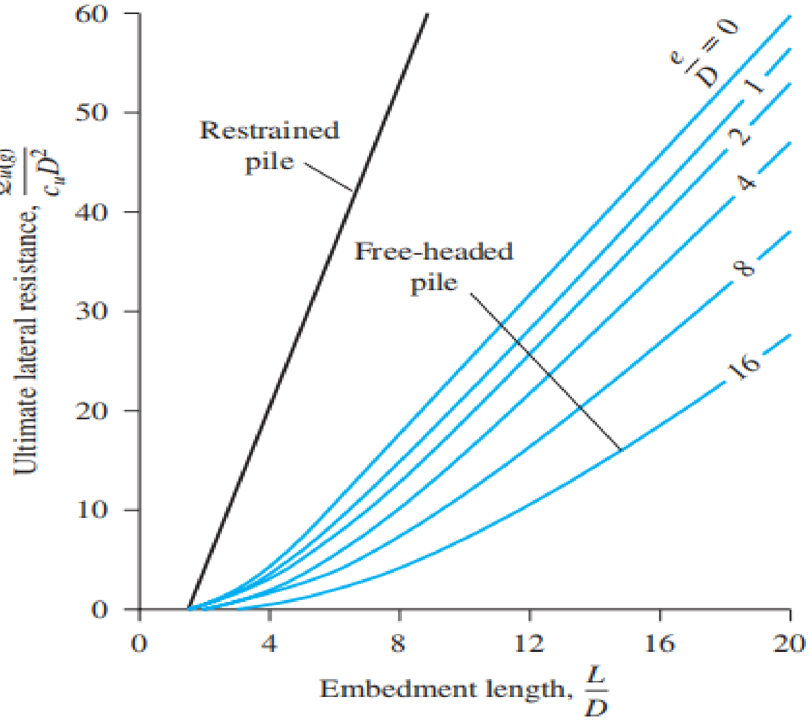

Figure 2-3: Brom's solution for ultimate lateral resistance of short piles in clay.

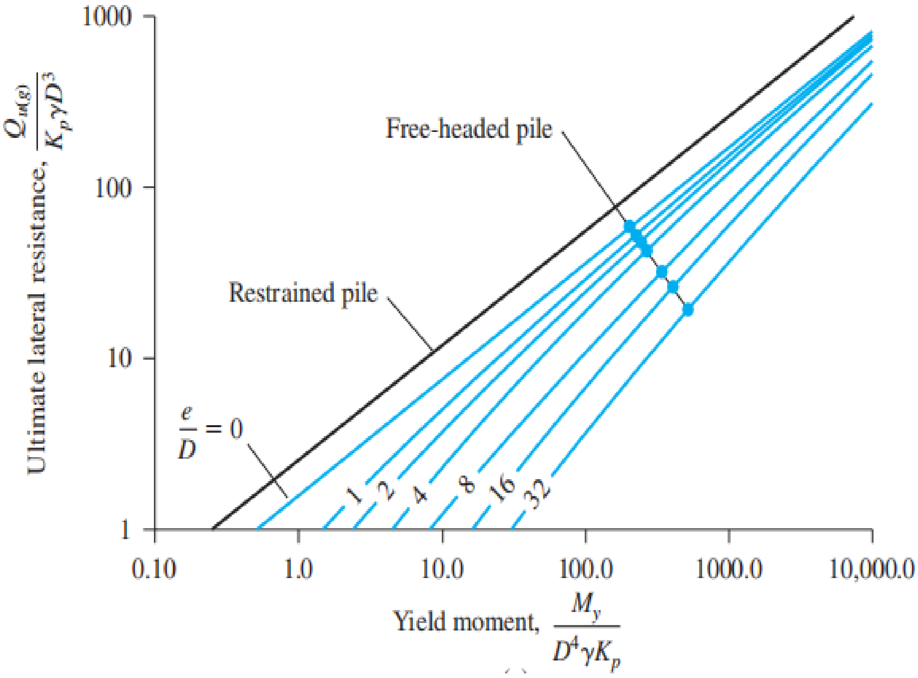

Figure 2-4: Brom's solution for ultimate lateral resistance of long piles in sand.

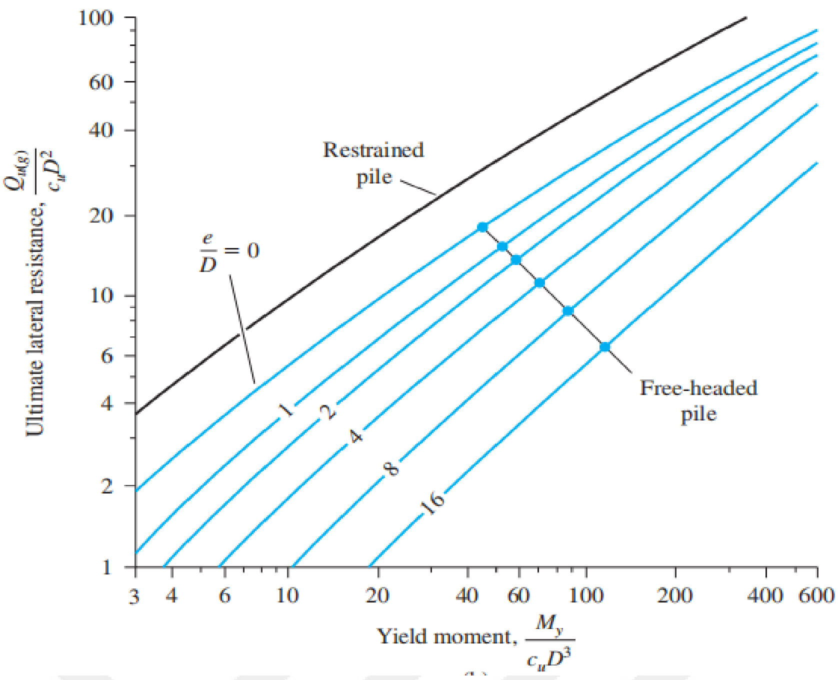

Figure 2-5: Brom's solution for ultimate lateral resistance of long piles in clay.

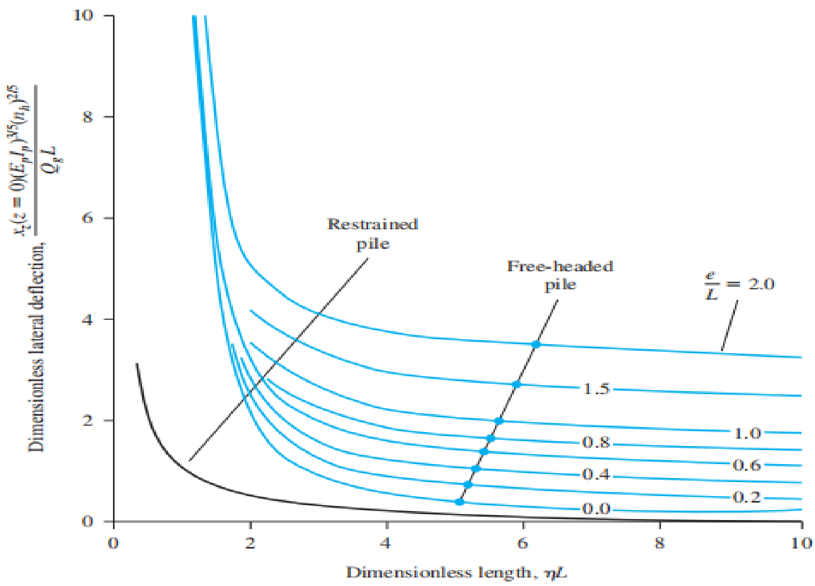

Figure 2-6: Brom's solution for estimating the deflection of pile head in sand.

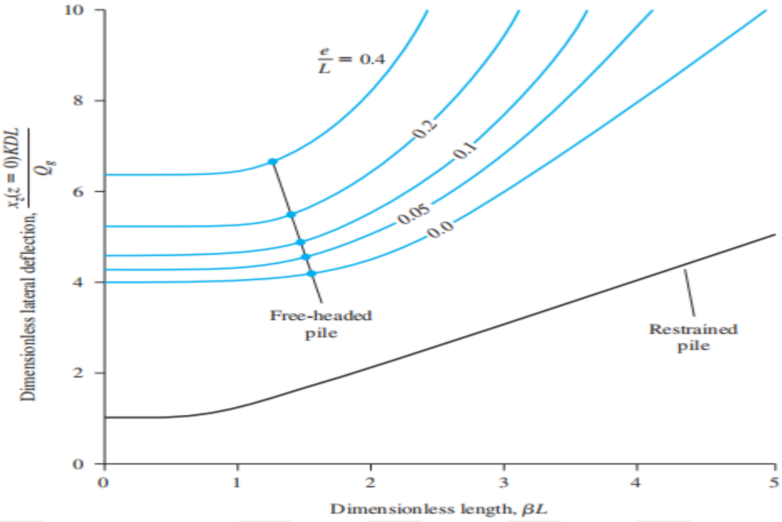

Figure 2-7: Brom's solution for estimating the deflection of pile head in clay**.**

2.1.2. Elastic solution and Winkler model

Matlock and Reese (1960), also known as the Matlock and Reese solution, is a method for estimating the moments and deflections of a vertical pile embedded in cohesionless soils (such as sand or gravel) when subjected to horizontal loads and bending moments at the ground surface. This method is based on the Winkler model, which treats the soil as an elastic medium that can be replaced by a series of nonlinear uncoupled elastic strings.

To use the Matlock and Reese solution, the engineer must first determine the horizontal loads and bending moments that the pile is expected to experience, as well as the properties of the soil in which the pile is embedded, such as the modulus of elasticity and the Poisson's ratio. The engineer can then use the Matlock and Reese solution to calculate the expected moments and deflections of the pile.

This information can be used to design the pile foundation and ensure that it can effectively resist lateral loads. It can also be used to predict the behavior of the pile under different loading conditions, such as changes in the magnitude or direction of the applied loads or the properties of the soil.

In the simpler Winkler's model, the soil, taken to be an elastic medium, can be replaced by a series of nonlinear uncoupled elastic strings. This gives the equation below;

$$k = \frac{p'}{x} \tag{1}$$

where;

k- modulus of subgrade reaction (kN/m^2)

p'- Pressure on the soil (kN/m)

x-pile deflection(m)

The modulus of subgrade reaction for cohesionless soils at a depth z is given as:

$$k_z = n_h * z \tag{2}$$

Where;

n_h - horizontal coefficient of subgrade reaction.

From the theory of beams on an elastic foundation;

$$E_P I_P * \frac{d^4 x}{dz^4} = p' \tag{3}$$

Where;

E_p- modulus of elasticity of the pile material

I_p-moment of inertia of the pile section

Based on Winkler's model,

$$p' = -k * x \tag{4}$$

Combining equations 3 and 4, we obtain;

$$E_P I_P * \frac{d^4 x}{dz^4} + kx = 0 \tag{5}$$

Solutions to equation 5 give the pile deflection and slope of the pile at any depth z as represented by equations 6 and 7 below respectively.

$$x(z) = \frac{A_x Q_g T^3}{E_P I_P} + \frac{B_x M_g T^2}{E_P I_P} \tag{6}$$

$$\theta(z) = \frac{A_\theta Q_g T^2}{E_P I_P} + \frac{B_\theta M_g T}{E_P I_P} \qquad 7$$

For the monopile, the deflection and slope at the mudline (z=0) is the parameter of interest in this study.

2.2. Modeling soil-structure interactions

There are three efficient techniques to take into account of soil-structure interactions for a monopile. The first approach is:

- **Use of nonlinear springs along the length of the pile**

Modeling the soil-structure interaction of a monopile structure, such as a wind turbine foundation or offshore platform, can be a complex task due to the nonlinear behavior of both the soil and the structure. One way to model this interaction is by using nonlinear springs along the length of the pile to represent the soil's reaction to the lateral loads applied to the structure.

In this approach, the soil is represented by a series of nonlinear springs that are attached to the pile at various points along its length. The stiffness of each spring is determined based on the soil properties at that location, such as the modulus of elasticity and Poisson's ratio. The nonlinear behavior of the springs is taken into account by using a nonlinear spring stiffness model, such as a power law model or a bilinear model.

This modeling approach helps to accurately represent the soil's reaction to the lateral loads applied to the monopile structure and to predict the resulting deflections and stresses in the pile. It can be used in conjunction with other modeling approaches, such as finite element analysis or experimental testing, to better understand the soil-structure interaction of the monopile structure.

- **Implementation of a translational and rotational spring at the mudline(seabed)**

Bouzid et al. (2018), defined a range of natural frequencies for the safe design purpose of offshore wind turbine foundations. An analytical expression of an OWT natural frequency as a function of soil-monopile interaction through monopile head springs characterized by lateral stiffness K_L, rotational stiffness K_R and cross-coupling stiffness K_{LR} was presented. After the determination of the monopile head movements (displacements and rotations), the values of K_L, $K_{R,}$ and K_{LR} were calculated and substituted into the analytical expression. From the research, the computed and measured natural frequency values were in fair agreement. The idealization of an offshore wind turbine foundation and the related terminology are presented in Figure 2-8.

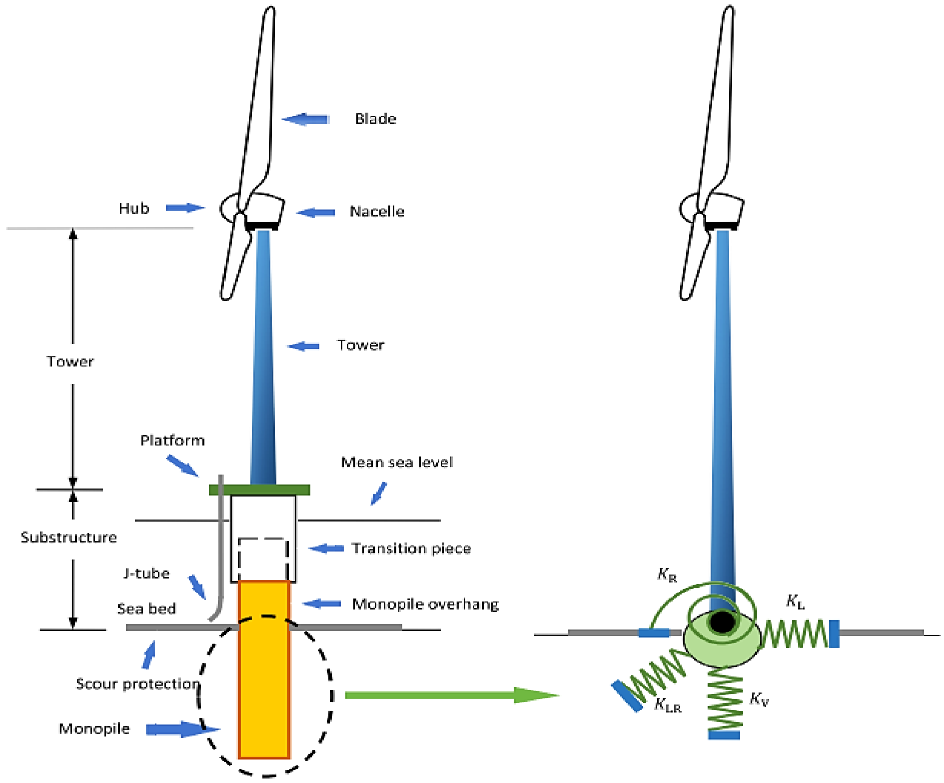

Figure 2-8: Idealization of a monopile foundation (Bouzid et al., 2018).

- **Use of an equivalent cantilever beam**

Another approach to model the soil-structure interaction of a monopile structure is by using an equivalent cantilever beam. In this approach, the soil is represented by an equivalent load applied to the base of the cantilever beam, which represents the pile. The magnitude and distribution of the equivalent load are determined based on the soil properties and the lateral loads applied to the monopile structure.

This modeling approach predicts the deflections and stresses in the pile by solving for the deflections and stresses in the equivalent cantilever beam. It is a relatively simple approach that can be used to quickly estimate the behavior of the monopile structure under different loading conditions. However, it may not be as accurate as more complex modeling approaches, such as those that use nonlinear springs to represent the soil's reaction to the lateral loads applied to the structure.

2.3. Foundations and structures of offshore wind turbines

The following foundation types are used in supporting OWTs:

- **Gravity foundations**

Gravity foundations are foundations that rely on their weight to resist lateral loads and support the structure they are supporting. These foundations are typically used in situations where the soil is relatively shallow and has sufficient bearing capacity to support the weight of the structure. Gravity foundations are typically simple and inexpensive to construct, but they are limited in their ability to resist lateral loads and may not be suitable for use in areas with deep or unstable soils.

- **Monopile foundations**

Monopile foundations consist of a single vertical pile, typically made of steel or concrete that is driven into the ground to support the structure. These foundations are typically used in offshore environments, such as for supporting wind turbines or oil platforms. Monopile foundations are relatively simple and inexpensive to construct, but they may not be as effective at resisting lateral loads as other types of foundations.

- **Monopiles with guy wires**

Monopile foundations with guy wires are similar to monopile foundations, but they also include guy wires that are anchored to the ground to provide additional lateral stability to the structure. These foundations are typically used in offshore environments where the lateral loads on the structure are expected to be relatively high.

- **Tripod foundations**

Tripod foundations are foundations that consist of three vertical piles that are connected at the top to form a tripod shape. These foundations are typically used in offshore environments, such as for supporting wind turbines or oil platforms. Tripod foundations are more effective at resisting lateral loads than monopile foundations, but they are also more complex and expensive to construct.

- **Jacket foundations**

Jacket foundations consist of a network of vertical piles and horizontal beams that are connected to form a frame or "jacket" shape. These foundations are typically used in offshore environments, such as for supporting wind turbines or oil platforms. Jacket foundations are highly effective at resisting lateral loads and are suitable for use in deep or unstable soils, but they are also more complex and expensive to construct than other types of foundations.

- **Tension leg with suction buckets**

Tension leg with suction buckets foundations are foundations that consist of a series of vertical piles that are anchored to the ground using suction buckets. These foundations are typically used in offshore environments, such as for supporting oil platforms. Tension leg with suction buckets foundations are highly effective at resisting lateral loads and are suitable for use in deep or unstable soils, but they are also complex and expensive to construct. All of the foundation types considered for the offshore wind turbines are depicted in Figure 2-9.

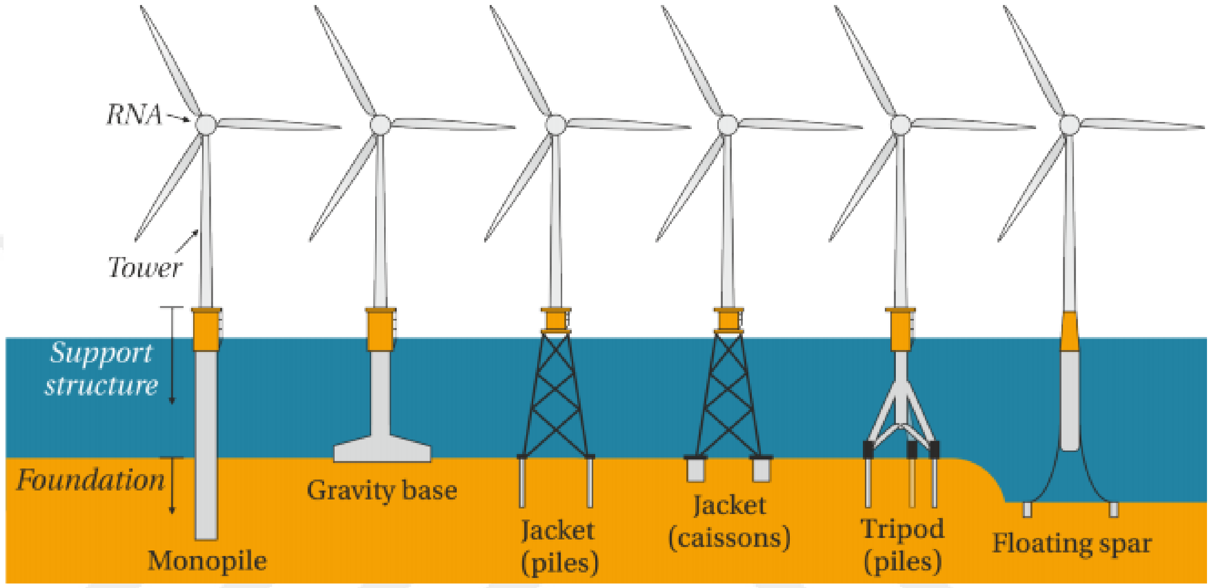

Figure 2-9: Foundation and structures of Offshore Wind Turbine (BW et al., 2017).

Monopile foundations are a common choice for supporting offshore wind turbines (OWTs) due to their simple and robust design, as well as their relatively low cost and ease of construction. They are typically used in relatively shallow water, with most installed windfarms being located in water depths between 30 and 45 meters (Kallehave et al., 2015). However, at greater depths, other foundation types may be preferred over monopile foundations due to their increased ability to resist lateral loads and the greater stability and reliability they offer. These foundation types include jacket foundations, tripod foundations, and tension leg with suction buckets foundations, which are all more complex and expensive to construct than monopile foundations but are suitable for use in deeper water and/or more unstable soils. Monopiles foundations are connected to the superstructure by a sleeve part called as transition piece. A sample transition piece is shown in Figure 2-10.

The choice of foundation type for an OWT project will depend on a number of factors, including the water depth, the soil conditions, and the loading conditions the foundation is expected to experience, and the cost and feasibility of constructing the foundation. Engineers will carefully consider all of these factors when selecting a foundation type to ensure that it is suitable for the specific project requirements.


Transition piece for Borkum Riffgrund Offshore Wind Farm. DONG Energy. (Online version in colour.

Figure 2-10: Sample transition piece for offshore wind farm (Kallehave et al., 2015).

Offshore wind energy has the potential to provide a significant amount of clean, renewable electricity using wind turbines that are supported by monopile foundations. These foundations are used to support large wind turbines in shallow to medium-depth waters, and they can be effective in helping to generate a significant amount of electricity from the wind. Monopile foundations are a popular choice for offshore wind turbines due to their simplicity and cost-effectiveness, making them an important part of the offshore wind energy industry (Arshad and O'Kelly, 2016).

Monopile foundations for offshore wind turbines are typically installed using hydraulic hammers. These foundations have a diameter (D) of 4 to 6 meters and an embedded length-to-diameter ratio (L/D) of approximately 5. The use of hydraulic hammers allows for the efficient installation of these foundations, which are critical for supporting the wind turbines and ensuring the stability of the offshore wind farm.

The deformation behavior of monopile foundations for offshore wind turbines is different from that of small-diameter piles. Monopiles are typically stiff and deform primarily through rigid body rotation about a pivot point, while small diameter piles deform through bending under lateral loads. This difference in deformation behavior is due to the larger size and greater stiffness of monopiles, which allows them to resist deformation through bending and instead rotate about a pivot point under load. The behavior of monopile foundations is important to consider in the design and analysis of offshore wind farms, as it affects the overall stability and performance of the wind turbines (Arshad and O'Kelly, 2016).   A typical p-y curve of a small diameter laterally loaded pile is shown in Figure 2-11.

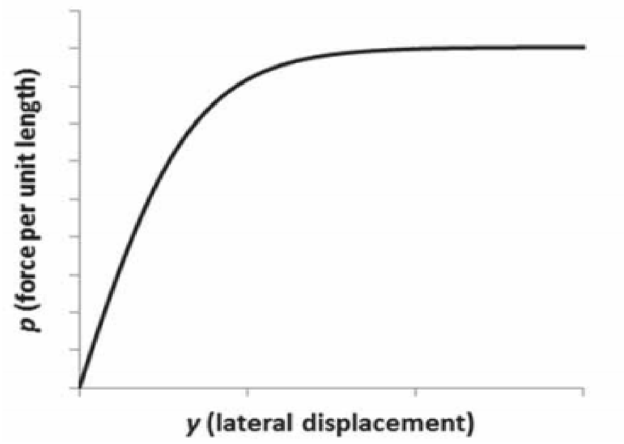

Figure 2-11: Illustration of p-y curve for piles.

2.4. Dynamic interaction and resonance

Offshore wind turbines are subjected to dynamic loads from various sources, including wind, waves, and the rotation of the turbine blades. These loads can vary significantly in magnitude and frequency. Besides they can have significant impacts on the structural integrity and performance of the wind turbines. To ensure the safety and reliability of offshore wind structures, it is important to carefully consider the dynamic loads that the wind turbines will be subjected to and to design the foundations and structures accordingly. This may involve the use of advanced analysis techniques, such as finite element analysis, to predict the response of the wind turbines to various loading conditions. In addition, offshore wind turbines are often designed with built-in redundancies and other safety features to ensure that they can withstand the dynamic loads that they may encounter during operation.

The response of the structure depends closely on the fundamental frequency f_0 (the first tower bending frequency) and the dynamic interaction with the external loads. Wind turbines are subjected to millions of periodic excitation cycles during their operating life. The rotor spinning at a given velocity induces mass imbalances-gyroscopic effects, causing a frequency of 1P. Also, the effect of a standard turbine having n blades induces further excitation due to the blades passing the tower. The frequency of this shadowing effect is equal to nP. The frequency bands for the design of modern offshore wind turbines are illustrated in Figure 2-12(a).

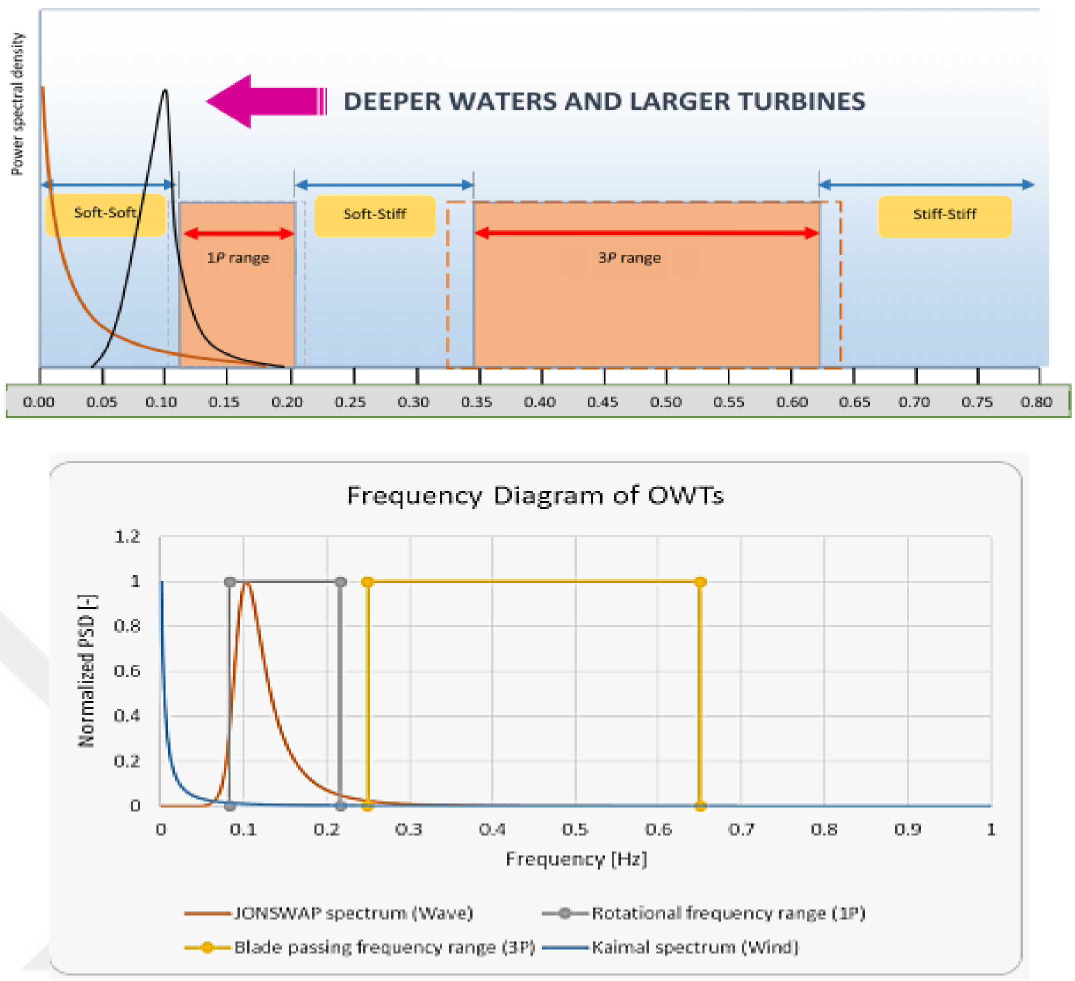

Figure 2-12: Illustration of typical excitation ranges of a modern offshore wind turbine (Arany et al., 2017).

The OWT design can be performed in such a way that the first Eigen frequency lies within 3 ranges: soft-soft, soft-stiff, and stiff-stiff.

- Soft-soft range: the natural frequency is less than the lower bound of 1P. This implies that the structure is too flexible. The frequency of the waves may lie in this range and therefore resonance can occur.
- Stiff-stiff range: this range is where the tower frequency is higher than the upper bound of the blade passing frequency 3P. This range is uneconomically feasible as it leads to a too-rigid structure-heavy and is expensive, making it inappropriate for design.
- Soft-stiff range: the natural frequency lies between 1P and 3P. This is the most optimum range for design.

Therefore, offshore wind turbines supported by monopile foundations are typically designed as soft-stiff structures. This is where, $f_{0,}$ is above the rotational frequency of the rotor, f_{1p}, which arises due to rotor imbalances, but below the blade-passing frequency, f_{3p}, which primarily arises due to aerodynamic impulse loads as the blades pass the tower. The spectral peak frequency of waves is between 0.1 and 0.3 Hz depending on the wind speed and site conditions. For a 6-8 MW offshore wind turbine on a monopile designed for the soft-stiff frequency range, f_0 would be around 0.2 - 0.23Hz. Typical ranges are illustrated in Figure 2-12(b).

2.5. Modeling of offshore wind turbine support structure

Wind loads acting on the turbine and tower along with the wave and current loading on the monopile and transition piece, apply substantial overturning moments to the foundation. Using available design procedures introduced in American Petroleum Institute API (2011) and Det Norske Veritas DNV (2004) codes suffer limitations. In the design and analysis of offshore wind turbine foundations, a common approach is to model the pile support structure as an elastic beam using either Bernoulli-Euler or Timoshenko beam elements. The soil-pile response is typically represented by a set of nonlinear springs, known as p-y springs, which describe the relation between the lateral soil resistance (p) and the lateral displacement (y) of the pile. The use of p-y curves in the design of large-diameter monopile foundations has been questioned due to the complex behavior of these foundations. As a result, numerical analysis using the finite element method is often used to more accurately capture the real behavior of monopile foundations under various loading conditions. This approach can help to ensure the structural integrity and performance of offshore wind farms by providing a more accurate prediction of the behavior of the foundations under various loading conditions.

2.6. Monopile foundation failure mechanism

Monopile foundations for offshore wind turbines can fail in two primary modes: ultimate limit state and serviceability limit state. In the ultimate limit state, failure can occur in two ways:

- When the supporting soil fails, which occurs when the soil's load-carrying capacity is overwhelmed by the applied loads on the foundation.
- When the pile itself fails by forming a plastic hinge, which occurs when the pile material is unable to withstand the loads acting on it and fails at some point along its length, resulting in a maximum stress that exceeds the pile's yield strength.

In the serviceability limit state, failure can occur in two ways:

- When the deformation of the foundation exceeds allowable limits. This can include an initial deflection of more than 0.2 meters, an initial tilt of more than 0.5 degrees, an accumulated deflection of more than 0.2 meters, and an accumulated tilt of more than 0.25 degrees.
- When the structural natural frequency of the wind turbine-tower-substructure-foundation system is too close to the frequency of the rotation of the rotor. To avoid

resonance, the structural natural frequency must be at least 10% different from the rotor frequency.

Proper design and analysis of monopile foundations are critical to ensure that they can withstand the loads that they will be subjected to during operation and avoid failure in both the ultimate limit state and the serviceability limit state. These modes of failure can be seen in Figure 2-13.

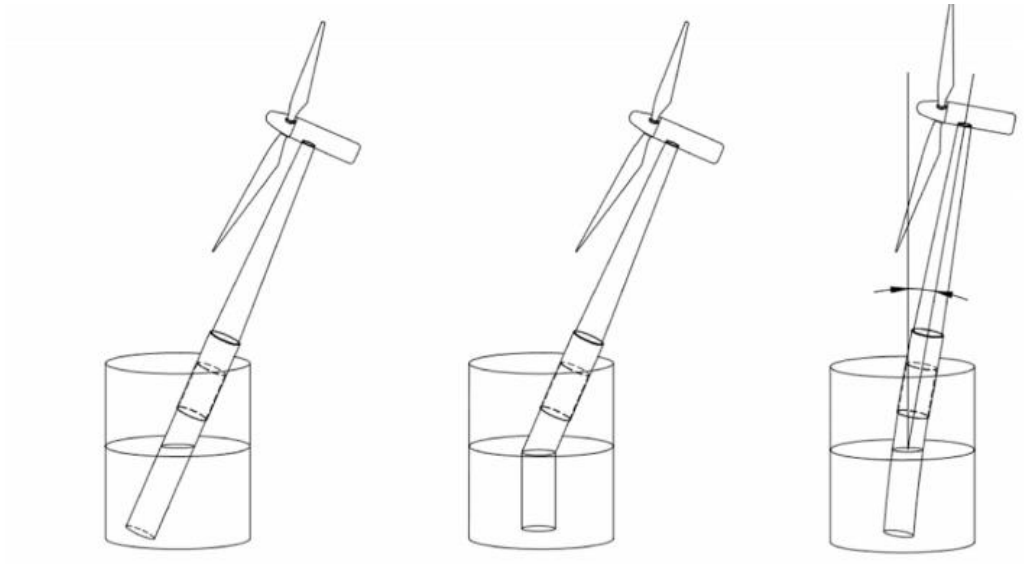

Figure 2-13: Examples of ULS and SLS failure modes (Arany et al., 2017b).

2.7. Finite element analysis

The finite element method (FEM) is a powerful tool for analyzing the structural behavior of complex systems such as offshore wind turbine foundations. In FEM, the structure being analyzed is divided into a collection of small, interconnected finite elements that represent a portion of the physical structure. These elements are joined by shared nodes, and together they form a mesh that can be used to approximate the behavior of the entire structure. The finite element analysis (FEA) process is typically carried out using specialized softwares, which allows users to define the geometry of the structure, apply loads and boundary conditions, and analyze the resulting stress and deformation.

One of the key advantages of FEA is its versatility, as it can be applied to a wide range of field problems including heat transfer, stress analysis, and magnetic fields. Additionally, FEA has no geometric restrictions, meaning that it can be used to analyze structures of any shape. It also allows for the application of arbitrary boundary conditions and loading, as well as the use of materials with varying properties, including anisotropic materials that have different properties in different directions. Furthermore, FEA allows for the use of graded meshes, which can improve the accuracy of the analysis by adding more elements where field gradients are high and more resolution is needed.

However, it is important to note that when using FEA software to model structures, it can be tempting to apply loads as nodal forces and moments, which are easy to apply but may lead to unrealistic results locally. This is because true loads do not typically act at a single point, and applying loads as pressure loads, which are distributed over a larger area, will often give more realistic results.

2.8. Soil characteristics and geotechnical data

Geotechnical ground surveys are a critical component of the design and construction of offshore wind turbine foundations, as they provide important information about the soil and seafloor conditions that the foundations will be built. These surveys typically involve a combination of in situ testing, such as cone penetration testing (CPT) and borehole drilling, as well as laboratory testing of soil samples. The scope and methods of the ground investigations will depend on various factors, including the size and importance of the wind turbine structure, the complexity of the soil, and the seafloor conditions.

The goal of soil investigations is to provide relevant information about the ground to a depth where the presence of weak formations will not affect the safety or performance of the wind turbine, support structure, and foundation. For the design of pile foundations against lateral loads, a combination of in situ testing and soil drilling should be performed to a sufficient depth, while for the design of piles against axial loads, at least one CPT and a nearby borehole should be drilled to the prescribed penetration depth for the pile plus the impact zone. In addition, samples should be taken from the seafloor to assess the potential for burrowing and other issues that could affect the stability of the foundation.

In seismically active areas, it may also be necessary to determine the shear modulus of the ground to great depths in order to ensure the safety and performance of the foundation. Overall, geotechnical ground surveys are a crucial step in the design and construction of offshore wind turbine foundations, as they provide the necessary information to ensure that the foundations are safe, reliable, and capable of withstanding the loads they will be subjected to during operation (DNV, 2011).

2.9. Potential of Offshore Wind energy in Turkey

According to a study by Argın and Yerci (2015), Turkey has significant potential for offshore wind power generation, with certain coastal regions, such as Bozcaada, Amasra, Samandagi, Gokceada, and Inebolu, being particularly suitable due to higher winds. Average wind speed for some offshore sites in Turkey are shown in Table 2-1. The majority of wind power plants in Turkey are located in the

Ege, Marmara, and Akdeniz regions, while 21.75% of the total capacity is located in Balıkesir. Izmir and Manisa also have significant installed capacity, at 18.20% and 12.89%, respectively. Locations of offshore wind farms in Turkey are indicated in Figure 2-14. The findings of this study highlight the potential for offshore wind energy in Turkey and suggest that these coastal regions could be well-suited for the development of wind power projects.

Table 2-1: Average wind speed at offshore sites in Turkey.

Average wind speed (m/s)					
Akçakoca	1,90	Didim	2,90	Ünye	1,48
Zonguldak	2,36	Bodrum	2,60	Çatalzeytin	2,09
İnebolu	4,03	Fethiye	1,32	Akçaabat	1,92
Sinop	2,95	Datça	3,63	Pazar(Rize)	2,09
Samsun	1,83	Marmaris	1,79	Karasu	3,02
Ordu	1,35	Antalya	2,17	Gemlik	3,67
Giresun	1,31	Alanya	1,53	Fatsa	2,49
Trabzon	2,02	Anamur	2,19	Aliağa	3,18
Rize	0,98	Silifke	1,61	Seferihisar	2,16
Hopa	2,67	Mersin	1,76	Kemer	1,68
Tekirdağ	2,63	İskenderun	2,12	Alata-Erdemli	1,51
Çanakkale	3,93	Finike	1,59	Dörtyol	0,95
Yalova	1,52	Kaş	2,58	Kale-Demre	1,55
Ayvalık	2,28	Amasra	4,57	Yumurtalık	2,04
Dikili	2,60	Cide	2,98	Karataş	2,58
İzmir	2,88	Bozkurt	2,24	Samandağ	4,24
Çeşme	2,57	Ereğli	2,05	Gökçeada,	4,12
Kuşadası	2,31	Alaçam	2,20	Bozcaada	5,60

Figure 2-14: Several offshore sites with potential for wind power generation in Turkey (Argın and Yerci, 2015).

2.10. Characteristic of the wind turbine

The analysed wind turbine in this study is the NREL offshore 5-MW baseline wind turbine. This unit is a conventional 3-bladed upwind variable-speed-variable blade, pitch-to-feather controlled turbine. The hub height for the baseline wind turbine is 90m. This gives a 15-m air gap between the blade tips at their lowest point when the wind turbine is undeflected and an estimated extreme 50-year individual wave height of 30m (Jonkman et al., 2009). Table 2-2 to Table 2-5 below gives the characteristics of the 5MW reference turbine.

Table 2-2: Wind turbine main parameters (Jonkman et al., 2009).

Rating	5 MW
Rotor Orientation, Configuration	Upwind, 3 Blades
Control	Variable Speed, Collective Pitch
Drivetrain	High Speed, Multiple-Stage Gearbox
Rotor	126 m
Hub Diameter	3 m
Hub Height	90 m
Cut-In, Rated, Cut-Out Wind Speed	3 m/s, 11.4 m/s, 25 m/s
Cut-In, Rated Rotor Speed	6.9 rpm, 12.1 rpm
Rated Tip Speed	80 m/s
Overhang, Shaft Tilt, Precone	5 m, 5º, 2.5º
Rotor Mass	110,000 kg
Coordinate Location of Overall Center of Mass	(-0.2 m, 0.0 m, 64.0 m)

Table 2-3: Undistributed blade structural properties (Jonkman et al., 2009).

Length (w.r.t. Root Along Preconed Axis)	61.5 m
Mass Scaling Factor	4.536 %
Overall (Integrated) Mass	17,740 kg
Second Mass Moment of Inertia (w.r.t. Root)	11,776,047 kg•m2
First Mass Moment of Inertia (w.r.t. Root)	363,231 kg•m
CM Location (w.r.t. Root along Preconed Axis)	20.475 m
Structural-Damping Ratio (All Modes)	0.477465 %

Table 2-4: Nacelle and hub properties (Jonkman et al., 2009).

Elevation of Yaw Bearing above Ground	87.6 m
Vertical Distance along Yaw Axis from Yaw Bearing to Shaft	1.96256 m
Distance along Shaft from Hub Center to Yaw Axis	5.01910 m
Distance along Shaft from Hub Center to Main Bearing	1.912 m
Hub Mass	56,780 kg
Hub Inertia about Low-Speed Shaft	115,926 kg•m2
Nacelle Mass	240,000 kg
Nacelle Inertia about Yaw Axis	2,607,890 kg•m2
Nacelle CM Location Downwind of Yaw Axis	1.9 m
Nacelle CM Location above Yaw Bearing	1.75 m
Equivalent Nacelle-Yaw-Actuator Linear-Spring Constant	9,028,320,000 N•m/rad
Equivalent Nacelle-Yaw-Actuator Linear-Damping Constant	19,160,000 N•m/(rad/s)
Nominal Nacelle-Yaw Rate	0.3 °/s

Table 2-5: Undistributed tower properties (Jonkman et al., 2009).

Height above Ground	87.6 m
Overall (Integrated) Mass	347,460 kg
CM Location (w.r.t. Ground along Tower Centerline)	38.234 m
Structural-Damping Ratio (All Modes)	1 %
Outer Base Diameter	6m
Thickness at Base	0.027m
Outer Top Diameter	3.87m
Thickness at Top	0.019
Young's Modulus (E)	210GPa
Shear Modulus (G)	80.8GPa
Steel Density (effective)	8500kg/m3

2.11. Simulation of loads

Simulating the loads that will be experienced by an offshore wind turbine and its support structure is a critical step in the design process, as it helps to ensure the safety and reliability of the system. These loads are dependent on a variety of factors, including site conditions such as wind, current, waves, and ice, as well as the mode of operation of the wind turbine. It is important to accurately predict and understand these loads in order to design a support structure that can safely and effectively support the wind turbine under a range of operating conditions.

To simulate the loads on an offshore wind turbine, a variety of tools and techniques can be used, including analytical methods, physical testing, and computer simulations. These approaches allow engineers to analyze the behavior of the wind turbine and support structure under different load conditions and evaluate their performance and structural integrity. By thoroughly understanding the loading conditions that the wind turbine and support structure will be subjected to, engineers can design systems that are safe, reliable, and capable of withstanding the forces they will encounter during operation.

2.11.1. Design Load Cases

Different design situations can be identified covering all expected operational situations as well as fault situations. These design situations are defined as follows in the standards for the design of offshore wind turbines (DNV, 2011; IEC, 2009a; IEC, 2005):

1. Power production
2. Power production plus the occurrence of a fault
3. Start-up
4. Normal shut-down
5. Emergency shutdown
6. Parked (standing still/idling)
7. Parked and fault conditions
8. Transport, assembly, maintenance, and repair

Hundreds of load cases that need to be analyzed to ensure the safe operation of wind turbines throughout their lifetime of 20-30 years are described in IEC codes and the DNV code (IEC, 2005; IEC, 2009a; IEC, 2009b; DNV, 2014).

For each of the defined load cases, load effects are calculated. This usually entails time domain simulation of the wind and wave loads on a dynamic structural model, including the aero-hydro-servo-elastic behavior of the turbine. The load effects are given by the response of the turbine to these loads in terms of displacements, rotations, and sectional forces at the nodes in the structural model.

All design load cases are built as a combination of four wind and four sea states. The wind conditions are; U-1 Normal turbulence scenario, U-2 Extreme turbulence scenario, U-3 Extreme gust at rated wind speed scenario, and U-4 Extreme gust at cut-out scenario. And the wave conditions are; W-1: 1-year Extreme Sea State ESS, W-2: 1-year Extreme Wave Height EWH, W-3: 50-year Extreme Sea State ESS, and W-4: 50-year Extreme Wave Height EWH (Arany et al., 2017).

2.11.2. Limit State Checks

Limit state analyses are an important part of the design process for offshore wind turbine foundations, as they allow engineers to evaluate the structural performance and safety of the system under different load conditions. There are several different limit states that must be considered in the analysis, including the ultimate limit state (ULS), serviceability limit state (SLS), accidental limit state (ALS), and fatigue limit state (FLS).

In the ULS analysis, the focus is on the structural strength of members and joints, as well as the stability of the structure as a whole. This includes checking for failures due to brittle fracture, overturning or capsizing of the structure, and transformation of the structure into a mechanism. The strength of the foundation must also be verified in the ULS analysis.

The SLS is concerned with the maximum acceptable deformations of the structure, foundation, and rotor-nacelle assembly (RNA) during operational conditions. This includes checking for deflections that may alter the effect of acting forces, excessive vibrations that could produce discomfort and motions that exceed the limitations of the equipment. Additionally, the SLS analysis must consider differential settlements of foundation soils that could cause an intolerable tilt of the wind turbine.

In the ALS, the focus is on the effects of unintended impact loads, such as ship impact and impacts due to dropped objects. Finally, the FLS analysis evaluates the ability of the structure to withstand the combined environmental loading over its intended design life. By thoroughly analyzing and understanding these limit states, engineers can design offshore wind turbine foundations that are safe, reliable, and capable of withstanding the loads they will be subjected to during operation.

2.11.3. Wind and wave load

2.11.3. Wind and wave load

Wind and wave loads play a vital role in the response of monopiles. In Figure 2-15, wave and wind loads acting to the typical offshore wind turbine is depicted. Since these forces are dynamic in nature, they may cause dynamic interactions with the structure which may cause resonance. Hence it is vital to take into account of wave and wind loads in a realistic approach.

Wind thrust on the tower

The wind turbine tower is subjected to wind thrust, which is the force that the wind exerts on the tower due to its drag. This wind thrust is a result of the tower being in an air flow, and it is distributed across the surface of the tower in the form of wind pressure. The magnitude of the wind thrust on the tower depends on a variety of factors, including the size and shape of the tower, the wind speed and direction, and the air density. To accurately predict the wind thrust on the tower, it is important to consider the effects of these factors on the wind flow around the tower. This can be done using computational fluid dynamics (CFD) simulations, which allow engineers to analyze the wind flow and predict the distribution of wind pressure on the tower. By understanding the wind thrust on the tower, engineers can design the tower and its support structure to safely and effectively withstand these forces during operation.

The wind pressure at a certain height depends on the air density ρ_a, the cross-section A, the wind speed V, and the drag coefficient C_{aero}:

$$F_{ae} = \frac{1}{2} * C_{ae} * \rho_a * A * V^2 \qquad 8$$

The drag coefficient is mainly related to the roughness of the surface, the shape of the structure, and the wind speed.

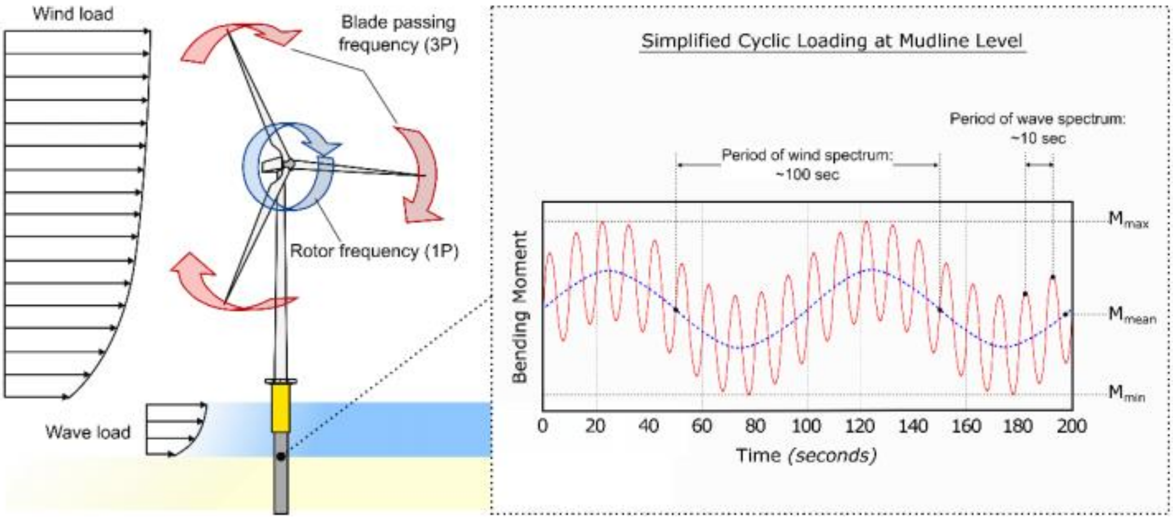

Figure 2-15: Loads acting on a typical offshore wind turbine foundation and typical mudline moment (Arany et al., 2017)

Wind thrust on the rotor

The wind turbine rotor is also subjected to wind thrust, which is the force that the wind exerts on the rotor blades due to their movement through the air. This wind thrust is responsible for turning the rotor, which in turn drives the generator to produce electricity. The magnitude of the wind thrust on the rotor depends on the size and shape of the rotor blades, the wind speed and direction, and the air density.

To accurately predict the wind thrust on the rotor, it is important to consider the effects of these factors on the wind flow around the rotor blades. This can be done using computational fluid dynamics (CFD) simulations, which allow engineers to analyze the wind flow and predict the distribution of wind thrust on the rotor. By understanding the wind thrust on the rotor, engineers can design the rotor and its drivetrain to efficiently and effectively convert wind energy into electricity.
The thrust force on a wind turbine rotor due to the wind is given by the equation below,

$$Th = \frac{1}{2} * \rho_a * A_R * C_T * U^2 \qquad 9$$

Where ρ_a -density of air, A_R -Rotor swept area, C_T -Thrust coefficient, U- Wind speed.

Wake effects

The wake effect refers to the way in which the wind flow is modified by the presence of offshore wind turbines. When a wind turbine is installed in an offshore location, it generates a wake behind it, which can affect the spatial distribution and value of wind speeds in the area. The wake effect can have several consequences, including an increase in turbulence intensity, a reduction in average wind speed in the wake, and an increase in site roughness, which can lead to increased wind shear.

To accurately predict the wake effect, it is important to consider the size and shape of the wind turbines, the wind speed and direction, and the distance between the turbines. This can be done using computational fluid dynamics (CFD) simulations, which allow engineers to analyze the wind flow and predict the distribution and intensity of the wake effect. By understanding the wake effect, engineers can design offshore wind farm layouts that maximize the energy output of the turbines while minimizing the impact on the surrounding wind flow.

Depending on the position of the structure in the wind farm, the value of the wake-induced loads is related to the wake of one single wind turbine or the superposition of several wakes. The wake effect will be more important if wind turbines are close to each other. The mutual influence of the wake effects should be taken into account if the distance between wind turbines is smaller than 10 times the rotor diameter (DNV, 2004). Micro siting of the wind turbines within a windfarm requires that local wake effects from adjacent wind turbines be considered part of the site conditions at each wind turbine structure of the farm (DNV, 2004).

In the study carried out by Arany et al. (2017b), for the ultimate limit state, two load combinations were considered;

- The Extreme Turbulence model (ETM) wind load at rated wind speed combined with the 50-year Extreme Wave Height EWH- the combination of wind scenario U-2 and wave scenario W-4. This provides higher loads in deeper water with higher waves.
- The 50-year Extreme Operating Gust (EOG) wind load combined with the 1-year maximum wave height. This provides higher loads in shallow water in sheltered locations where the wind load dominates.

For a detailed procedure on how to derive the wind and wave loads check the Simplified Design Procedure (SDP) introduced in (Arany et al., 2017).

2.11.4. Wave load

MacCamy and Fuchs (1954) identified three phenomena that exert influence on the total wave loads acting on offshore structures: drag, inertia, and diffraction. Drag is the force that the waves exert on the structure due to the resistance of the water to the movement of the structure. Inertia is the force that the waves exert on the structure due to the acceleration of the water as it moves around the structure. Diffraction is the bending of the wave as it passes around the structure, which can result in additional wave loads on the structure.

The relative importance of these three wave loads depends on the size and shape of the structure. For small and slender structures, drag is the dominant wave load. For larger structures, inertia becomes the dominant wave load, and for very large structures, diffraction becomes the dominant wave load.

MacCamy and Fuchs' theory is based on diffraction and can be used to predict the wave loads acting on large structures, defined as structures with a ratio of body size (D) to wave length (L) greater than 0.2. This theory has been widely used in the design of offshore structures, including wind turbine foundations, to ensure their safety and reliability under a range of wave conditions. By thoroughly understanding and analyzing the wave loads acting on an offshore structure, engineers can design systems that are capable of withstanding the forces they will encounter during operation.

2.12 Previous studies

DNV (2014)**,** provides guidelines concerning monopile foundation design. It mentions the pile penetration depth adjustment to suit the actual environmental and soil conditions. It was observed that monopile foundations are becoming more advantageous and suitable for areas with moveable seabed having scour effect. The monopile structures in deep waters having high flexibility possess a disadvantage. The limiting condition of the monopile foundation is considered as the deflection and vibration of the system.

Abdel-Rahman and Achmus (2005), conducted research on a 7.5 m diameter monopile in dense sand soil conditions. The results obtained indicated that with the API method, the deformations of the monopile are smaller as compared to what was obtained from finite element analyses. It was also indicated that for lateral forces less than 6MN, the results from both methods were in fair agreement.

Kallehave et al. (2015), highlights the reliance of the offshore wind industry on subsidy schemes in order to be competitive with fossil-fuel-based energy sources. It was suggested that a cost reduction for future projects would make the wind industry feasible. According to their findings, project cost can be reduced by focusing on the better design of the monopile structure by taking into consideration of cheaper production techniques and quicker installation procedures.

Byrne et al. (2020), focused on the application of one dimensional (1D) computational model for the analysis and design of laterally loaded monopile foundations for offshore wind applications. In their study, typical soil reaction curves were employed to represent the different aspects of soil reaction acting on the monopile. Stiff glacial clay till soil conditions were considered in the study. Results indicated that the model applies well to homogenous soil deposits only contrary to offshore sites which usually consist of layered profiles, involving interbedded clays and sand. By applying the PISA design model by assigning clay soil reaction curves to the clay layers and employing the 1D computational model for the sand layers, this issue could be practically solved.

Gupta et al. (2020), provided perspectives on the design of offshore wind turbine monopile foundations. In their study, an analysis procedure was described considering the balance between accuracy and computational efficiency. The suggested analysis framework consists of dynamic analysis with linear visco-elastic soil as well as static analysis with nonlinear elastic soil. Timoshenko beam theory is shown to produce the most accurate monopile response although in the same line, Euler-Bernoulli beam theory produces optimal results providing a balance between accuracy and computational efficiency. The same analysis indicated that static analysis is sufficient and optimal in producing monopile-soil stiffness values that may be applied in determining the natural frequency of vibration of the OWTs.

BW et al. (2017), showed that wind loads acting on the turbine and tower in combination to wave and current loading on the monopile and transition piece are causing substantial overturning moment to the monopile foundation. Deeper waters imposed even greater loads on the monopile. The design method developed in this study was based on detailed 3-dimensional finite element analyses. A combination of finite element analysis and the benefits of the existing conventional p-y framework was investigated in the study.

Kuo et al. (2012), investigated the minimum required embedded length of cyclic horizontally loaded monopiles using numerical simulations. A new approach called the stiffness degradation method was applied and it was recommended that the requirement of a critical pile length which leads to the minimum pile deflection under extreme load should be used as a design criterion.

Liu et al. (2017), investigated the loads acting on offshore horizontal axis wind turbines. In the study, Blade Element-Momentum (BEM) theory, including dynamic inflow and dynamic stall effects was used. Morison’s equation was used in the determination of the wave loads. Specifically, the design was carried out on a 5MW reference offshore HAWT and the influence of aerodynamic damping on the fatigue load was investigated.

Nygaard (2016), introduced a numerical approach considering hydrodynamic forces on monopiles with secondary structures. The numerical models used in this study were BEM models and CFD models. In the study, models with and without the secondary structure were analyzed while varying the wave conditions i.e., wave height and wave period. It was concluded that the BEM model might not be a suitable method to determine forces because of drag which is significant in the case of monopiles. Therefore, the CFD model was recommended.

Malik (2016), indicated that the typical highest structural eigen periods of wind turbine structures lie between 3 and 5 seconds and often coincide with the wave frequencies. Results indicated that the estimation of the fatigue life is significantly dependent on accurate hydrodynamic modeling of the wave forces. It was mentioned that the often-used Morison’s equation is no longer accurate because it does not account for diffraction. A 5MW reference wind turbine was selected in their study to compare the standard Morison’s equation and Mac Camy Fuchs diffraction theory. It was found that the 5MW wind turbine structure was more sensitive to aerodynamic loads rather than hydrodynamic loads as would be expected from a monopile structure at shallow water depth.

Haiderali et al. (2013), investigated the lateral and axial load-bearing capacity of monopiles in clays using the finite element modeling code, Abaqus/standard. In the analyses, three-dimensional modeling was adopted since one or two-dimensional finite element analyses inaccurately represent stress and strain fields around a laterally loaded pile. Additionally, three dimensional constitutive models which do not assume the values and directions of any of the principal stresses and strains in the soil can be used to model the behavior of actual soils. In the study, monopiles with diameters of 4m, 5m, 6m, and 7.5m were analyzed. The embedded length “L” was kept constant at 35m for all the analyses. A combination of axial and lateral loads was applied to the monopiles. Results of lateral pile displacement versus depth profiles indicated that monopiles deformed mainly through rotation about a pivot point with the toe of the monopile undergoing negative displacement. Also, the axial loads had no significant influence on either the monopile ultimate lateral capacity or lateral displacement.

Velarde and Bachynski (2017), studied large wind turbine foundations in deep waters. Depths of 20m, 30m, 40m, and 50m and DTU 10MW reference wind turbines were taken into account. The study concluded that with increasing water depths, the contribution of hydrodynamic loading to fatigue damage increased.

3. MATERIALS AND METHODS

In this chapter, the materials and methods used to analyze the behavior of a 7.5m diameter monopile foundation are introduced. The monopile foundation is a type of support structure commonly used to anchor offshore wind turbines to the seabed. These foundations are typically made of steel and are driven into the seabed using specialized equipment. The materials used to construct the monopile foundation as well as the properties of the soil in which it is installed play major roles in monopile behavior. In our study, the behavior of a monopile installed in the seabed consisting of dense sand is investigated.

To investigate the behavior of the monopile foundation, the simplified design procedure developed by Arany et al. (2017), the Winkler approach and finite element analysis using Abaqus software are utilized. The simplified design procedure takes into account of met ocean data, soil properties and structural characteristics to calculate the lateral load capacity of monopile foundations. The Winkler approach is a mathematical model that represents the soil-pile interaction using a series of springs and damper elements. Finite element analysis is a powerful numerical method that allows engineers to analyze the behavior of complex structures under a wide range of load conditions. By using a combination of these methods, a thorough understanding of the behavior of the monopile foundation under various load conditions can be gained while allowing them to design systems that are safe, reliable, and capable of withstanding the forces they will encounter during operation.

3.1. Materials

In the numerical modeling part of the study, monopile body is considered using mechanical properties of high strength steel whereas the seabed material where the monopile is embedded is modeled by using typical parameters of granular material. As it is known, most offshore sites are underlain by sandy soils. In the analyses, tower structure, transition structure and the turbine unit are not modeled since the presence of these elements will increase the complexity of the model while increasing the runtime of the models significantly. Only monopile body is considered by the addition of required moments and forces on top of the monopile.

3.1.1. Dense sand

For the numerical analyses, a site underlain by dense sand is chosen for comparison purposes. The geotechnical parameters considered in this study include the strength and stiffness parameters of the soil. The chosen parameters are indicated in Table 3-1.

Table 3-1: Soil properties considered in the numerical analyses (Abdel-Rahman & Achmus, 2005).

Material properties	**value**	**unit**
dense sand		
unit buoyant weight, γ'	11	KN/m^3
oedometric stiffness parameter, k	600	
oedometric stiffness parameter, λ	0.55	
Poisson’s ratio	0.25	
internal friction angle	35	degree
dilation angle	5	degree
cohesion	0	kN/m^3
depth of soil sample, Z	45	m
reference atmos. Stress	100	KN/m^2
current mean principal stress, σ	495	KN/m^2
stiffness modulus for oedometric compression, E_s	144605.3	kN/m^2

Values of stiffness modulus E_s, unit buoyant weight γ', and horizontal coefficient of subgrade reaction n_h, are used to understand the effect of their increase on the pile deflection and rotation. The values of the parameter are indicated in Table 3-2. These values were estimated using Eqs. 10 and 11.

$$E_S = k * \sigma_{at} * \left(\frac{\sigma}{\sigma_{at}}\right)^{\lambda} \tag{10}$$

Where; $\boldsymbol{\sigma_{at}}$ =100kPa reference stress (Achmus & K., 2005).

$$n_h = A * \frac{\gamma'}{1.35} \tag{11}$$

The modulus of the subgrade reaction is chosen as suggested by Terzaghi (1955). The soil’s modulus of subgrade reaction is approximated as linearly increasing with depth given by Eq 11, where; A = 100-300 for loose sand, and 300-1000 for medium-dense sand (Arany et al., 2017).

Table 3-2: Soil parameters for the FEA, Winkler approach, and SDP comparison.

γ' (kN/m^3)	**E_s(kPa)**	**n_h (kN/m^3)**	**’ (^{0})**
11	144605.3	4888.889	30

In addition to the above parameters, values of internal friction angle **ϕ**’, embedded length L_p, soil Young’s modulus E_s, and pile wall thickness t_p as indicated in Table 3-3 were used in the finite element model to understand their effect on the monopile behavior considering the serviceability limit state.

Table 3-3: Soil and structural properties applied in FEA.

Pile wall thickness, t_p(mm)	**Embedded length,L_p(m)**	**Friction angle,ϕ (^{0})**	**Young's modulus (MPa)**
80	20	20	100
85	25	30	200
90	30	40	300
95			

3.1.2. Steel

The material properties of steel are taken to be in the linear elastic range with values indicated in Table 3-4. To take into account of plasticity, the plastic range was added to the steel material definition in a separate simulation as indicated in Table A(2).

Table 3-4: Material properties of steel.

Mass density, ρ	**Young’s modulus, E**	**Poisson’s ratio, ν**	**Thickness, t_p**
7850 kg/m^3	210 GPa	0.2	90 mm

3.2. ANALYSIS METHODOLOGIES

In this study, the Simplified Design Procedure was implemented alongside the Winkler approach, elastic solution, and Finite Element Analysis (FEA) to investigate the structural behavior and performance of offshore wind turbines. Multiple regression analysis using Statistica software was carried out to generate closed-form formulae that can be used in the preliminary design of large-diameter monopile foundations.

3.2.1. Finite element Modeling

The analyses were carried out using commercial numerical modeling software Abaqus/Standard 2021. Three dimensional model was considered to accurately represent stress and strain fields around a laterally loaded pile. Also, a 3D constitutive model that can take into account of the values and directions of any of the principal stresses and strains in the soil is an important criterion for modeling the behavior realistically. The three-dimensional finite element mesh comprises three parts, the hollow steel pile, the soil plug, and the surrounding soil. This is considered as a non-displacement pile (monopile).

3.2.1.1. Geometry and boundary conditions of the FEA model

The horizontal loading of a monopile implies a plane of symmetry in the problem geometry and it is therefore sufficient to discretize only half of the geometry into a FE mesh as shown in Figure 3-1.

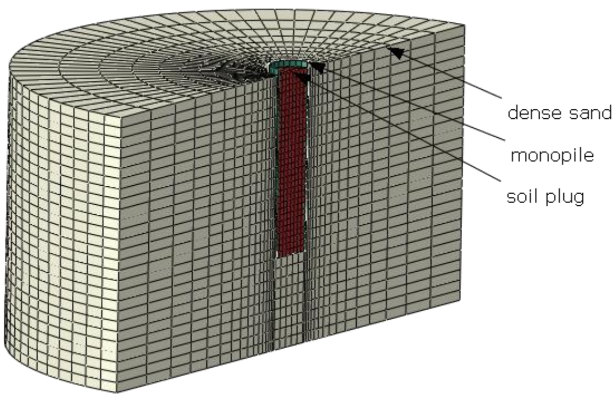

Figure 3-1: Model geometry.

This problem is symmetrical about a plane that contains the axis of the pile and the line of action of the lateral load. The finite element mesh of half of the pile and the surrounding soil was considered. The base of the sand strata is fixed in the x, y and z-directions. There is one plane of symmetry that allows sliding in the x and z directions. It is noted that the mesh is finer in the vicinity of the pile since this is considered as the zone of stress concentration.

In addition, the displacements normal to the vertical cylindrical boundary are also set to zero, together with zero forces in the vertical Z direction and directions tangential to this boundary. To ensure that the X-Z plane at Y = 0 is a plane of symmetry, the displacements normal to this plane (i.e., in the Y-direction) are set to zero, as are the forces in the X and Z-directions. Additionally, the rotational degrees of freedom with respect to X and Z-axes along the edges of pile shell elements in the Y = 0 plane are also set to zero.

According to the simpilified procedure suggested by Arany (2017), the pile wall thickness, t_P was given by the equation,

$$t_p \geq 6.35 + \frac{D}{100} \qquad 12$$

where D is the diameter of the monopile. In Figure 3-2, ahalf portion of the monopile was depicted whereas in Figure 3-3, the soil plug is visualized.

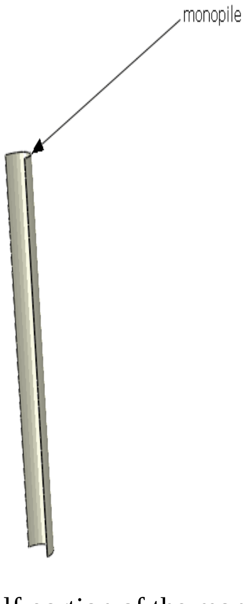

Figure 3-2: A half portion of the monopile.

A monopile of diameter 7.5m was analyzed during this study. The total length of the steel pile was 31m whereas the embedded length was 30m. The pile protrudes 1m above the seabed to prevent the soil from going over the pile which would violate the ultimate limit state and generate unrealistic results.

The pile is assumed to have a soil plug throughout its embedded length. Both linear elastic and elastoplastic behavior were considered separately within the analysis to model the steel for comparison purposes.

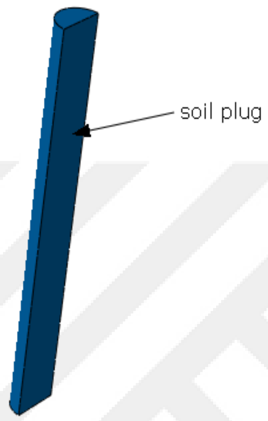

Figure 3-3: Soil plug considered in the analyses.

The overall model dimensions comprised a diameter of 12D from the pile center and a height equal to 1.5L. The model dimensions are chosen such that there are no artificial boundary effects on the pile -soil behavior.

3.2.1.2. Pile-soil interaction

Interface elements that are capable of simulating the frictional interaction between the pile surface and the soil are used. Interaction between the steel pile and the soil is simulated using penalty-type interface elements with a friction factor of 0.4. This type of interface is capable of describing the frictional interaction (Coulomb type) between the pile surface and the soil in contact.

3.2.1.3 Element type

The pile was constructed using 4-noded (tetrahedral) doubly curved linear shell elements with finite membrane strains S4R. The soil and the plug were constructed using an 8-node brick, trilinear displacement, reduced integration, and hourglass control C3D8R. To minimize the occurrence of shear locking, reduced integration elements with one integration point were used.

3.2.1.4. Running the simulation

The vertical and horizontal effective stress profiles of the sand strata are part of the input data that must be supplied to the FE program for this static analysis. The initial horizontal effective stress is assumed to be 50% of the vertical effective stress. A Mohr-Coulomb model was used in this simulation.

The simulation was run in two steps. In step 1, the effective self-weight of the sand layer was applied using the “body force” option. During step 1, the geostatic command was invoked to make sure that equilibrium is satisfied within the soil layer. This step runs for 1seconds.

In step 2, a force-deformation analysis was invoked and the monopile lateral load and overturning moment were applied using the concentrated load option. A time period of 100s was taken in this step. Due to symmetry, only half of the lateral load was applied. The horizontal load applied to the monopile is incrementally applied over time using the ramp option available.

3.2.2. Simplified design procedure (Arany et al., 2017)

This method introduces a simplified way to carry out the preliminary design of monopile foundations based on the least amount of data. Characteristics of site soils, wind and wave parameters, and turbine characteristics are considered as the basic input for this analysis procedure. In this study, a 5MW NREL reference wind turbine was considered. The whole procedure was implemented using Excel software. Example sheets from the excel file is shown in the Appendix A.

3.2.2.1. The design criteria

Based on design codes related to the design of monopiles for offshore applications, the following conditions illustrated in Figure 3-4 must be satisfied during design.

- Foundation load carrying capacity must be higher than the maximum load.
- The pile’s yield strength must be higher than the maximum stress.
- The lifetime of the foundation has to be at least 50 years.
- The initial deflection must be less than 0.2m.
- The initial rotation must be less than 0.5^0.
- The accumulated rotation must be less than 0.25^0.
- The natural frequency of the system must be greater than 0.24Hz.

1.ULS: A.foundation's load carrying capacity has to exceed the maximum load(for horizontal and vertical load and overturning moment) $M_{ULS}<M_f$ B.The pile's yield strength should exceed the maximum stress $F_{ULS}<F_f$. C. Global(Euler type or column) buckling has to be avoided $V_{ULS}<V_f$. D.Local(shell) buckling has to be avoided $\sigma_m<f_{yk}$. 2.FLS: A.The lifetime of the foundation has to be atleast 50 years T_L>50yrs. 3.SLS: A.Initial deflection must be less than 0.2m $\rho_0<0.2$m . B.initial tilt must be less than 0.5^0 $\Theta_0<0.5^0$. C. Accumulated deflection must be less than 0.2m $\rho_{acc}<0.2$m. D. Accumulated tilt must be less than 0.25^0 $\Theta_{acc}<0.25^0$ 4. SLS(Natural frequency): A. The stuctural natural frequency of the wind turbine -tower-substructure-foundation system has to avoid the frequency of rotation of the rotor(1p)by atleast 10% $f_0>1.1*f_{1p,max}=0.24$Hz. 5. Installation: pile wall thickness(initial guess) $t_p>=6.35+D_p/100$ (mm).

Figure 3-4: Design criteria of the monopiles

3.2.2.2. Wind turbine data

For the proper design of a monopile foundation of an offshore wind energy unit, the characteristics of the superstructure should be known. For this study, 5MW capacity NREL wind turbine was considered since the characteristics of the turbine unit and the tower structure are well known. The properties of the turbine unit and tower structure are indicated in Table 2-5 and Table 3-5.

Table 3-5: Turbine characteristics for 5MW NREL wind turbine and tower structure

PARAMETER	SYMBOL	VALUE	UNIT
Hub height	z_{hub}	90	m
rotor diameter	D	126	m
tower height	L_T	87.6	m
tower top diameter	D_t	3.87	m
tower bottom diameter	D_b	6	m
tower wall thickness	T_t	0.027	m
density of the tower material	ρ_t	7860	kg/m^3
tower mass	M_t	250	tons
rated wind speed	U_R	12	m/s
mass of the rotor -nacelle assembly (RNA)	m_{RNA}	243	tons
Operational rotational speed range of the turbine	Ω	(5-13)	rpm

A water depth of 30m was considered for the monopile design. By considering the lateral load acting at 30 m above the mudline (eccentricity), the bending moment acting on the pile head was calculated. The forces and moments considered in the first part of the study were as indicated in

Table 3-6 below. The geotechnical and other material parameters considered in this modeling study are shown in Table 3-7.

Table 3-6: Loading applied on pile head.

Applied load (MN)	Bending moment (MNm)
0	0
2	60
4	120
6	180
8	240
10	300
12	360
14	420
16	480
18	540
20	600

Table 3-7: Material parameters

PARAMETER	SYMBOL	VALUE	UNIT
Soil's submerged unit weight	γ'	11	kN/m^3
Soil's angle of internal friction	Ø'	35	degree
constant	A	600	
soil's coefficient of subgrade reaction(horizontal)	η_h	4888.889	kN/m^3
pile wall material-S355 steel-Young's modulus	E_p	210	GPa
pile wall material-S355-steel-density	ρ_p	7860	kg/m^3
pile material-S355-Yield stress	f_{yk}	355	MPa

3.2.2.3. Pile dimensions

A 7.5 m diameter monopile with a wall thickness of 90 mm was considered. The embedded length was taken equal to 30 m for verification of results with the research previously conducted by (Abdel-Rahman & Achmus, 2005).

3.2.2.4. Estimation of the geotechnical load-carrying capacity of the monopile

According to the design criteria, monopiles should not fail at the ultimate limit state. Hence, a check was made to ensure that the soil does not fail at the ultimate limit state. Using Eqs.13 and 14 introduced in the simplified procedure of Arany et al. (2017), parameters F_R and M_R indicated in Table 3-8 were calculated and compared against the lateral loads and moments applied to the pile head.

$$F_R = \frac{3}{2} * \gamma' * D_P * K_P * f^2 \tag{13}$$

$$M_R = F_R * \left(e + \frac{2}{3} f \right) \tag{14}$$

Table 3-8: Soil load bearing capacity parameters.

PARAMETER	SYMBOL
passive lateral earth pressure coefficient	K_p
eccentricity	e
Horizontal load carrying capacity (assuming soil failure)	F_R
zero shear force point location below mudline	f
Moment capacity of the foundation (assuming soil failure)	M_R

3.2.2.5. Estimation of deformations and foundation stiffness

By evaluating the foundation stiffness K_L, K_{LR}, and K_R in Table 3-9 using Eqs. 15, 16, 17 and 18, the pile head lateral deformation ρ and rotation Θ were determined. The values were checked against the stated design criteria in Figure 3-4.

$$K_L = 1.074 n_h^{\frac{3}{5}} (E_P I_P)^{\frac{3}{5}} \tag{15}$$

$$K_{LR} = -0.99 n_h^{\frac{2}{5}} (E_P I_P)^{\frac{3}{5}} \tag{16}$$

$$K_R = 1.48 n_h^{\frac{1}{5}} (E_P I_P)^{\frac{4}{5}} \tag{17}$$

$$\begin{bmatrix} F_x \\ M_y \end{bmatrix} = \begin{bmatrix} K_L & K_{LR} \\ K_{LR} & K_R \end{bmatrix} \begin{bmatrix} \rho \\ \theta \end{bmatrix} \tag{18}$$

Where; F_x and M_y are the lateral force and overturning moment respectively.

Table 3-9: Foundation stiffness, displacement, and rotation parameters at the pile head

PARAMETER	**SYMBOL**	**UNIT**
lateral stiffness of the foundation	K_L	N/m
Cross-coupling stiffness of the foundation	K_{LR}	N
Rotational stiffness of the foundation	K_R	N/rad
displacement in the x-direction	ρ	m
Rotation at mudline	ϴ	degrees

3.2.2.6. Estimation of the natural frequency

By determining the foundation flexibility coefficients C_R, C_L, C_S, and the fixed base natural frequency of the tower f_{FB}, indicated in Table 3-10 below, the first natural frequency of the turbine-tower-substructure-foundation system f_0 was calculated using Eq 19.

$$f_0 = C_L C_R C_S f_{FB} \qquad (19)$$

Table 3-10: Natural frequency estimation

PARAMETER	SYMBOL	UNIT
Young's modulus of tower material	E_T	GPa
the second moment of the area of the tower	I_T	m^4
fixed base (cantilever beam) natural frequency of the tower	f_{FB}	Hz
the average diameter of the tower	D_T	m
tower thickness	t_T	m
constant	q	
constant	f(q)	
equivalent bending stiffness of the tower	$EI_ŋ$	
non-dimensional foundation stiffness value-L	$ŋ_L$	
non-dimensional foundation stiffness value-LR	$ŋ_{LR}$	
non-dimensional foundation stiffness value-LR	$ŋ_R$	
constant	a	
constant	b	

platform height above mudline	L_S	m
bending stiffness ratio	X	
length ratio	Ψ	
rotational foundation flexibility coefficient	C_R	
lateral foundation flexibility coefficient	C_L	
substructure flexibility coefficient	C_S	
first natural frequency	f_0	Hz

The obtained value of the natural frequency must be greater than 0.24Hz to satisfy the pre-set design criterion.

3.2.3. Elastic solution and Winkler approach

Using the theory of beams on an elastic foundation in combination with the Winkler model as indicated in Eqs. 6 and 7 and coefficients from Table A(1), values of deflection x(z) and slope Θ(z) at the mudline were obtained. Table A(4) indicates the calculation procedure and the required parameters.

Table 3-11: Parameters applied in the Winkler approach**.**

PARAMETER	SYMBOL	UNIT
Modulus of subgrade reaction	k	kN/m^2
Pressure on soil	p'	kN/m
Horizontal coefficient of subgrade reaction	n_h	N/m^3
Depth	z	m
Modulus of elasticity of pile material	E_p	Pa
Moment of inertia of the pile section	I_p	m^4
Length of pile	L	m
Lateral force	Q_g	N
Moment	M_g	Nm
The characteristic length of the soil-pile system	T	
Constant L/T	β	
Non-dimensional depth, z/T	Z	
deflection coefficient	A_x	
deflection coefficient	B_x	
slope coefficient	$A_Θ$	
slope coefficient	$B_Θ$	

Moment coefficient	A_m	
Moment coefficient	B_m	
Shear coefficient	A_v	
Shear coefficient	B_v	
soil reaction coefficient	$A_{p'}$	
soil reaction coefficient	$B_{p'}$	
pile deflection at any depth	x(z)	m
the slope of the pile at any depth	ϴ(z)	degrees
moment of the pile at any depth	M(z)	Nm
shear force on the pile at any depth	V(z)	N
Soil reaction at any depth	p'(z)	kN/m

3.2.4 Multiple regression analysis

Multiple regression analysis is a statistical technique used to examine the relationship between a dependent variable and two or more independent variables. The dependent variable is the variable that is being predicted or explained, while the independent variables are the variables that are used to predict or explain the dependent variable. The multiple regression analysis estimates the coefficients of the independent variables in a linear equation that predicts the value of the dependent variable. The equation takes the form

$$Y = b_0 + b_1 * X_1 + b_2 * X_2 + ... + b_n * X_n \tag{19}$$

Where Y is the dependent variable, b_0 is the intercept, b_1, b_2, … b_n are the coefficients of the independent variables X_1, X_2, … X_n.

The coefficients of the independent variables indicate the strength and direction of the relationship between the independent variables and the dependent variable. A positive coefficient indicates a positive relationship, while a negative coefficient indicates a negative relationship. In addition to estimating the coefficients of the independent variables, multiple regression analysis also provides information about the overall fit of the model. The R-squared value, also known as the coefficient of determination, represents the proportion of the variance in the dependent variable that can be explained by the independent variables. A high R-squared value indicates a good fit for the model, while a low R-squared value indicates that the model does not explain much of the variation in the dependent variable.

In this study, data was collected from 324 simulations performed in Abaqus CAE a finite element analysis software. Parameters that were varied in the determination of the rotation, ϴ, and lateral deflection of the pile, ρ, at the mudline included; pile wall thickness, pile embedded length, soil's Young's modulus, internal angle of friction and the lateral force applied to the pile head. The data saved in an Excel file was imported into Statistica software and multiple regression analysis was conducted.

In this regression analysis, variables were selected. The rotation, Ɵ, and lateral deflection at mudline ,ρ, were taken to be the dependent variables while the pile wall thickness, pile embedded length, soil's Young's modulus, internal angle of friction, and the lateral force applied to the pile head were the 5 independent variables.

4. RESULTS AND ANALYSIS

The results obtained from the three different methods adopted in this study were discussed and presented in this chapter. A comparison in the estimation of displacement and rotation of the monopile as indicated by the applied methods was also discussed. The effect of different soil parameters on the foundation capacity, natural frequency, displacement, and rotation of the monopile was also discussed. Lastly, the regression equations obtained from the multiple regression analysis were presented.

4.1 Comparison of the results obtained with different methods

In this part the results obtained using the Simplified Design Procedure, Winkler approach and the FEA were compared.

4.1.1 Monopile behavior

The 7.5m diameter monopile having an embedded length of 30m showed a semi-flexible – semi-rigid behavior under different loading conditions. From the elastic solution method, L/T was found to be greater than 2 as shown in Table A(4). The deformed shapes of the monopile under lateral load and bending moment are shown in Figure 4-1 below. While increasing the lateral load, the depth/location of the point of zero displacement along the monopile embedded length was found to increase as shown in Table 4-1 and Figure 4-2.

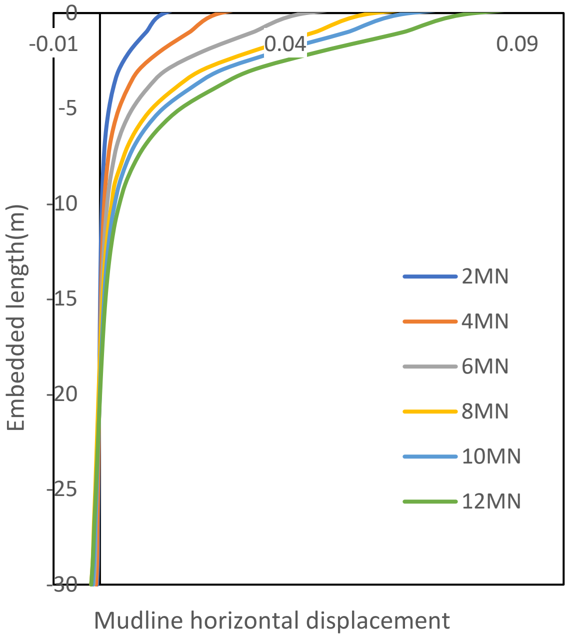

Figure 4-1: Deflected shape of the monopile under different horizontal loads and bending moment

Table 4-1: Location of point of zero displacement along the monopile length.

Applied load (MN)	Point of zero displacement(m)
2	15.88
4	17.50
6	18.40
8	18.96
10	19.90
12	20.20

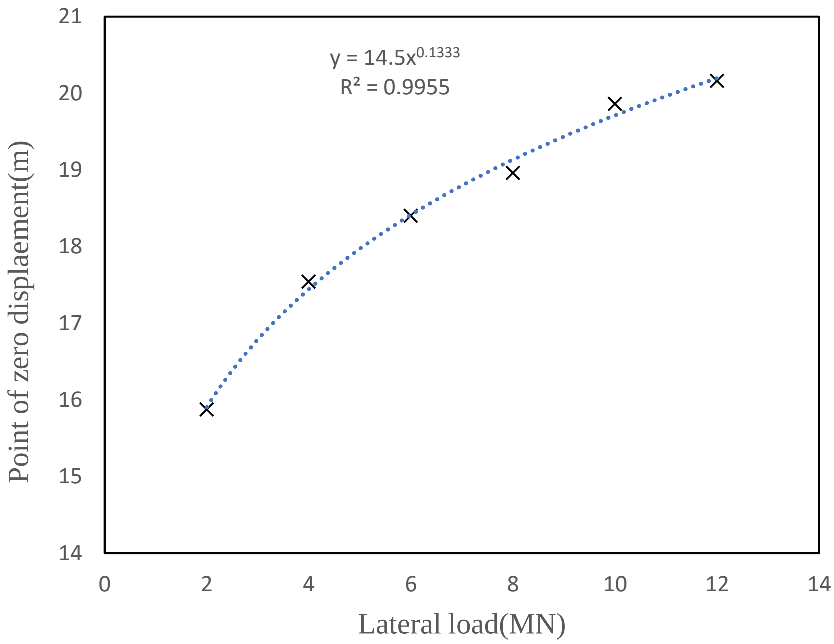

Figure 4-2: Variation of point of zero displacement along the monopile embedded length with increasing horizontal load**.**

4.1.2. Monopile capacity

A comparison of the results of mudline displacement, rotation, and pile yield capacity from FEA, the Simplified Design Procedure, and the Winkler model was conducted at this part. The analytical procedure introduced by Winkler and the simplified design procedure tends to underestimate the values of the mudline rotation and displacement.

4.1.2.1. Mudline displacement

The SDP and the elastic solution methods were found to underestimate the value of the mudline displacement in the monopile when compared to the FEA results. There is a small difference in the results for lateral forces less than 6MN but the difference in the results increases for greater lateral forces as shown in Figure 4-3 below. For example, for a lateral force of 8MN, there is an underestimation of 15.98% in the value of the mudline horizontal displacement. The SDP and the Winkler model gave similar mudline displacement values for all the lateral loads. The Winkler approach and the simplified design procedure overestimate the soil’s bearing resistance leading to an underestimation of the mudline displacement values.

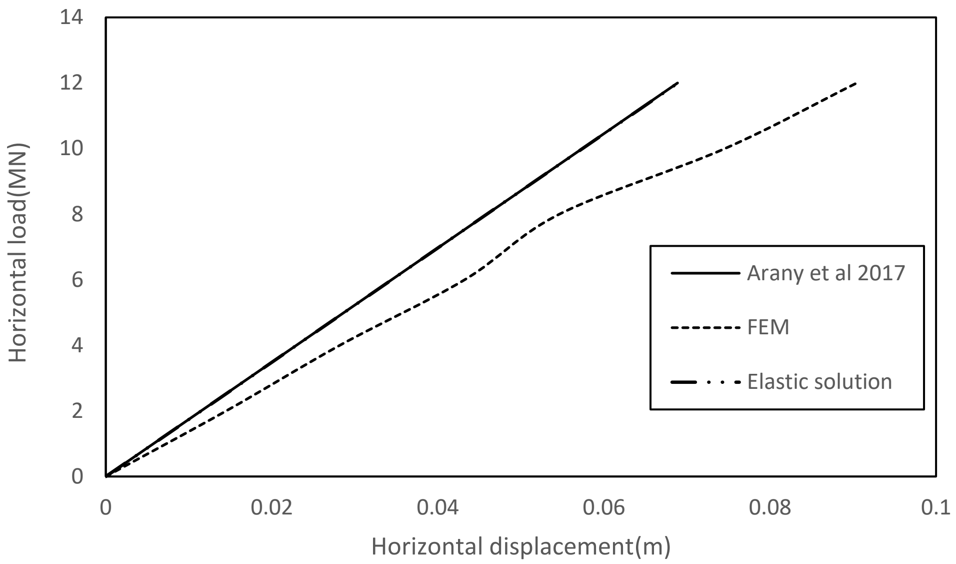

Figure 4-3: Lateral load vs Mudline displacement

4.1.2.2. Mudline rotation

In Figure 4-4, the rotation angles for the monopiles were compared for different methodologies. It was observed that the Winkler approach yielded very small values of the mudline rotation as compared to the finite element analysis and the SDP. The results obtained using the SDP are close to those obtained from the FEA. The Winkler approach and the simplified design procedure overestimate the soil's bearing resistance leading to an underestimation of the mudline rotation values.

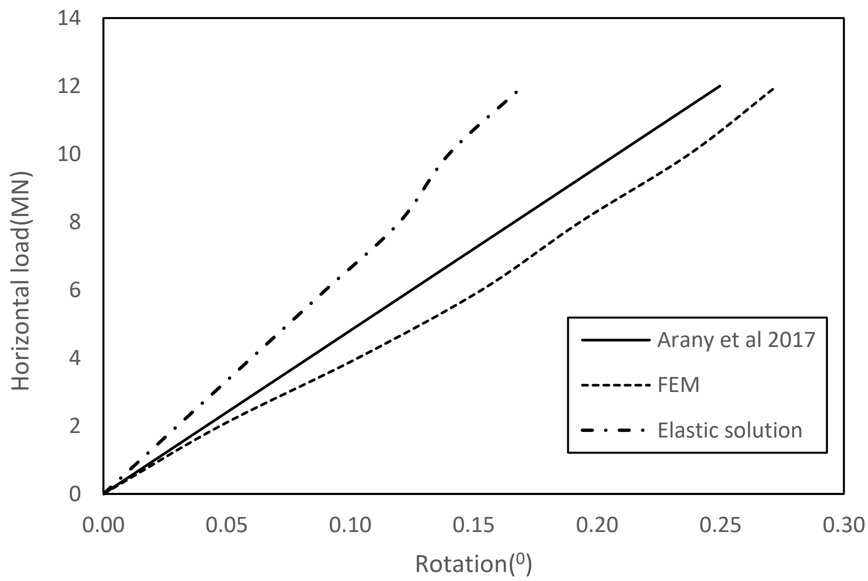

Figure 4-4: Lateral load vs Mudline rotation

4.1.2.3. Pile yield capacity

Considering a lateral load of 8 MN and a bending moment of 240MN, the monopile body was found to yield near the point of load application as shown in Figure 4-5(a). When linear elastic steel behavior is considered, failure is not observed in the monopile body as depicted in Figure 4-5(b).

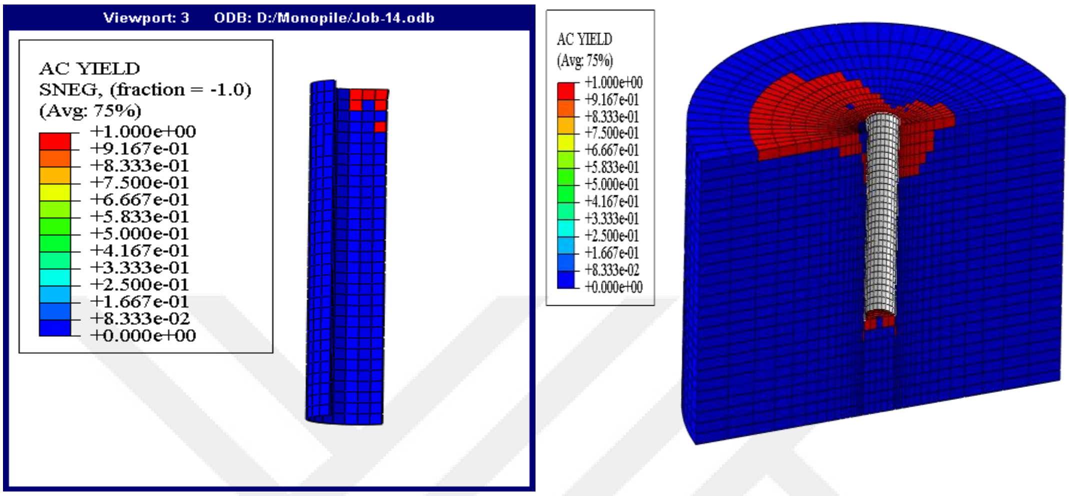

a b

Figure 4-5: Active yielding of the monopile

The results obtained with the SDP indicated no cases of yielding for the same monopile dimensions and applied load combination.

4.1.3. Effect of material definition in Abaqus

In Figure 4-6 and 4-7 below, the first figure on the left represents a monopile with the steel material behavior defined as linear elastic, and on the right, the steel material exhibits elastic and plastic behavior. The steel plasticity values are indicated in Table A (2).

4.1.3.1. Von Mises stress

In Figure 4-6 below, the linear elastic steel material in the monopile experiences maximum Von Mises stress of 376.6MPa at node 32 while the elastoplastic steel material of the monopile experiences a lower maximum value of Von Mises stress of 203.2MPa. This indicated a 46.04% reduction in maximum stress value occurring in the monopile at node 32. The stress values were from a simulation for an applied lateral load of 2MN and 60MN.m overturning moment.

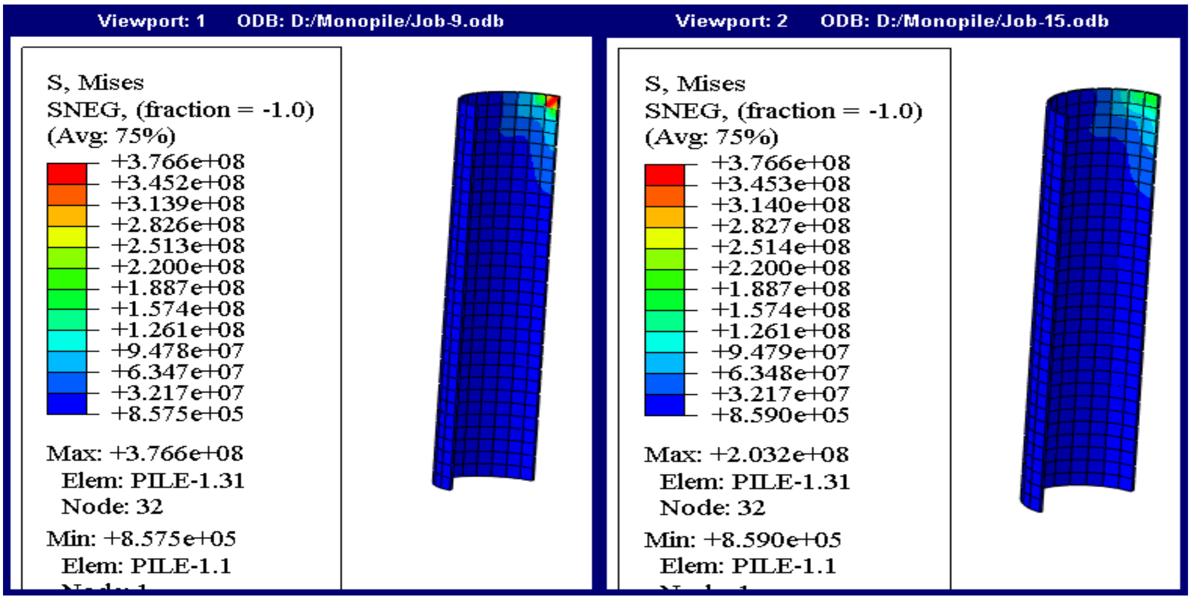

Figure 4-6: Von Mises stress in the monopile

4.1.3.2. Logarithmic strain LE

In Figure 4-7 below, the linear elastic steel material for the monopile reached a maximum logarithmic strain value of 0.14% while the elastoplastic steel material reached 0.21% strain. There was a 32.46% increase in the value of strain in the monopile material when defined as elastoplastic.

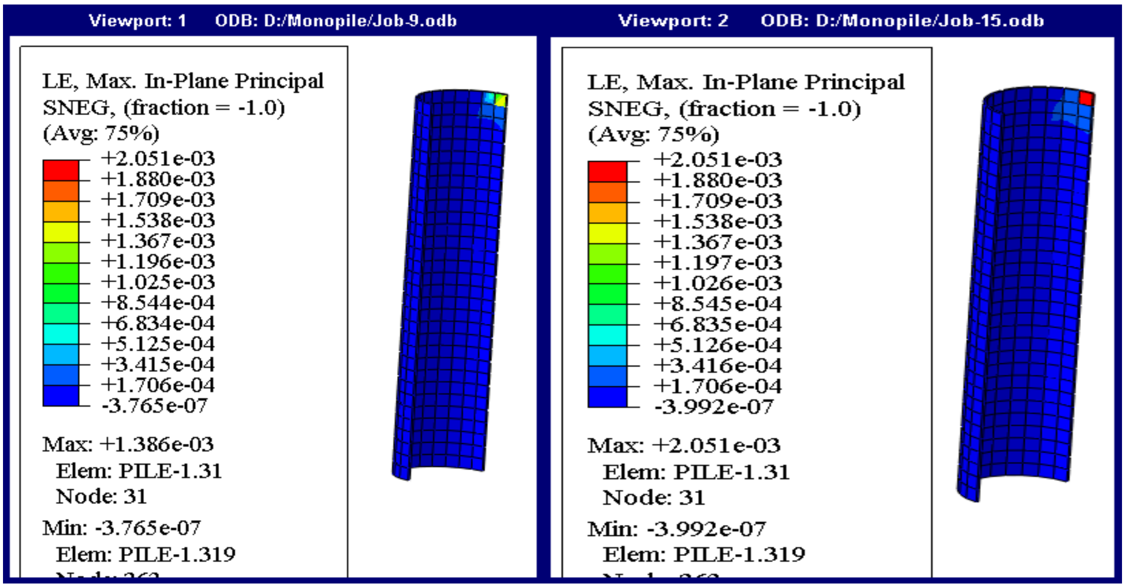

Figure 4-7: Logarithmic strain LE in the monopile

4.1.3.3. Pile deflection

In Figure 4-8, the deformed shape of the monopile when a lateral load of 2MN and overturning moment of 60MN.m was applied is shown. When the steel material was defined as linear elastic the monopile mudline horizontal displacement was 13.94mm while for the elastoplastic definition, the mudline displacement was 14.47mm. A 3.67% increase in mudline horizontal displacement was shown.

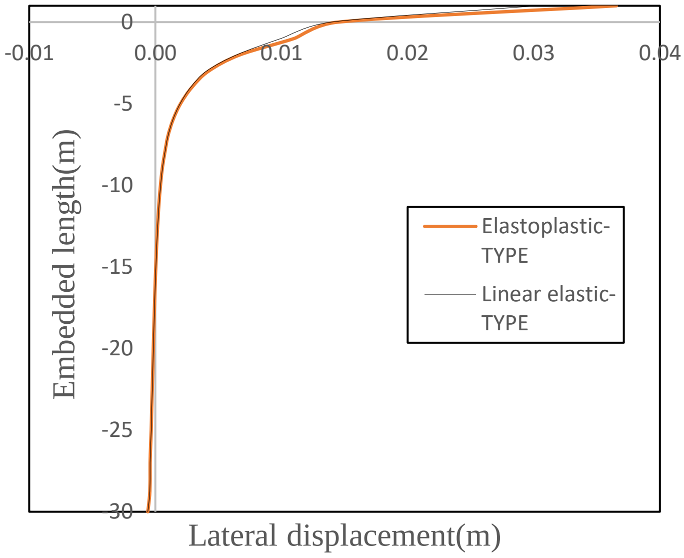

Figure 4-8: Deformed shape of the monopile 2MN

4.1.3.4. Stress vs Strain

Figure 4-9 illustrates the stress-strain behavior of the 7.5m diameter monopile when a lateral load of 2MN and 8MN was applied. The results were compared for the linear elastic and elastoplastic behavior of the steel. In Figure 4-9(a), it was observed that the material experiences a maximum stress of 135.34MPa at a strain of 0.000972 for the elastoplastic case. While the linear elastic definition is adopted for steel behavior, maximum stress reaches a greater value of 255.78MPa at a strain of 0.001386. Figure 4-9(b), it was observed that the material experiences a maximum stress of 190.6MPa at a strain of 0.011903 for the elastoplastic case. While the linear elastic definition is adopted for steel behavior, it was observed that maximum stress reaches a greater value of 921.5MPa at a strain of 0.004836.

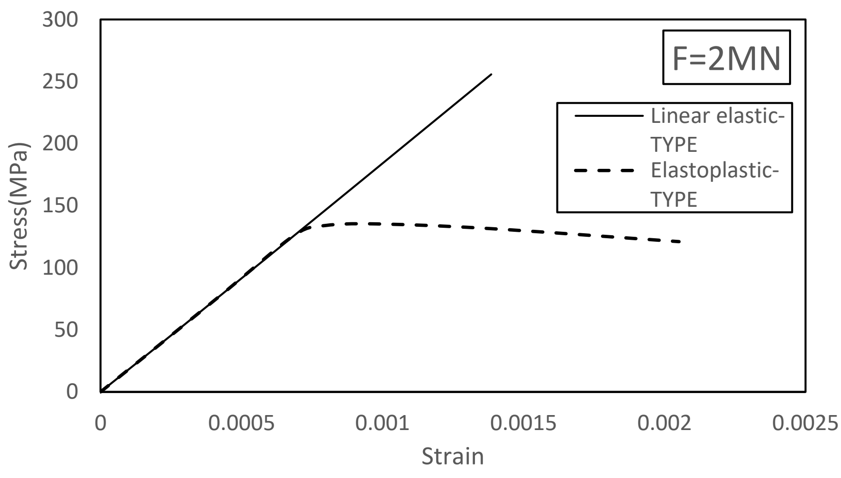

(a)

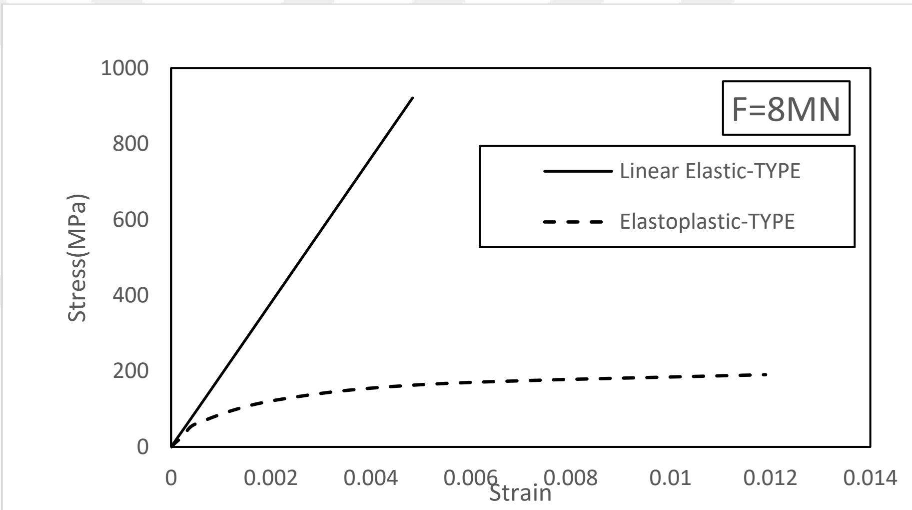

(b)

Figure 4-9: Stress vs Strain behavior in the monopile for 2MN horizontal load

4.1.3.5. Bedding soil pressure

The horizontal bedding stresses acting on the monopile in the plane of symmetry are shown in Figure 4-10. The characteristic loading behavior of the monopile with bedding stresses of opposite signs above and below the point of rotation can be seen. In Figure 4-10(a), the bedding stresses build up in the sand layer covered a short length of the pile shaft and reached a maximum negative value of 78.04kPa when a lateral force of 4MN was applied on the pile head whereas in Figure 4-10(b), a greater build-up of the bedding stresses along a greater length of the pile shaft is seen when a lateral load of 12MN was applied. A minimum bedding stress of 103.2kPa is reached in this case. It is believed that the bedding stresses build up as the soil tries to push back against the monopile when a lateral load is applied.

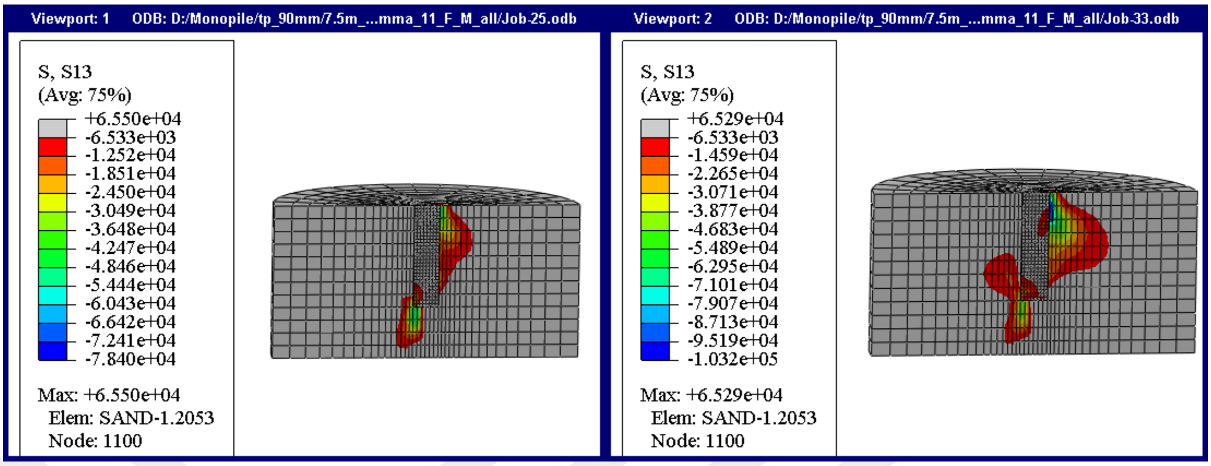

(a) (b)

Figure 4-10: Mobilized bedding pressure for monopile body

4.1.3.6. Geotechnical capacity of the foundation

Considering lateral loads of 4MN and 12MN, active yielding was seen in the dense sand from as shown in Figure 4-11. In Figure 4-11(b), it was observed that yielding covered a larger depth along the pile shaft for a higher applied lateral of 12MN as compared to the 4MN in Figure 4-11(a). Based on the calculations according to the SDP as shown in Table A(6), the value of lateral load capacity F_R (68.496MN) and bending moment capacity M_R (2055.43MNm) were found to be greater than the values of the applied load (8MN) and bending moment (240MNm) by a factor of about 8 while indicating that the foundation soil is stable. Therefore, it can be inferred that the simplified design procedure overestimates the soil's resistance and cannot be relied on during the detailed design of the monopile foundation. At this point, results obtained with the finite element analysis found to be more realistic.

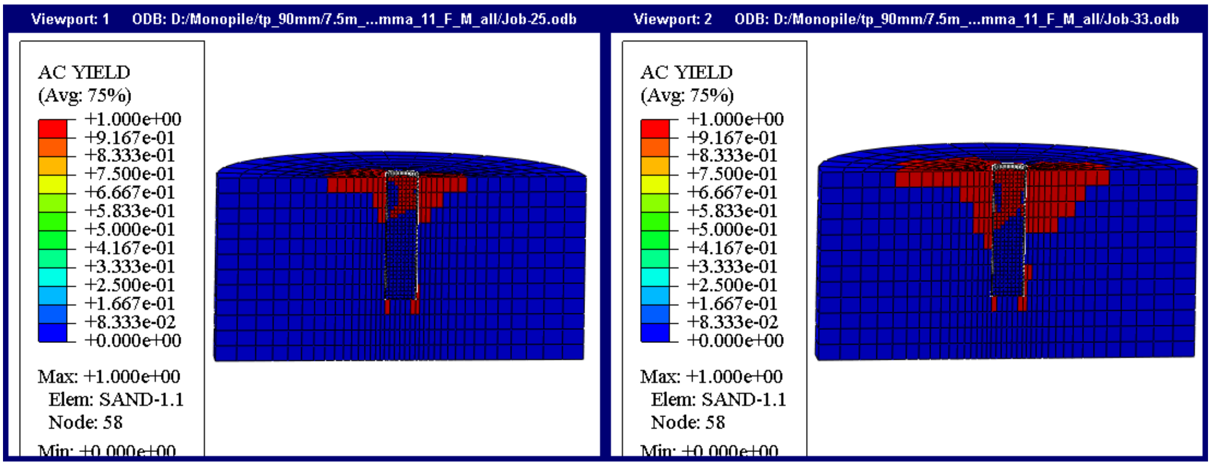

(a) (b)

Figure 4-11: Active Yielding in the dense sand

4.1.3.7. Natural frequency of the foundation

Using the SDP as illustrated in Table A(8), the first natural frequency of the turbine-tower-substructure-foundation system f_0 was found to be equal to 0.27Hz which is greater than 0.24Hz. This indicated no cases of resonance in the system. The design criterion regarding the natural frequency is met.

4.2 Effect of soil and structural properties on the monopile behavior according to FE Analyses

Using the parameters given in Table 3-3, a total number of 324 simulations were conducted with the finite element analysis software Abaqus to understand the effect of pile wall thickness, embedded length, internal friction angle, and Young's modulus on the serviceability limit state behavior of the 7.5 m diameter monopile. The monopile body was considered to behave linear elastic for simplification.

4.2.1. Soil Young's modulus

In this research, soil Young's modulus varied from 100MPa to 300MPa. This range is considered to be representative for very dense to stiff sands. The effect of the increasing value of Young's modulus of the soil on the mudline displacement and rotation was illustrated in the subsequent sections below.

4.2.1.1. Mudline displacement

When a horizontal force of 12MN was applied on the 7.5 m diameter monopile with a wall thickness of 85mm embedded 25 m into sand having internal friction angle of 20 degrees, a 20.53% decrease in mudline displacement value occurred by increasing the soil's Young's modulus from 100MPa to 200MPa. While an 8.4% decrease in mudline displacement occurred when the soil's Young's modulus was increased from 200MPa to 300MPa under the same loading conditions and material properties. In Figure 4-12, the horizontal displacement versus soil Young's Modulus behavior for the simulations performed with different internal friction angles of 20, 30 and 40 degrees were depicted.

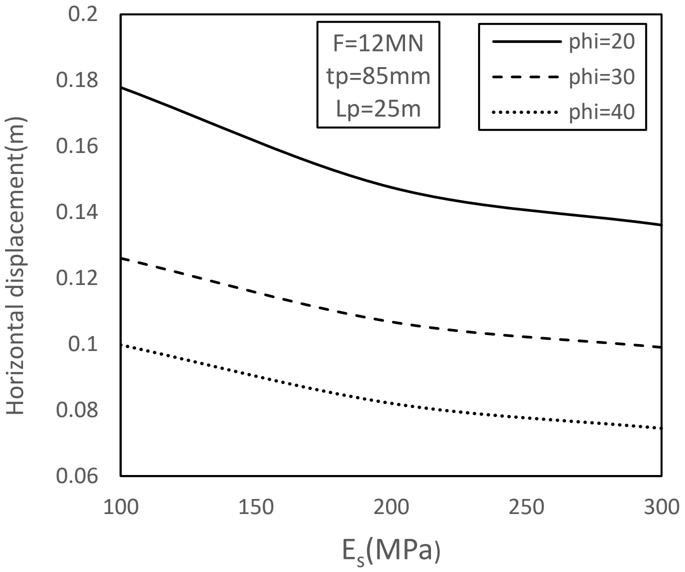

Figure 4-12: Effect of soil Young's modulus on the monopile mudline lateral displacement

4.2.1.2. Mudline rotation

Taking the 12MN lateral load and similar soil and structural properties as with the previous part, the effect of increasing the soil's Young's modulus on the mudline rotation for different internal friction angles was shown in Figure 4-13 below. Taking internal friction angle of 20 degrees, when the soil's Young's modulus is increased from 100MPa to 200MPa, a 6.74% decrease in the mudline rotation is seen while from 200MPa to 300MPa, a 2.5% decrease occurred in the value of mudline rotation.

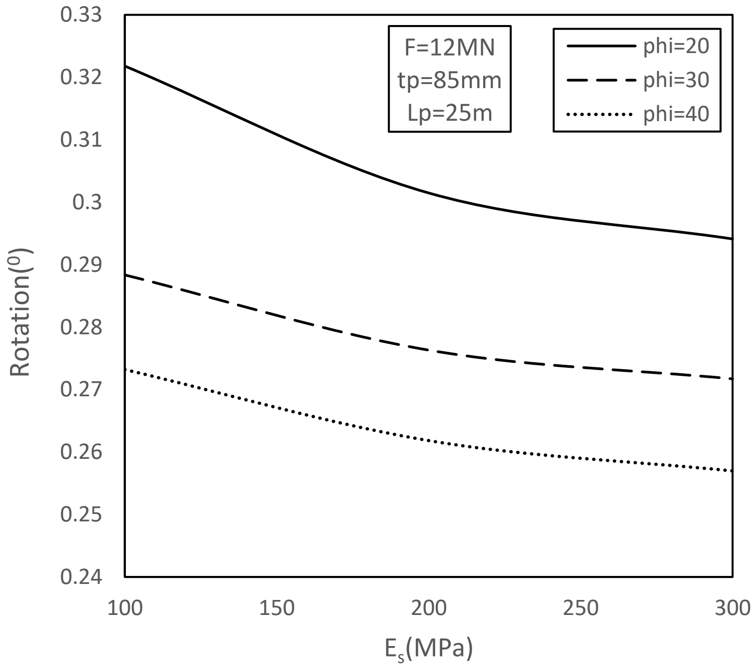

Figure 4-13: Effect of soil Young's modulus on the monopile mudline rotation

4.2.2. Effect of internal angle of friction

The angle of internal friction for a bedding soil is the slope angle of the failure line on the Mohr's Circles plot of the shear stress and normal effective stresses at which shear failure occurs. The angle of Internal Friction, ϕ, can be determined in the laboratory by the direct shear tests or triaxial tests. In this study, the friction angle was varied from 20^0 to 40^0 and the effect of the increase on the mudline displacement and rotation was illustrated below.

4.2.2.1. Mudline displacement

In Figure 4-14 below, effect of soil internal friction angle on the mudline displacement for an applied horizontal load of 12MN for a 7.5 m diameter monopile with a thickness of 80mm were investigated. The dept of embedment for the monopile was taken as 20m. Considering Young's modulus value of 100MPa, a 65% decrease in the value of horizontal displacement occurred as the internal friction angle increased from 20^0 to 30^0. While a 35.87% decrease in horizontal displacement occurred when the friction angle was increased from 30^0 to 40^0. There is a more pronounced reduction in the monopile mudline displacement as the friction angle increases for soils with lower values of the soil

Young's modulus as compared to soils with higher values of Young's modulus. There is a well emphasized value of the angle of friction at around 34^0 where the reduction trend nearly flattens off.

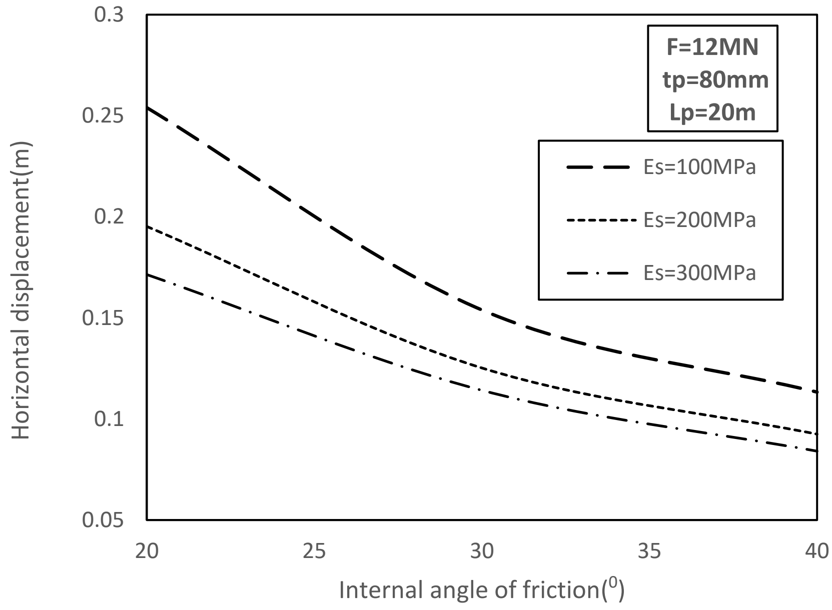

Figure 4-14: Effect of internal friction angle on the mudline displacement

4.2.2.2 Mudline rotation

As in the section on mudline displacement above, considering similar loading and soil parameters; increasing the internal friction angle from 20^0 to 30^0, a 25.9% decrease in the monopile rotation occurred while changing internal angle of friction from 30^0 to 40^0, only a 10.21% decrease in monopile rotation occurred as clearly illustrated in Figure 4-15. There is a more pronounced reduction in the monopile rotation as the friction angle increases for soils with lower values of the soil Young's modulus as compared to soils with higher values of Young's modulus. There is a well observed value of the angle of friction at around 34^0 where the reduction trend nearly becomes flat.

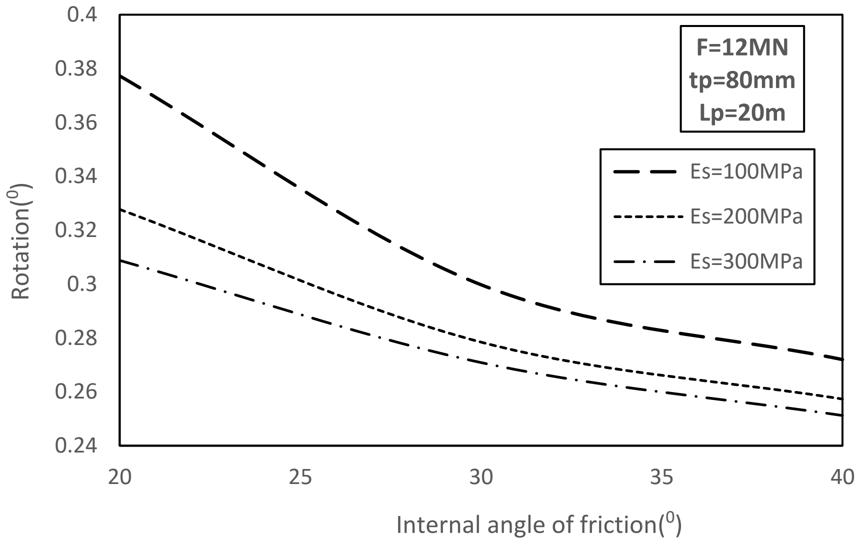

Figure 4-15: Effect of internal friction angle on the rotation angles of the monopile

4.2.3 Pile wall thickness

In real-site conditions, the monopile wall thickness can vary along the length of the monopile but in this study, it was assumed to be uniform throughout the pile length. To check for the effect of pile wall thickness on the lateral displacement and rotation, the thickness value was varied from 80mm to 95mm. The figures in the subsequent section illustrate the effect.

4.2.3.1 Mudline displacement

Taking an embedded length of 20m, E_s of 200MPa, and ϕ of 30^0, when the pile wall thickness was increased from 80mm to 85mm, an 8.68% decrease in the mudline lateral displacement occurs, from 85mm to 90mm, 8.05% decrease occurs and lastly from 90 mm to 95mm, a 7.74% decrease occurs as illustrated in Figure 4-16 below.

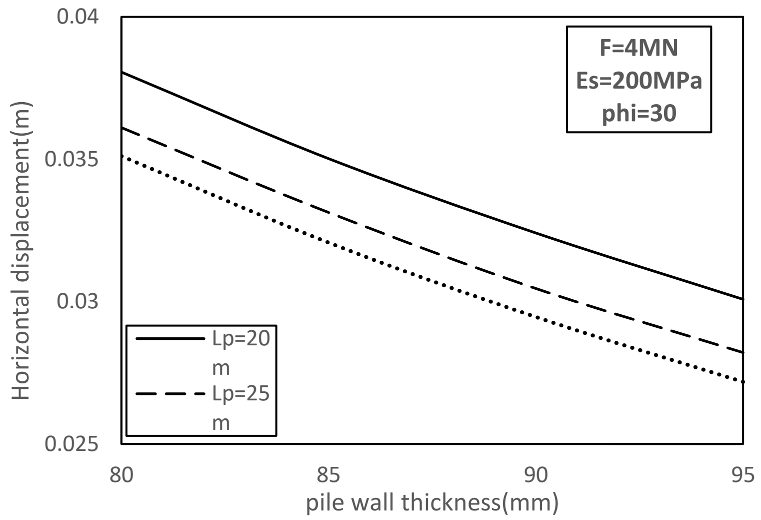

Figure 4-16: Effect of pile wall thickness on the lateral displacement of the monopile

4.2.3.2 Mudline rotation

When the wall thickness is increased from 80mm to 85mm, a 1.54% decrease in mudline rotation occurs, while from 90mm to 95mm, a 3.83% decrease in the rotation occurs as illustrated in Figure 4-17.

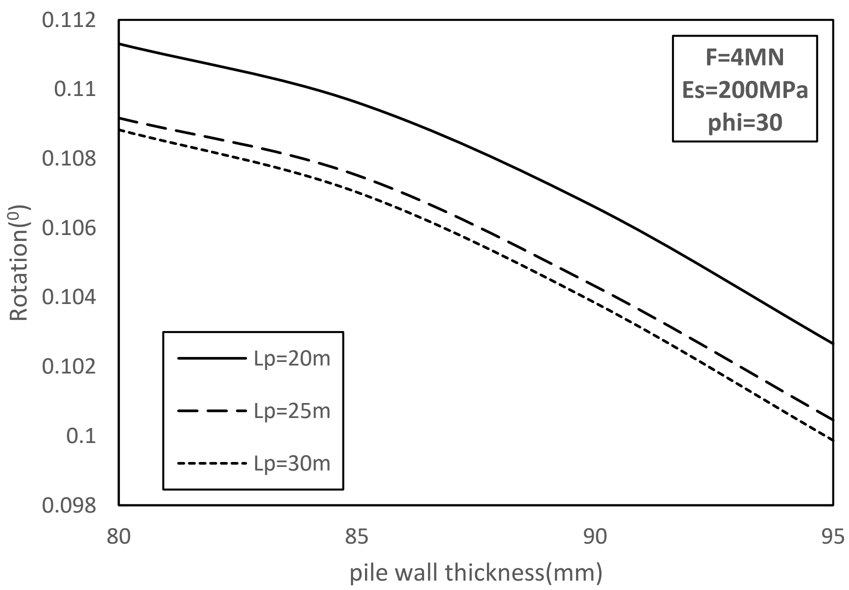

Figure 4-17: Effect of pile wall thickness on the rotation

4.2.4 Embedded length

For this study, the embedded length was varied between 20m and 30m. The effect of embedded length on lateral displacement and rotation was discussed in the following parts.

4.2.4.1 Mudline displacement

For an 8MN lateral load, 100MPa soil Young's modulus, ϕ angle of 30^0 and pile wall thickness of 80mm, when the embedded length was varied from 20m to 25m, an 11% decrease in the monopile lateral displacement occurred while from 25m to 30m, 3.88% decrease in displacement occurred.

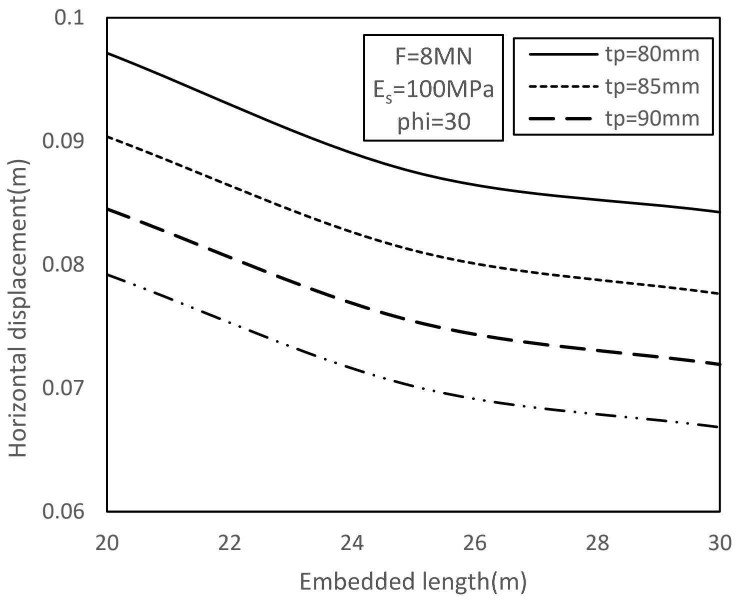

Figure 4-18: Horizontal displacement vs embedded length

4.2.4.2 Mudline rotation

For an 8MN lateral load,100MPa soil Young's modulus, ϕ angle of 30^0 and pile wall thickness of 80mm, when the embedded length was varied from 20 to 25 m, an 5.35% decrease in the monopile rotation occurred while from 25m to 30m, 1.5% decrease in rotation occurred.

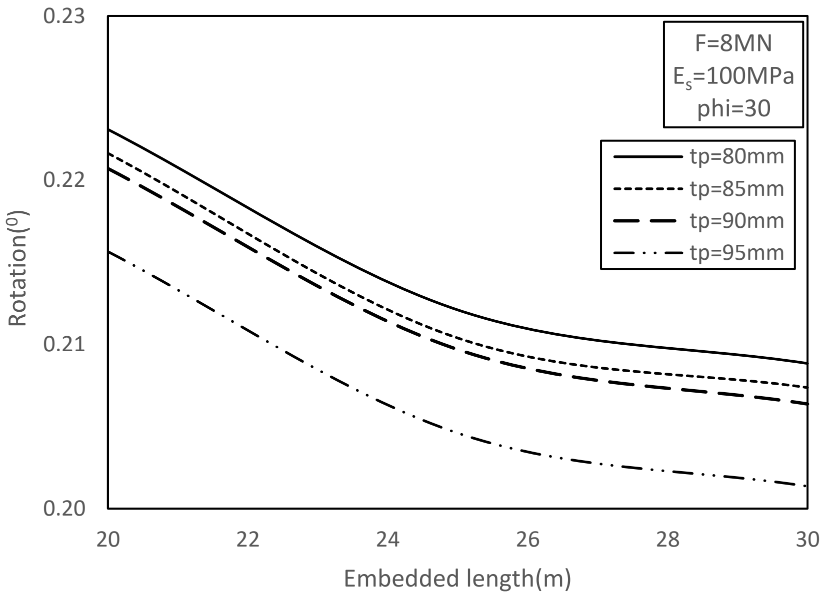

Figure 4-19: Rotation vs embedded length

4.2.5 Multiple regression analysis

From the multiple regression analyses performed using Statistica software, the coefficients of determination obtained for the two dependent variables; rotation at mudline, Ө, in degrees and lateral deflection, ρ, at mudline in meters were 0.97 and 0.89 respectively. The high values of R^2 for both cases indicated that the models fit the data well and also indicated that almost all of the variability with the variables specified in the model was accounted for.

Using the coefficients for each of the independent variables, regression Eqs. 20 and 21 were formulated as given below.

$$\theta = 0.137107 + 0.022114 * F - 0.000134 * t_p - 0.001437 * L_P - 0.000087 * E_S - 0.00162 * \phi \quad (20)$$

$$\rho = 0.213993 + 0.010246 * F - 0.0011 * t_P - 0.001404 * L_P - 0.000111 * E_S - 0.002243 * \phi \quad 21$$

Where; **ϕ** - Internal angle of friction in degrees, $\mathbf{E_s}$ -Elastic modulus of the soil in MPa, $\mathbf{L_P}$ - Pile embedded length in meters, $\mathbf{t_P}$ - Pile wall thickness in mm, and **F** - Total lateral force applied to the pile head in MN.

When dimensionless parameters were incorporated, the coefficients of determination R^2 obtained were 0.5 and 0.7 for the rotation at mudline Θ in degrees and lateral deflection at mudline ρ in meters respectively. Using the coefficients for the two independent variables in this case, regression Eqs. 22 and 23 were formulated as follows.

$$\theta = 0.173847 + 3.260309 * C - 0.00162 * \phi \quad 22$$

$$\rho = 0.097601 + 1.939268 * C - 0.002243 * \phi \quad 23$$

Where;

$$C = \frac{F}{L_P * t_P * E_S}$$

and ϕ - Internal angle of friction in degrees, E_s -Elastic modulus of the soil in MPa, L_P - Pile embedded length in meters, t_P - Pile wall thickness in meters, and F - Total lateral force applied to the pile head in MN. C is a dimensionless parameter.

Eqs. 20, 21, 22, and 23 can be used to understand the behavior of the 7.5 m diameter monopile in dense sand soil conditions and can also serve as a initial attempt for the preliminary design of a monopile having similar characteristics.

4.2.6 Pile failure mechanism

For the uniform soil exhibiting constant stiffness parameters with depth, Poulos and Hull (1989), suggested that a pile behaves rigidly if the length is less than 1.48R and behaves flexibly if the length exceeds 4.44R. While a non-homogenous soil where the stiffness increases linearly with depth from zero at the surface, a pile behaves rigidly if the length is less than 1.1R and behaves flexibly if the length exceeds 3.3R. In this study, the 7.5 m diameter monopile was analyzed at different values of embedded length i.e., 20m, 25m, and 30m. Using the criteria, the monopile was found to exhibit a semi-rigid semi-flexible behavior as shown in Figure 4-20 below.

$$R = \sqrt[4]{(E_P * I_P)/E_S} \qquad (12)$$

Where R is the rigidity parameter.

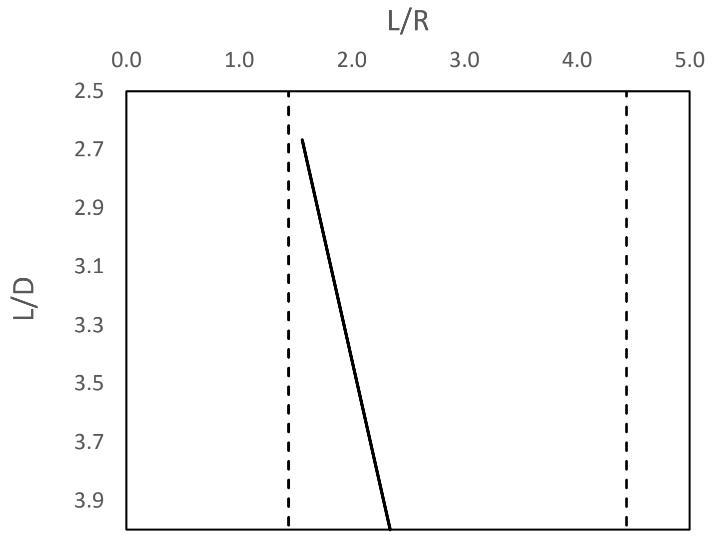

Figure 4-20: Pile failure mechanism

5. CONCLUSIONS AND SUGGESTIONS

Within this study, a 7.5m diameter monopile embedded in a dense sand soil was analysed using finite element method and the simplified design procedures available in the literature. The effect of structural and soil parameters on the monopile behavior was examined, and results indicated that the stiffness of the soil and internal friction angle have a nonlinear and negative relationship with the monopile's lateral displacement and rotation. The simplified design procedure and elastic solution in combination with the Winkler model underestimated the pile displacement and rotation, while the finite element analysis accurately predicted the behavior of the monopile. Based on the results obtained from the finite element simulations, regression equations that can be used for the initial design of monopiles embedded in dense sand soil conditions were presented.

Results of the analyses indicated that soil Young’s Modulus and internal friction angle have a nonlinear relation with the rotation and displacement that occurs along the monopile. The greater the stiffness of the soil, the lower the value of the monopile lateral displacement and rotation. As the internal friction angle increases, the mudline displacement and rotation decrease. For the stiffer/ dense sands with Young’s modulus values above 100MPa, the monopile mostly exhibits a failure mechanism that lies between rigid and flexible behavior. The study mostly focused on the deformational behavior rather than the ultimate resistance because the lateral design of large-diameter monopiles is in most cases governed by the deformation behavior. In all simulations, the monopile tended to behave in a more rigid way rotating about the point of zero displacement. The Young’s modulus values were taken high only covering the dense/stiff sands.

The simplified design procedure gave values that were close to the data obtained from finite element analyses as compared to the elastic solution. Due to the absence of site data i.e., the wind and wave data, arbitrary values of lateral load, bending moment, and water level were taken in the analyses. The simplified design procedure overestimated the soil resistance values and cannot take into account of yielding in the soil. Considering this in mind, it can be concluded that simplified design procedure estimations should be considered with caution and supporting the results with finite element analyses is advised. In the finite element analyses, defining the pile material as linear elastic significantly oversimplifies the problem. A more realistic material behavior should be adopted for steel when performing the finite element analyses. Additionally, for the soils Mohr Coulomb model can yield for quick analyses however use of improved constitute models is required. In the analyses, dry soil conditions were considered but on a real site, pore pressure poses a challenge. Therefore, pore pressure should be incorporated in future analyses.

From the multiple regression analyses performed using Statistica software, regression equations that can be used to estimate the behavior of the 7.5 m diameter monopile embedded in dense sand soil conditions having different mechanical characteristics were formulated within this study.

Finite element analyses gave good results for the mudline rotation and displacement of the monopile with monotonic loading applied but the real loading on the monopile is more complicated. Therefore, further research concerning the more realistic loading of the monopiles will be carried out as a future study. Additionally, it is planned to conduct analyses on monopiles having different diameters embedded in both clayey and sandy soil conditions. Using the data obtained from finite element analyses, multiple variate nonlinear regression analyses will be performed to suggest closed form formulae which would be used for preliminary design of the monopile foundations.

6. REFERENCES

Abdel-Rahman, K., & Achmus, M. (2005, October). Finite element modelling of horizontally loaded monopile foundations for offshore wind energy converters in Germany. In Proceedings of the international symposium on frontiers in offshore geotechnics. Taylor and Francis, Perth (pp. 391-396).

American Petroleum Institute (API), (2011). Geotechnical considerations and foundation design for offshore structures. Washington, D.C., USA: ANSI/API specification RP 2GEO.

Arany, L., Bhattacharya, S., Macdonald, J., & Hogan, S. J. (2017). Design of monopiles for offshore wind turbines in 10 steps. Soil Dynamics and Earthquake Engineering, 92, 126-152.

Arany, L., Bhattacharya, S., Macdonald, J., & Hogan, S. J. (2017b). Design of monopiles for offshore wind turbines in 10 steps. Soil Dynamics and Earthquake Engineering, 92, 126-152.

Argın, M., & Yerci, V. (2015, November). The assessment of offshore wind power potential of Turkey. In 2015 9th International Conference on Electrical and Electronics Engineering (ELECO) (pp. 966-970). IEEE.

Arshad, M., & O'Kelly, B. C. (2016). Analysis and design of monopile foundations for offshore wind-turbine structures. Marine Georesources & Geotechnology, 34(6), 503-525.

Bouzid, D. A., Bhattacharya, S., & Otsmane, L. (2018). Assessment of natural frequency of installed offshore wind turbines using nonlinear finite element model considering soil-monopile interaction. Journal of Rock Mechanics and Geotechnical Engineering, 10(2), 333-346.

BW, B., Zdravkovic, L., Gavin, K. G., & Muirwood, A. (2017). Offshore site investigation and geotechnics smarter solutions for future offshore developments. Proceedings of the 8th International Conference 12-14 September 2017 Royal Geographical Society. London, UK.

Byrne, B. W., Houlsby, G. T., Burd, H. J., Gavin, K. G., Igoe, D. J., Jardine, R. J., ... & Zdravković, L. (2020). PISA design model for monopiles for offshore wind turbines: application to a stiff glacial clay till. Géotechnique, 70(11), 1030-1047.

Det Norske, V. (2004). Design of Offshore Wind Turbine Structure. Offshore Standard DNV-OS-J101. DNV, D. N. V. (2011). Offshore Standard, DNV-OS-J101. Marine Operations.

Gupta, B. K., & Basu, D. (2020). Offshore wind turbine monopile foundations: Design perspectives. Ocean Engineering, 213, 107514.

Haiderali, A., Cilingir, U., & Madabhushi, G. (2013). Lateral and axial capacity of monopiles for offshore wind turbines. Indian Geotechnical Journal, 43, 181-194.

International Electrotechnical Commission (IEC). (2009a). International Standard IEC 61400-3 Wind turbines - Part 3: Design requirements for offshore wind turbines, 1.0 ed.

International Electrotechnical Commission (IEC). (2009b). International Standard IEC-61400-1 Amendment 1 - Wind turbines - Part 1: Design requirements, 3rd Edition.

International Electrotechnical Commission. (2005). International standard IEC 61400-1. Wind turbines–Part, 1, 22-23.

Jonkman, J., Butterfield, S., Musial, W., & Scott, G. (2009). Definition of a 5-MW reference wind turbine for offshore system development (No. NREL/TP-500-38060). National Renewable Energy Lab. (NREL), Golden, CO (United States).

Kallehave, D., Byrne, B. W., LeBlanc Thilsted, C., & Mikkelsen, K. K. (2015). Optimization of monopiles for offshore wind turbines. Philosophical Transactions of the Royal Society A: Mathematical, Physical and Engineering Sciences, 373(2035), 20140100.

Kuo, Y. S., Achmus, M., & Abdel-Rahman, K. (2012). Minimum embedded length of cyclic horizontally loaded monopiles. Journal of Geotechnical and Geoenvironmental Engineering, 138(3), 357-363.

Liu, X., Lu, C., Li, G., Godbole, A., & Chen, Y. (2017). Tower load analysis of offshore wind turbines and the effects of aerodynamic damping. Energy Procedia, 105, 373-378.

MacCamy, R. C., & Fuchs, R. A. (1954). Wave forces on piles: a diffraction theory (No. 69). US Beach Erosion Board.

Malik, M. G. (2016). Hydrodynamic Modelling Effects on Fatigue Calculations for Monopile Offshore Wind Turbines (Master's thesis, NTNU).

Matlock, H., & Reese, L. C. (1960). Generalized solutions for laterally loaded piles. Journal of the Soil Mechanics and foundations Division, 86(5), 63-92.

Nygaard, M. (2016). Hydrodynamic forces on monopiles with secondary structures: Numerical approach. 1–53.

Piante, C., Jeffries, E., Mulazzani, A., Agin, G., Monnier, M., Bordenave, T., & Laurent, C. (2019). PHAROS4MPAS-Safeguarding marine protected areas in the growing Mediterranean blue economy.

Recommendations for the offshore wind energy sector+ Policy brief: priority actions for public authorities.

Poulos, H. G., & Hull, T. S. (1989). The role of analytical geomechanics in foundation engineering. In Foundation engineering: Current principles and practices (pp. 1578-1606). ASCE.

Velarde, J., & Bachynski, E. E. (2017). Design and fatigue analysis of monopile foundations to support the DTU 10 MW offshore wind turbine. Energy Procedia, 137, 3-13.

Veritas, D. N. (2004). Offshore Standard DNV-OS-J101: Design of Offshore Wind Turbine Structures. Det Norske Veritas, Høvik, Norway.

Veritas, D. N. (2014). Offshore Standard DNV-OS-J101: Design of Offshore Wind Turbine Structures. Det Norske Veritas, Høvik, Norway.

Appendix A

Table A(1): From Drilled Pier Foundations, by R. J. Woodward, W. S. Gardner, and D. M. Greer.

Table 11.14 Coefficients for Long Piles, $k_z = n_h z$

Z	A_x	A_θ	A_m	A_v	A'_p	B_x	B_θ	B_m	B_v	B'_p
0.0	2.435	−1.623	0.000	1.000	0.000	1.623	−1.750	1.000	0.000	0.000
0.1	2.273	−1.618	0.100	0.989	−0.227	1.453	−1.650	1.000	−0.007	−0.145
0.2	2.112	−1.603	0.198	0.956	−0.422	1.293	−1.550	0.999	−0.028	−0.259
0.3	1.952	−1.578	0.291	0.906	−0.586	1.143	−1.450	0.994	−0.058	−0.343
0.4	1.796	−1.545	0.379	0.840	−0.718	1.003	−1.351	0.987	−0.095	−0.401
0.5	1.644	−1.503	0.459	0.764	−0.822	0.873	−1.253	0.976	−0.137	−0.436
0.6	1.496	−1.454	0.532	0.677	−0.897	0.752	−1.156	0.960	−0.181	−0.451
0.7	1.353	−1.397	0.595	0.585	−0.947	0.642	−1.061	0.939	−0.226	−0.449
0.8	1.216	−1.335	0.649	0.489	−0.973	0.540	−0.968	0.914	−0.270	−0.432
0.9	1.086	−1.268	0.693	0.392	−0.977	0.448	−0.878	0.885	−0.312	−0.403
1.0	0.962	−1.197	0.727	0.295	−0.962	0.364	−0.792	0.852	−0.350	−0.364
1.2	0.738	−1.047	0.767	0.109	−0.885	0.223	−0.629	0.775	−0.414	−0.268
1.4	0.544	−0.893	0.772	−0.056	−0.761	0.112	−0.482	0.688	−0.456	−0.157
1.6	0.381	−0.741	0.746	−0.193	−0.609	0.029	−0.354	0.594	−0.477	−0.047
1.8	0.247	−0.596	0.696	−0.298	−0.445	−0.030	−0.245	0.498	−0.476	0.054
2.0	0.142	−0.464	0.628	−0.371	−0.283	−0.070	−0.155	0.404	−0.456	0.140
3.0	−0.075	−0.040	0.225	−0.349	0.226	−0.089	0.057	0.059	−0.213	0.268
4.0	−0.050	0.052	0.000	−0.106	0.201	−0.028	0.049	−0.042	0.017	0.112
5.0	−0.009	0.025	−0.033	0.015	0.046	0.000	−0.011	−0.026	0.029	−0.002

Table A(2): Steel plasticity

Yield stress (MPa)	Plastic strain
200.20	0
246.00	0.0235
294.00	0.0474
374.00	0.0935
437.00	0.1377
480.00	0.18

Table A(3): Displacement(m) along the Embedded length of the monopile.

U_X 2MN	U_X 4MN	U_X 6MN	U_X 8MN	U_X10MN	U_X12MN	Z
3.02E-02	5.33E-02	9.11E-02	1.13E-01	1.24E-01	1.47E-01	1
1.39E-02	2.60E-02	4.44E-02	5.91E-02	6.69E-02	8.08E-02	0
9.97E-03	1.93E-02	3.31E-02	4.64E-02	5.34E-02	6.54E-02	-1
6.46E-03	1.30E-02	2.23E-02	3.29E-02	3.85E-02	4.78E-02	-2
4.05E-03	8.33E-03	1.42E-02	2.19E-02	2.61E-02	3.28E-02	-3
2.80E-03	5.90E-03	1.01E-02	1.59E-02	1.92E-02	2.44E-02	-4
1.96E-03	4.13E-03	7.05E-03	1.13E-02	1.37E-02	1.75E-02	-5
1.38E-03	2.92E-03	5.00E-03	8.16E-03	9.99E-03	1.29E-02	-6
9.96E-04	2.10E-03	3.59E-03	5.96E-03	7.35E-03	9.57E-03	-7
7.55E-04	1.60E-03	2.74E-03	4.46E-03	5.52E-03	7.21E-03	-8
5.56E-04	1.19E-03	2.04E-03	3.14E-03	4.13E-03	5.43E-03	-9
4.19E-04	9.16E-04	1.57E-03	2.55E-03	3.20E-03	4.22E-03	-10
3.09E-04	7.03E-04	1.20E-03	1.93E-03	2.47E-03	3.26E-03	-11
2.28E-04	5.48E-04	9.37E-04	1.47E-03	1.93E-03	2.55E-03	-12
1.54E-04	4.10E-04	7.02E-04	1.10E-03	1.50E-03	2.00E-03	-13
9.39E-05	3.04E-04	5.20E-04	8.07E-04	1.17E-03	1.56E-03	-14
4.38E-05	2.17E-04	3.70E-04	5.65E-04	8.97E-04	1.21E-03	-15
-6.23E-06	1.33E-04	2.27E-04	3.50E-04	6.64E-04	9.05E-04	-16
-4.51E-05	6.44E-05	1.10E-04	1.70E-04	4.70E-04	6.54E-04	-17
-8.60E-05	-2.24E-06	-3.82E-06	3.93E-07	2.91E-04	4.25E-04	-18
-1.22E-04	-6.31E-05	-1.08E-04	-1.51E-04	1.32E-04	2.22E-04	-19
-1.60E-04	-1.25E-04	-2.14E-04	-3.01E-04	-2.08E-05	2.93E-05	-20
-1.93E-04	-1.81E-04	-3.09E-04	-4.38E-04	-1.63E-04	-1.50E-04	-21
-2.26E-04	-2.37E-04	-4.06E-04	-5.78E-04	-3.04E-04	-3.28E-04	-22
-2.62E-04	-2.98E-04	-5.09E-04	-7.18E-04	-4.45E-04	-5.04E-04	-23
-2.97E-04	-3.57E-04	-6.11E-04	-8.62E-04	-5.88E-04	-6.81E-04	-24
-3.26E-04	-4.10E-04	-7.02E-04	-1.00E-03	-7.26E-04	-8.54E-04	-25
-3.75E-04	-4.84E-04	-8.27E-04	-1.16E-03	-8.84E-04	-1.05E-03	-26
-4.16E-04	-5.47E-04	-9.35E-04	-1.32E-03	-1.03E-03	-1.24E-03	-27
-4.16E-04	-5.74E-04	-9.82E-04	-1.44E-03	-1.15E-03	-1.39E-03	-28
-4.56E-04	-6.45E-04	-1.10E-03	-1.61E-03	-1.32E-03	-1.59E-03	-29
-5.98E-04	-8.19E-04	-1.40E-03	-1.89E-03	-1.57E-03	-1.88E-03	-30

Table A(4): Determination of pile deflection and slope according to Elastic solution and Winkler model.

PARAMETER	SYMBOL	VALUE	UNIT	COMMENT
Modulus of subgrade reaction	k	0.00E+00	kN/m^2	
Pressure on soil	p'	0.00E+00	kN/m	
Horizontal coefficient of subgrade reaction	n_h	4.89E+06	N/m^3	
Depth	z	0	m	
Modulus of elasticity of pile material	E_p	2.10E+11	Pa	
Moment of inertia of the pile section	I_p	14.39	m^4	
Length of pile	L	31	m	
Lateral force	Q_g	1.20E+07	N	
Moment	M_g	3.60E+08	Nm	
Characteristic length of the soil-pile system	T	14.395071		
Constant L/T	β	2.15351415		semi flexible
Non-dimensional depth, z/T	Z	0		
deflection coefficient	A_x	2.435		
deflection coefficient	B_x	1.623		
slope coefficient	A_Θ	-1.623		
slope coefficient	B_Θ	-1.75		
Moment coefficient	A_m	0		
Moment coefficient	B_m	1		
Shear coefficient	A_v	1		
Shear coefficient	B_v	0		
soil reaction coefficient	$A_{p'}$	0		
soil reaction coefficient	$B_{p'}$	0		
pile deflection at any depth	x(z)	0.06890845	m	
slope of the pile at any depth	Θ(z)	-0.17	degrees	
moment of pile at any depth	M(z)	360000000	Nm	
shear force on pile at any depth	V(z)	12000000	N	
Soil reaction at any depth	p'(z)	0	kN/m	

Table A(5): Comparison of Mudline displacement using Simplified Design Procedure, Winkler approach and Finite Element Analysis.

$y'=11kN/m3$, $Ø'=35^0$, $E_s=144605.3kN/m2$, $n_h=4888.889kN/m3$			
Displacement-Arany et al 2017(m)	**Displacement-FEM(m)**	**Displacement-Winkler(m)**	**Applied load (MN)**
0.00000	0.00000	0.00000	0
0.01148	0.01394	0.01150	2
0.02296	0.02599	0.02297	4
0.03443	0.03750	0.03445	6
0.04591	0.05569	0.04590	8
0.05739	0.06686	0.05742	10
0.06887	0.08081	0.06891	12

Table A(6): Geotechnical capacity of the soil (Arany et al 2017).

TOTAL LOAD	F_T	8	MN
TOTAL OVERTURNING MOMENT	M_T	240	MNm
Geotechnical load BEARING capacity estimation			
PARAMETER	**SYMBOL**	**VALUE**	**UNIT**
passive lateral earth pressure coefficient	K_p	3.69	
eccentricity	e	30	
horizontal load carrying capacity (assuming soil failure)	F_R	68.49	MN
zero shear force point location below mudline	f	0.006081442	
moment capacity of the foundation (assuming soil failure)	M_R	2055.43	MNm

Table A(7): Mudline deflection and rotation values (Arany et al 2017)

Deformation and foundation stiffness estimation				
PARAMETER	**SYMBOL**	**VALUE**	**UNIT**	**COMMENT**
lateral stiffness of the foundation	K_L	1088062827	N/m	
Cross-coupling stiffness of the foundation	K_{LR}	-14437920580	N	
Rotational stiffness of the foundation	K_R	3.10707E+11	N/rad	
displacement in the x-direction	ρ	0.045910979	m	<0.2m
		0.002905822	rad	

slope of the deflection (tilt or rotation)	0.166491347	degrees	<0.5 degrees

Table A(8): Natural frequency of the wind turbine structure (SDP).

Natural frequency calculation				
PARAMETER	**SYMBOL**	**VALUE**	**UNIT**	**COMMENT**
young's modulus of tower material	E_T	210	GPa	
second moment of area of tower	I_T	1.452385042	m^4	
fixed base(cantilever beam) natural frequency of the tower	f_{FB}	0.337927103	Hz	
average diameter of the tower	D_T	4.935	m	
tower thickness	t_T	0.02341943	m	
constant	q	1.550387597		
constant	f(q)	2.712005202		
equivalent bending stiffness of the tower	EI_η	8.27164E+11		
non dimensional foundation stiffness value-L	η_L	884.249272		
non dimensional foundation stiffness value-LR	η_{LR}	-133.9433881		
non dimensional foundation stiffness value-LR	η_R	32.90511835		
constant	a	0.5		
constant	b	0.6		
platform height above mudline	L_S	43.72	m	
bending stiffness ratio	X	0.100923449		
length ratio	Ψ	0.499086758		
rotational foundation flexibility coefficient	C_R	0.883306655		
lateral foundation flexibility coefficient	C_L	0.994135243		
substructure flexibility coefficient	C_S	0.898362938		
first natural frequency	f_0	0.266582615	Hz	>0.24

Table A(1): Sample Metocean data used for deriving of the wind load.

metocean data			
parameter	**symbol**	**value**	**unit**
wind speed Weibull distribution shape parameter	s	1.8	[-]

wind speed Weibull distribution scale parameter	K	8	m/s
reference turbulence intensity	I	18	%
turbulence intergral length scale	L_k	340.2	m
density of air	ρ_a	1.225	kg/m^3
significant wave height with 50-year return period	$H_{s,50}$	6.6	m
peak wave period	$T_{s,50}$	9.1	s
maximum wave height(50-year)	$H_{m,50}$	12.4	m
maximum wave period	$T_{m,50}$	12.5	s
maximum water depth (50-year high water level)	S	30	m
density of sea water	ρ_w	1030	kg/m^3

Table A(2): Wind load and moment estimation example.

Highest wind load calculation: scenario U-3

PARAMETER	**SYMBOL**	**VALUE**	**UNIT**
50-year extreme wind speed	$U_{10,50\text{-year}}$	35.7	m/s
1-year extreme wind speed	$U_{10,1\text{-year}}$	28.6	m/s
characteristic standard deviation of wind speed	$\sigma_{U,C}$	3.142	m/s
		22.4	m/s
		8.0	m/s
TOTAL WIND LOAD	$F_{wind,EOG}$ or Th_{EOG}	1781962.315	N
MUDLINE BENDING MOMENT WITHOUT LOAD FACTOR	$M_{wind,EOG}$	213835477.7	N
load factor	γ_L	1.35	
MUDLINE BENDING MOMENT WITH LOAD FACTOR	$M_{wind,EOG}$	288677895	N

Table A(3): Estimation of initial pile dimensions and yielding capacity of the pile material.

Initial pile dimensions calculation

PARAMETER	**SYMBOL**	**VALUE**	**UNIT**	
pile thickness	t_p	90	mm	81.35
monopile diameter	D_p	7.5	m	
material factor	γ_M	1.1		
pile's second moment of area	I_p	14.39095727	m^4	2.788732394

limiting value for pile yield	f_{yk}/γ_M	322.7	
Embedded length	L_p	28.79053651	m

Table A(4): Critical wave load and moment calculation example.

Critical wave load calculation			
PARAMETER	**SYMBOL**	**VALUE**	**UNIT**
1-year significant wave height	$H_{s,1}$	5.28	m
1-year peak wave period	$T_{s,1}$	8.143393788	s
Number of waves in a 3-hour period	N	1186.813187	
ratio of maximum wave height to significant wave height	H_m/H_s	1.881359482	
1-year maximum wave height	$H_{m,1}$	10	m
range of wave period	$T_{m,1}$	11.16969539	
Maximum wave load	F_{wave}	2130000	N
Maximum wave moment	M_{wave}	53800000	Nm

Table A(5): Rotation values from the Simplified Design Procedure, Finite Element Analysis and Elastic solution for the applied horizontal loads.

LOAD (MN)	**Rotation-Winkler**	**Rotation-arany(^{0})**	**Rotational displacement(m)**	**Rotation-FEM (^{0})**
0	0.000	0.000	0.000	0.000
2	0.030	0.042	0.003	0.047
4	0.060	0.083	0.007	0.103
6	0.090	0.125	0.010	0.153
8	0.120	0.166	0.013	0.193
10	0.140	0.208	0.016	0.237
12	0.170	0.250	0.018	0.273
14	0.200	0.291	0.020	0.304
16	0.230	0.333	0.022	0.333
18	0.260	0.375	0.023	0.358
20	0.290	0.416	0.025	0.381

Table A(6): Displacement and Rotation values at different soil Young's Modulus.

Ø=20 Lp=25m tp=85mm			
Es	**U 4MN**	**U 8MN**	**U 12MN**
100	0.05185	0.10941	0.17784
200	0.04368	0.09225	0.14754
300	0.04045	0.08525	0.13611
	Ө 4MN	**Ө 8MN**	**Ө 12MN**
100	0.12426	0.23258	0.3218
200	0.11733	0.22034	0.30148
300	0.11459	0.21548	0.29412

a

Ø=30 Lp=25m tp=85mm		
U 4MN	**U 8MN**	**U 12MN**
0.03986	0.08116	0.12604
0.03313	0.06842	0.10676
0.03029	0.06323	0.09902
Ө 4MN	**Ө 8MN**	**Ө 12MN**
0.1135	0.2121	0.28836
0.10752	0.20309	0.27632
0.10479	0.19932	0.27172

b

Ø=40 Lp=25m tp=85mm		
U 4MN	**U 8MN**	**U 12MN**
0.03181	0.06536	0.09976
0.02581	0.05357	0.08205
0.02319	0.04805	0.07446
Ө 4MN	**Ө 8MN**	**Ө 12MN**
0.10712	0.20166	0.27321
0.10143	0.19279	0.26184
0.09876	0.18887	0.25698

c

Table A(7): Displacement and Rotation values at different horizontal coefficients of subgrade reaction.

n_h (kN/m3)	displacement(m)	Rotation (^{0})
3555.556	0.080	0.272
4000.000	0.076	0.263
4444.444	0.072	0.256
4888.889	0.069	0.250
5333.333	0.066	0.244

Table A(8): Displacement and rotation at different values of internal friction angle.

Es=100,000kPa Lp=20m tp=80mm			
Ø	**U 4MN**	**U 8MN**	**U 12MN**
20	0.06581	0.14558	0.25402
30	0.04667	0.09714	0.15392
40	0.03742	0.07447	0.11329
	Ɵ 4MN	**Ɵ 8MN**	**Ɵ 12MN**
20	0.13915	0.26189	0.37729
30	0.11974	0.22164	0.29976
40	0.11126	0.20642	0.27197

a

Es=200,000kPa Lp=20m tp=80mm		
U 4MN	**U 8MN**	**U 12MN**
0.05302	0.11499	0.19524
0.03806	0.07979	0.12523
0.02969	0.05979	0.0925
Ɵ 4MN	**Ɵ 8MN**	**Ɵ 12MN**
0.12642	0.23535	0.32772
0.11131	0.2078	0.27845
0.10343	0.19258	0.25732

b

Es=300,000kPa Lp=20m tp=80mm		
U 4MN	**U 8MN**	**U 12MN**
0.04802	0.1036	0.17143
0.03467	0.07292	0.11417
0.02646	0.05383	0.08408
Ɵ 4MN	**Ɵ 8MN**	**Ɵ 12MN**
0.12156	0.22586	0.30879
0.10796	0.20237	0.27087
0.09972	0.1876	0.25121

c

Table A(9): Effect of embedded length on the rotation and mudline displacement

Es=100,000kPa Ø=30 tp=80mm			
Lp	**U 4MN**	**U 8MN**	**U 12MN**
20	0.04667	0.09714	0.15392
25	0.04315	0.08752	0.13565
30	0.04123	0.08425	0.12852
	Ɵ 4MN	**Ɵ 8MN**	**Ɵ 12MN**
20	0.11974	0.22164	0.29976
25	0.11533	0.21039	0.27924

30	0.11394	0.20737	0.2727

a

Es=100,000kPa Ø=30 tp=85mm		
U 4MN	**U 8MN**	**U 12MN**
0.0433	0.09037	0.14367
0.03986	0.08116	0.12604
0.03784	0.07764	0.1194
Ɵ 4MN	**Ɵ 8MN**	**Ɵ 12MN**
0.13667	0.22309	0.30865
0.1135	0.2121	0.28836
0.11192	0.20884	0.28225

b

Es=100,000kPa Ø=30 tp=90mm		
U 4MN	**U 8MN**	**U 12MN**
0.04041	0.08451	0.13521
0.03692	0.07542	0.11757
0.03492	0.07192	0.11102
Ɵ 4MN	**Ɵ 8MN**	**Ɵ 12MN**
0.11469	0.22071	0.31115
0.11015	0.20969	0.29064
0.10854	0.20637	0.28451

c

Es=100,000kPa Ø=30 tp=95mm		
U 4MN	**U 8MN**	**U 12MN**
0.03782	0.0792	0.12734
0.03435	0.07016	0.11021
0.03235	0.06683	0.10349
Ө 4MN	**Ө 8MN**	**Ө 12MN**
0.11059	0.21565	0.30865
0.10603	0.2046	0.28834
0.10435	0.20136	0.28198

d

Table A(10): Effect of pile wall thickness on rotation and mudline displacement

	Es=200,000kPa Ø=30 Lp=20m		
tp mm	**U 4MN**	**U 8MN**	**U 12MN**
80	0.03806	0.07979	0.12523
85	0.03502	0.07381	0.11637
90	0.03241	0.06839	0.10834
95	0.03008	0.06362	0.1012
	Ө 4MN	**Ө 8MN**	**Ө 12MN**
80	0.11131	0.2078	0.27845
85	0.10962	0.20946	0.2877
90	0.1066	0.20695	0.28985
95	0.10266	0.20205	0.28724

a

Es=200,000kPa Ø=30 Lp=25mm		
U 4MN	**U 8MN**	**U 12MN**
0.03611	0.07438	0.11572
0.03313	0.06842	0.10676
0.03046	0.06311	0.09911
0.02821	0.05851	0.0919
Ɵ 4MN	**Ɵ 8MN**	**Ɵ 12MN**
0.10917	0.20136	0.26713
0.10752	0.20309	0.27632
0.10432	0.2007	0.27874
0.10046	0.19596	0.27611

b

Es=200,000kPa Ø=30 Lp=30mm		
U 4MN	**U 8MN**	**U 12MN**
0.03511	0.07217	0.11084
0.03207	0.06638	0.10246
0.02946	0.0613	0.09459
0.02718	0.05663	0.08767
Ɵ 4MN	**Ɵ 8MN**	**Ɵ 12MN**
0.10883	0.19958	0.26312
0.10703	0.20153	0.2727
0.10384	0.19936	0.27496
0.09987	0.19444	0.2726

c

Table A(11): pile failure mechanism

			Es=100,000kPa Ø=20 tp=80mm F=4MN			
Lp	**Dp**	**Rrigidity**	**Lp/Dp**	**Lp/R**	**1.44Lp/R**	**4.44Lp/R**
			0		1.44	4.44
20	7.5	12.813	2.7	1.6	1.44	4.44
25	7.5	12.813	3.3	2.0	1.44	4.44
30	7.5	12.813	4.0	2.3	1.44	4.44

Appendix B. Design charts

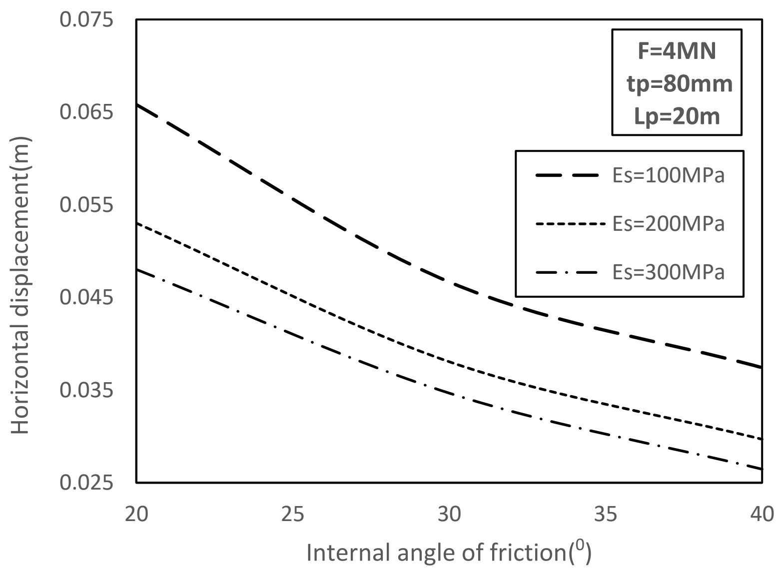

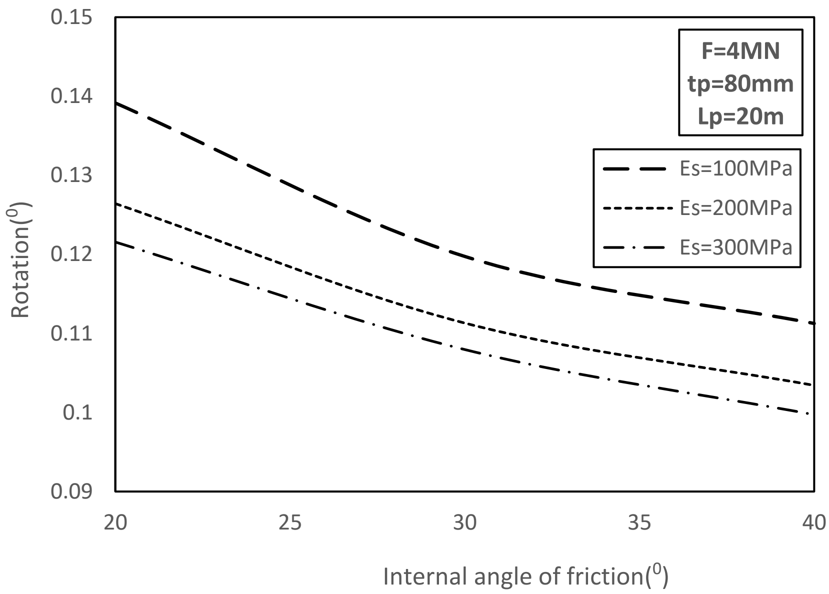
F=4MN
tp=80mm
Lp=20m
Es=100MPa
Es=200MPa
Es=300MPa
Rotation(^{0})
0.15
0.14
0.13
0.12
0.11
0.1
0.09
20
25
30
35
40
Internal angle of friction(^{0})

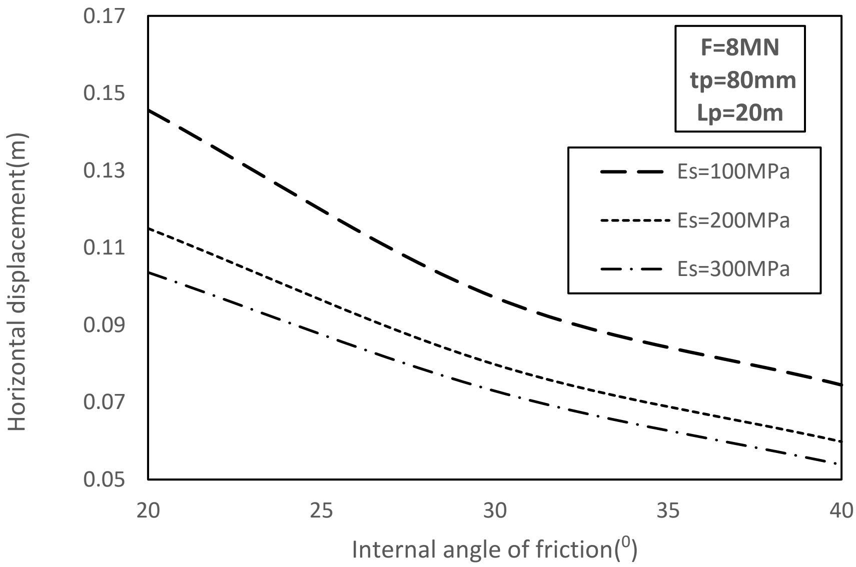
F=8MN
tp=80mm
Lp=20m
Es=100MPa
Es=200MPa
Es=300MPa
Horizontal displacement(m)
0.17
0.15
0.13
0.11
0.09
0.07
0.05
20
25
30
35
40
Internal angle of friction(^{0})

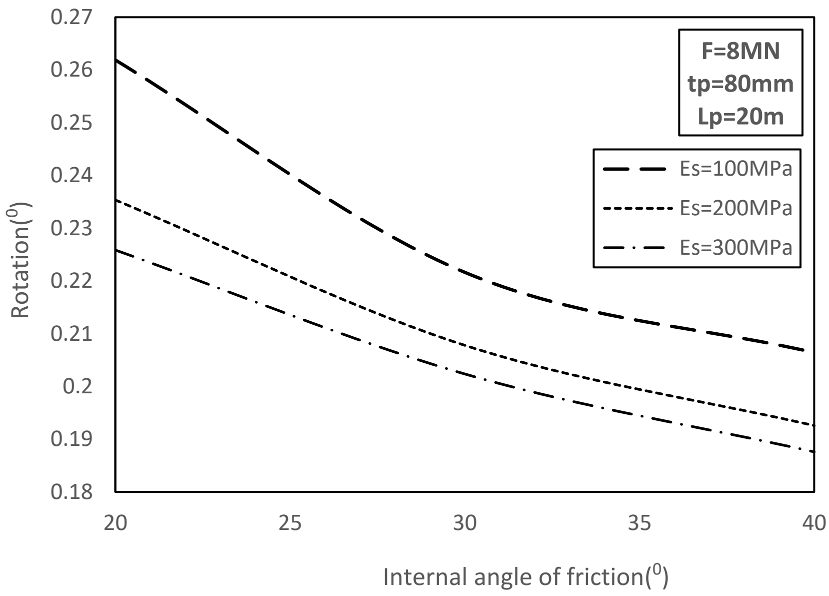
F=8MN
tp=80mm
Lp=20m
Es=100MPa
Es=200MPa
Es=300MPa
Rotation(0)
Internal angle of friction(0)
0.27
0.26
0.25
0.24
0.23
0.22
0.21
0.2
0.19
0.18
20
25
30
35
40

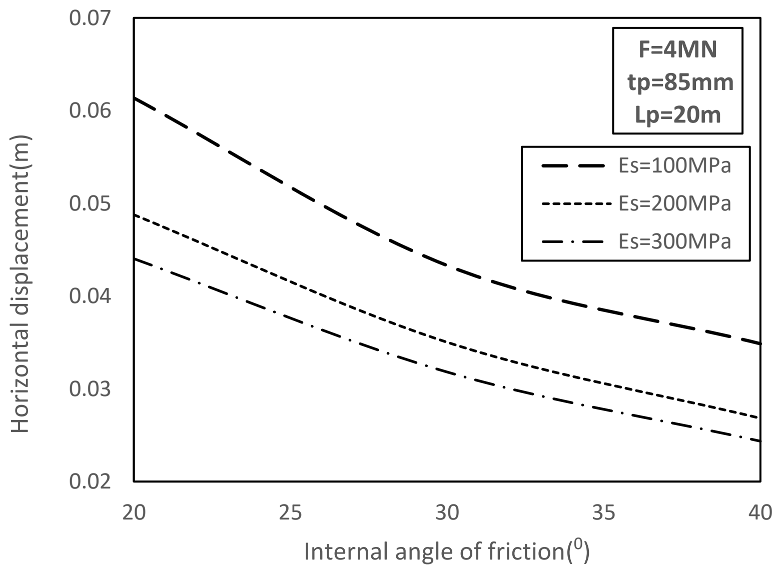
F=4MN
tp=85mm
Lp=20m
Es=100MPa
Es=200MPa
Es=300MPa
Horizontal displacement(m)
Internal angle of friction(0)
0.07
0.06
0.05
0.04
0.03
0.02
20
25
30
35
40

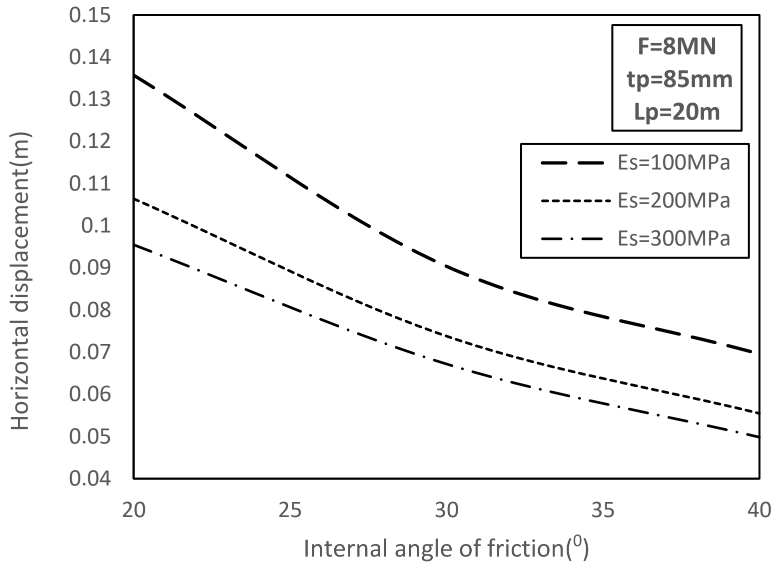
F=8MN
tp=85mm
Lp=20m
Es=100MPa
Es=200MPa
Es=300MPa
Horizontal displacement(m)
0.15
0.14
0.13
0.12
0.11
0.1
0.09
0.08
0.07
0.06
0.05
0.04
20
25
30
35
40
Internal angle of friction(^{0})

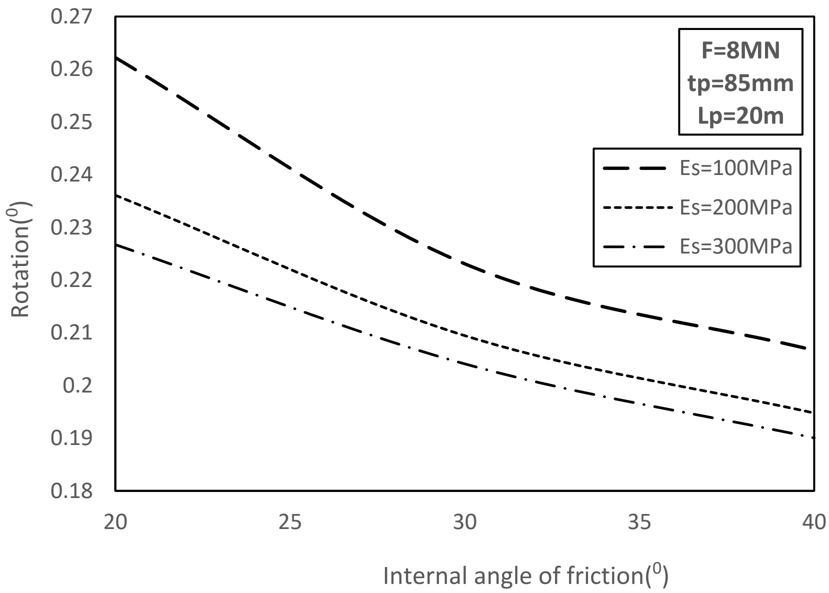
F=8MN
tp=85mm
Lp=20m
Es=100MPa
Es=200MPa
Es=300MPa
Rotation(^{0})
0.27
0.26
0.25
0.24
0.23
0.22
0.21
0.2
0.19
0.18
20
25
30
35
40
Internal angle of friction(^{0})

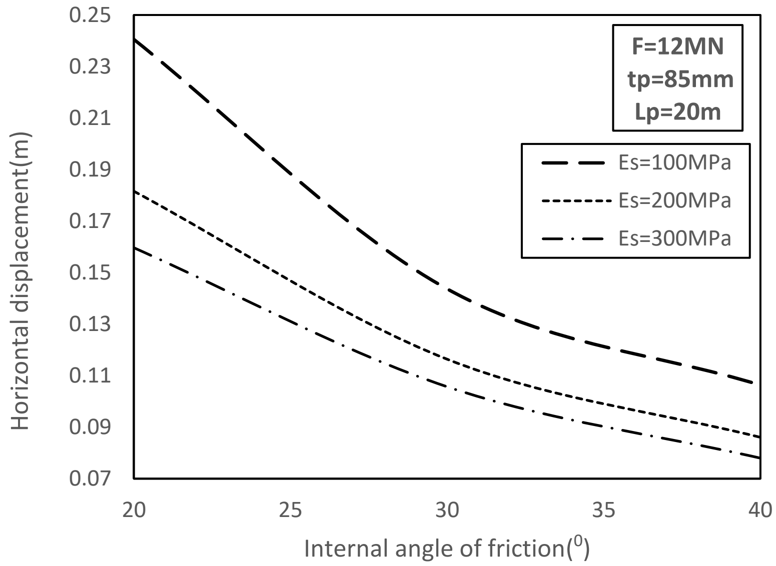
F=12MN
tp=85mm
Lp=20m
Es=100MPa
Es=200MPa
Es=300MPa
Horizontal displacement(m)
0.25
0.23
0.21
0.19
0.17
0.15
0.13
0.11
0.09
0.07
20
25
30
35
40
Internal angle of friction(0)

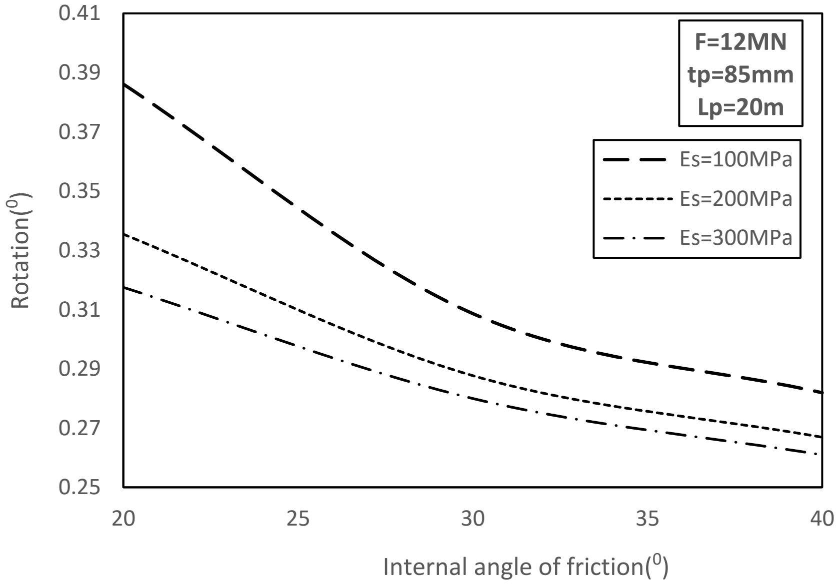
F=12MN
tp=85mm
Lp=20m
Es=100MPa
Es=200MPa
Es=300MPa
Rotation(0)
0.41
0.39
0.37
0.35
0.33
0.31
0.29
0.27
0.25
20
25
30
35
40
Internal angle of friction(0)

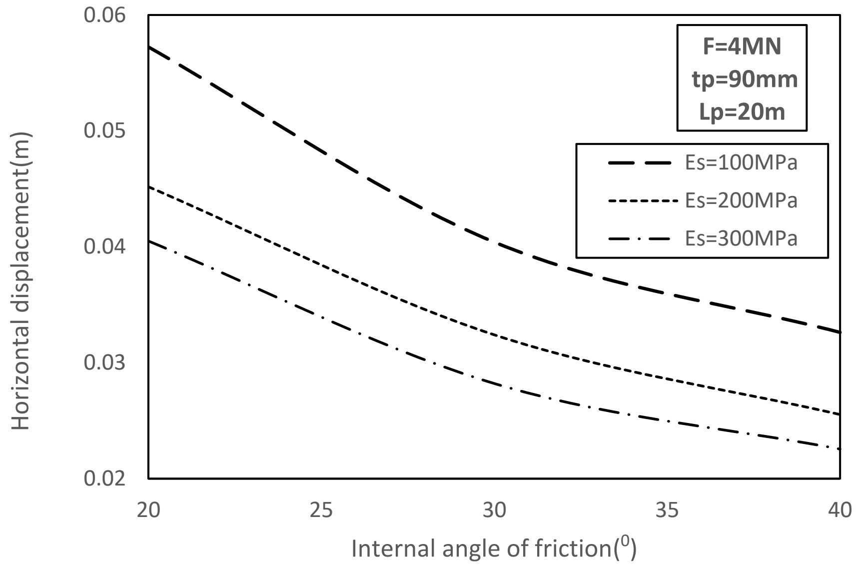
0.06
0.05
0.04
0.03
0.02
20
25
30
35
40
Horizontal displacement(m)
Internal angle of friction(0)
F=4MN
tp=90mm
Lp=20m
Es=100MPa
Es=200MPa
Es=300MPa

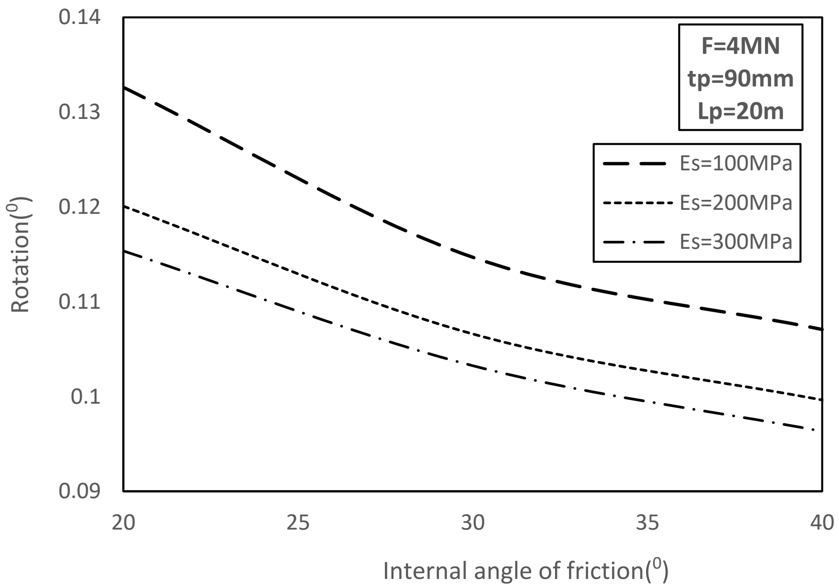
0.14
0.13
0.12
0.11
0.1
0.09
20
25
30
35
40
Rotation(0)
Internal angle of friction(0)
F=4MN
tp=90mm
Lp=20m
Es=100MPa
Es=200MPa
Es=300MPa

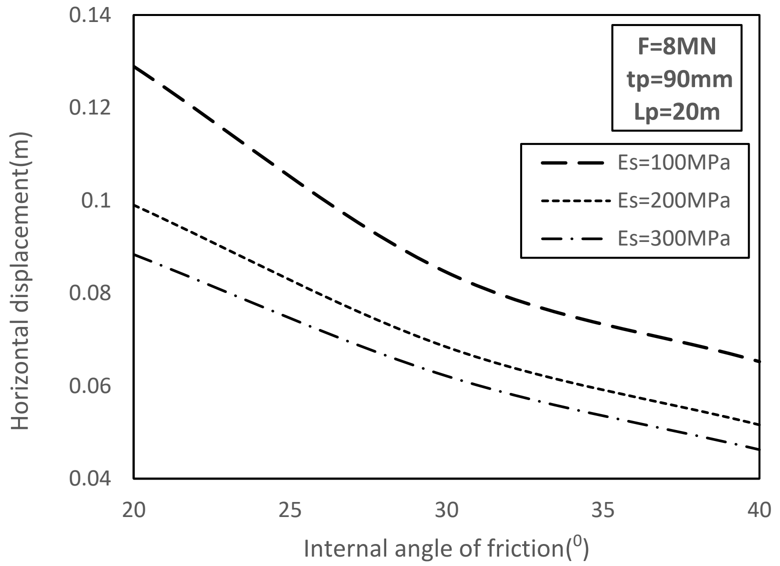
F=8MN
tp=90mm
Lp=20m
Es=100MPa
Es=200MPa
Es=300MPa
Horizontal displacement(m)
0.14
0.12
0.1
0.08
0.06
0.04
20
25
30
35
40
Internal angle of friction(0)

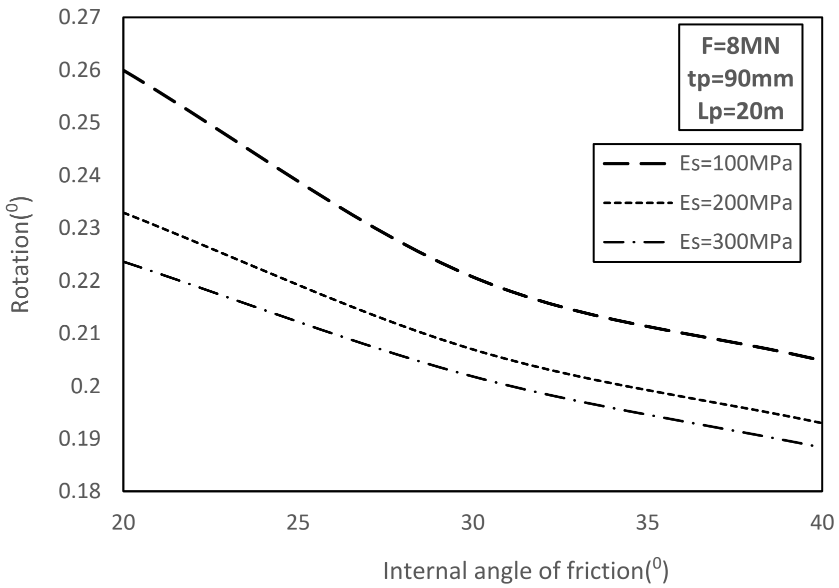
F=8MN
tp=90mm
Lp=20m
Es=100MPa
Es=200MPa
Es=300MPa
Rotation(0)
0.27
0.26
0.25
0.24
0.23
0.22
0.21
0.2
0.19
0.18
20
25
30
35
40
Internal angle of friction(0)

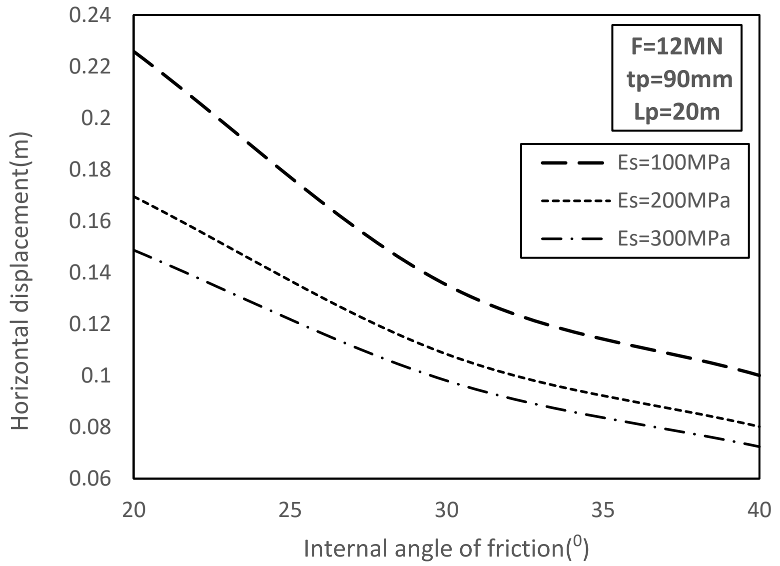
F=12MN
tp=90mm
Lp=20m
Es=100MPa
Es=200MPa
Es=300MPa
Horizontal displacement(m)
0.24
0.22
0.2
0.18
0.16
0.14
0.12
0.1
0.08
0.06
20
25
30
35
40
Internal angle of friction(0)

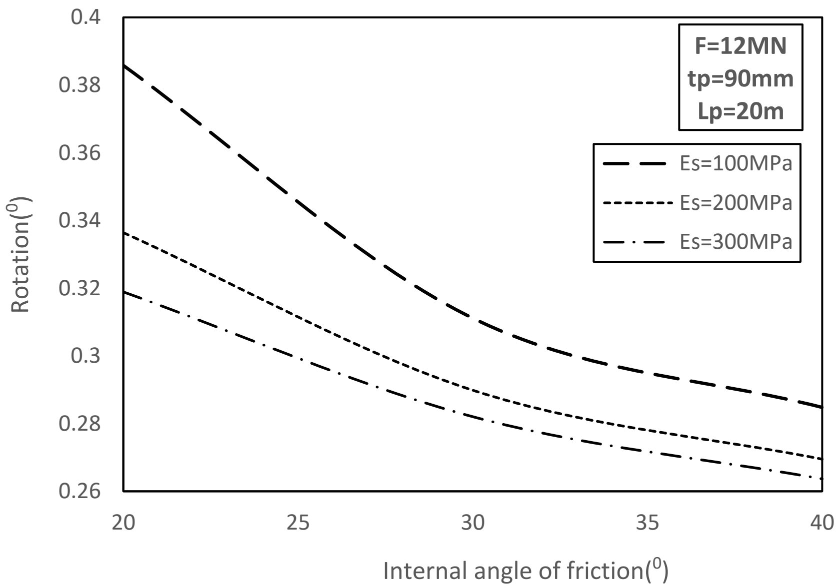
F=12MN
tp=90mm
Lp=20m
Es=100MPa
Es=200MPa
Es=300MPa
Rotation(0)
0.4
0.38
0.36
0.34
0.32
0.3
0.28
0.26
20
25
30
35
40
Internal angle of friction(0)

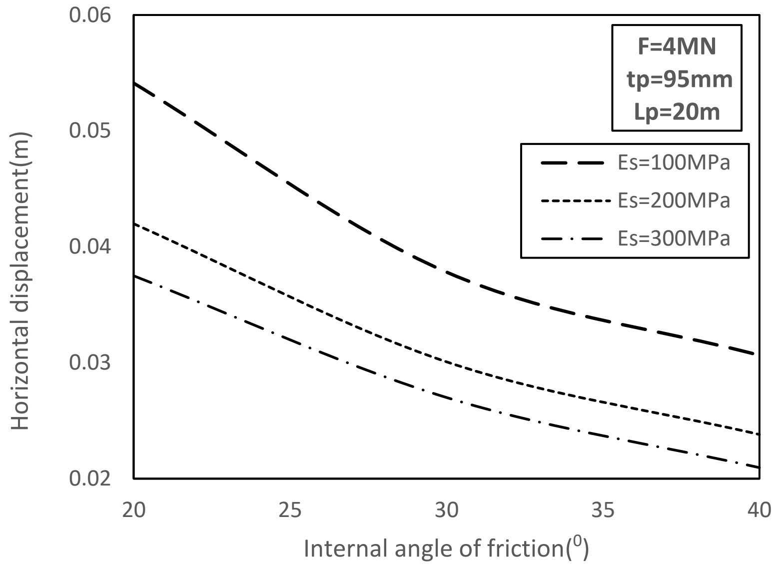
F=4MN
tp=95mm
Lp=20m
Es=100MPa
Es=200MPa
Es=300MPa
Horizontal displacement(m)
0.06
0.05
0.04
0.03
0.02
20
25
30
35
40
Internal angle of friction(^{0})

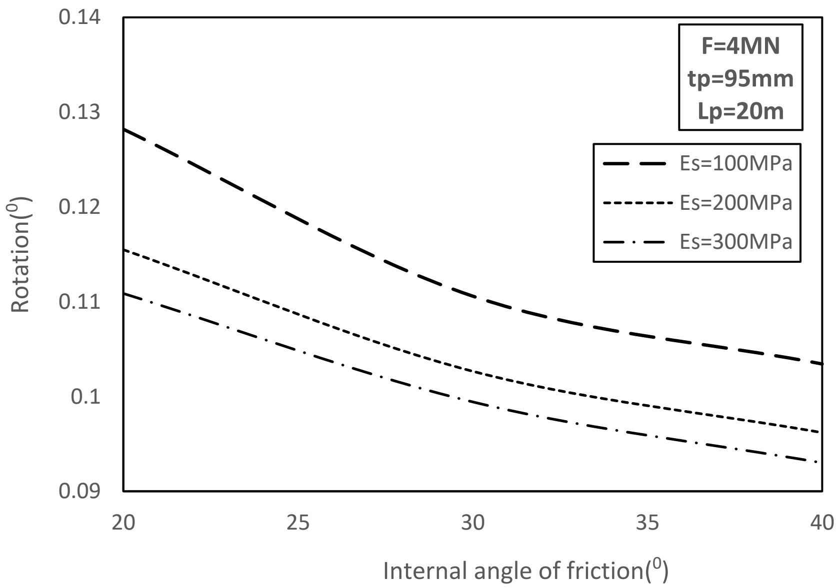
F=4MN
tp=95mm
Lp=20m
Es=100MPa
Es=200MPa
Es=300MPa
Rotation(^{0})
0.14
0.13
0.12
0.11
0.1
0.09
20
25
30
35
40
Internal angle of friction(^{0})

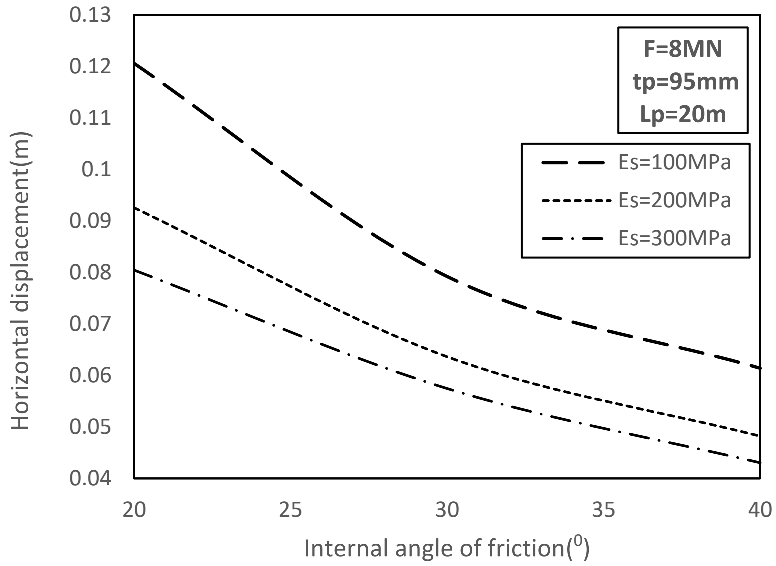
F=8MN
tp=95mm
Lp=20m
Es=100MPa
Es=200MPa
Es=300MPa
Horizontal displacement(m)
0.13
0.12
0.11
0.1
0.09
0.08
0.07
0.06
0.05
0.04
20
25
30
35
40
Internal angle of friction(0)

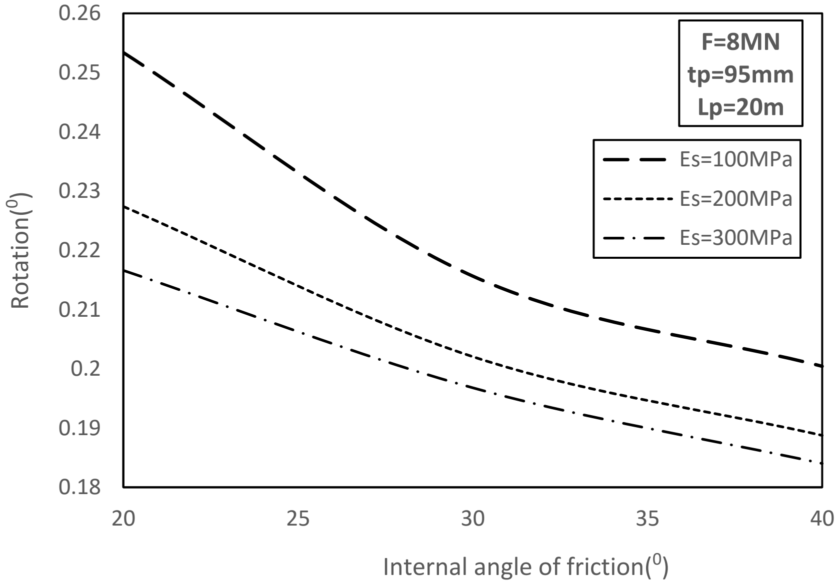
F=8MN
tp=95mm
Lp=20m
Es=100MPa
Es=200MPa
Es=300MPa
Rotation(0)
0.26
0.25
0.24
0.23
0.22
0.21
0.2
0.19
0.18
20
25
30
35
40
Internal angle of friction(0)

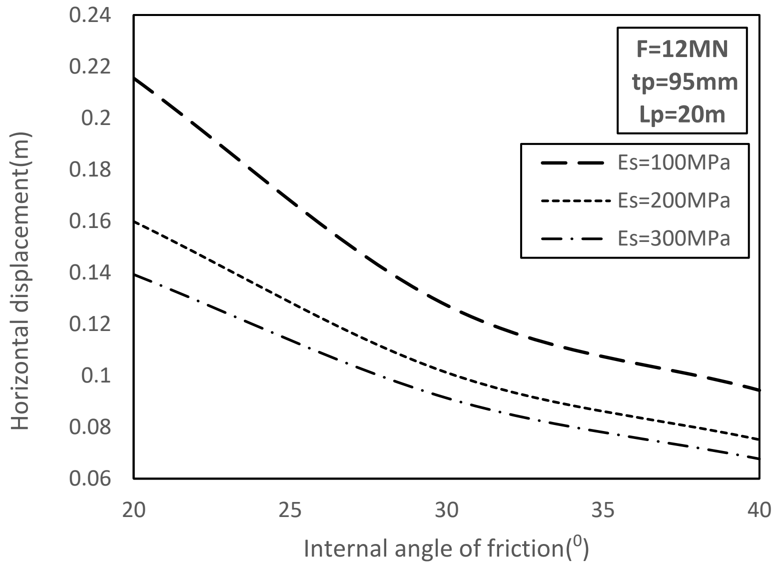
F=12MN
tp=95mm
Lp=20m
Es=100MPa
Es=200MPa
Es=300MPa
Horizontal displacement(m)
0.24
0.22
0.2
0.18
0.16
0.14
0.12
0.1
0.08
0.06
20
25
30
35
40
Internal angle of friction(0)

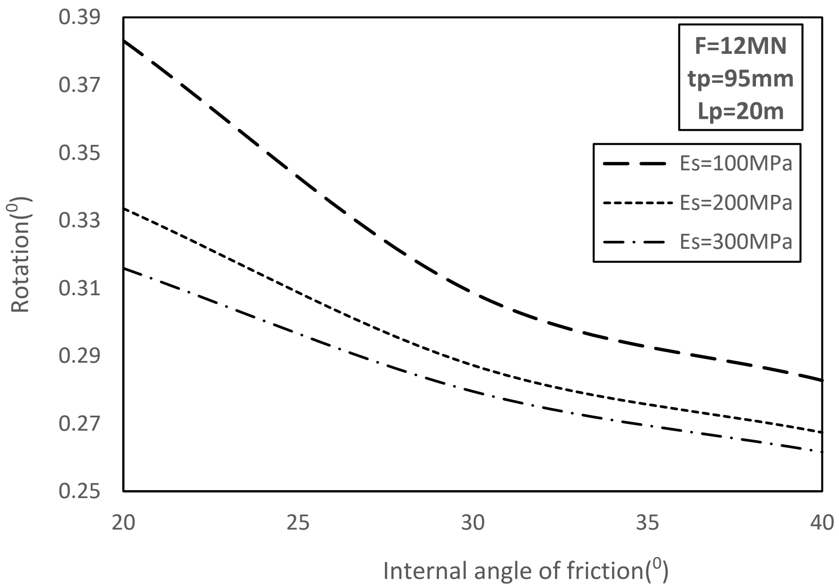
F=12MN
tp=95mm
Lp=20m
Es=100MPa
Es=200MPa
Es=300MPa
Rotation(0)
0.39
0.37
0.35
0.33
0.31
0.29
0.27
0.25
20
25
30
35
40
Internal angle of friction(0)